

Evaluating the robustness of a physics-informed machine learning ship performance model for maritime voyage optimization

Julie Vanackere

Student number: 01511540

Supervisors: Prof. dr. ir. Sidharta Gautama, dhr. Casimir Morobe (Toqua)
Counsellor: Ir. Casper Van Gheluwe

Master's dissertation submitted in order to obtain the academic degree of
Master of Science in Industrial Engineering and Operations Research

Academic year 2021-2022

Permission

The author gives permission to have this master dissertation available for consultation and to copy parts for personal use. Any other use is subject to copyright regulations, in particular the obligation to state expressly the source when quoting results from this master dissertation.

Ghent, 2th of September, 2022

Julie Vanackere

Preface

After completion of this master dissertation, a 7-year period of academic study at Ghent University will lie behind me. I will have succeeded the Master of Science in Business Engineering with the specialization, Data Analytics and the Master of Science in Industrial Engineering and Operations Research. Despite the challenges, I look back at this period with gratitude and could never accomplished this end result without the help of several people.

First of all, I would like to thank my supervisors, Prof. dr. ir. Sidharta Gautama and Ir. Casper Van Gheluwe, for their aid, knowledge sharing and detailed feedback. He gave me the opportunity to dive deep into this topic and acquire fundamental insights concerning my field of study. I also wish to thank the maritime start-up, Toqua, more precisely Casimir Morobé, Michaël Deschoolmeester and Camille Colle for their guidance, the thoughtful insights and mostly the enjoyable collaboration.

Furthermore, I would like to thank my sister and brother-in-law for the endless mental support, the warm welcomes in Ghent and co-working opportunities. Apart from them, I want to express gratitude towards the amazing friends I met during my studies. Without them, the group assignments, the exams and the life in Ghent would not have been as inspiring as it was now.

Finally, special thanks go out to my parents. They gave me the chance to fulfil my studies and provided me with ongoing encouragement throughout my course of study. They are always there to foster my dreams and show interest in all that I am pursuing.

Julie Vanackere, 2th of September, 2022

Evaluating the robustness of a physics-informed machine learning ship performance model for maritime voyage optimization

by

Julie VANACKERE

Master's dissertation submitted in order to obtain the academic degree of

INDUSTRIAL ENGINEERING AND OPERATIONS RESEARCH

Academic year 2021–2020

Supervisors: Prof. Dr. Ir. S. GAUTAMA, Dhr. C. MOROBÉ

Counselors: Ir. C. VAN GHELUWE

Ghent University

Faculty of Engineering and Architecture

Department of Industrial Systems Engineering and Product Design

Abstract

In this work, an overview is given of the aspects involved in weather routing among which traditionally used and recently developed ship performance models as well as the weather routing algorithms. This research mainly attempts to quantify the individual predictions of different types of ship performance models in estimating the power of a vessel. Following research is centered around the machine learning models of Toqua including a physics-informed ship performance model. The focus lies on the implementation of these models in weather routing. To this end, the weather avoidance and the fuel efficiency potential is tested. Furthermore, emphasis lies on creating a decision framework in applying the models.

Keywords

Weather routing, ship-hydrodynamic models, fuel oil consumption, A-star, simulated annealing, robustness, weather avoidance, fuel efficiency, physics-informed machine learning model

Evaluating the robustness of a physics-informed machine learning ship performance model for maritime voyage optimization

Julie Vanackere

Supervisor(s): Prof. dr. ir. Sidharta Gautama,
ir. Casper Van Gheluwe, dhr. Casimir Morobe

Abstract—This article forms an overview of a master’s dissertation on how different kind of ship hydrodynamic models predict the power of a vessel and how they differ from one another depending on the severity of the weather. Furthermore, the paper explains how the weather routing optimization is influenced by the model’s predictions in minimizing the fuel oil consumption (FOC) of a route. In particular, the robustness of the models comprising the sensitivity to avoid bad weather and the fuel efficiency potential is tested. Four types of FOC models are examined among which the sea trial curve, the sea trial curve with correction factor, the original machine learning and physics-informed machine learning model of Toqua. For the maritime voyage optimization, the A-star algorithm is applied for which the objective function, constraints and geographical representation is explained. The simulated annealing algorithm and the parameter fineting is also explained in depth.

Keywords—Weather routing, ship-hydrodynamic models, fuel oil consumption, A-star, simulated annealing, robustness, weather avoidance, fuel efficiency, physics-informed machine learning model

I. INTRODUCTION

THE international shipping is responsible for 80-90% of the global trade and remains the most fuel- and cost-efficient mode of transport [1, 2]. Moreover, shipping has a significant role in climate change. A 50% reduction in green house gas (GHG) emissions should be reached by 2050. The pressure to decarbonize asks for the use of new technology, ship designs, alternative fuels and operational adjustments [2]. In light of new technology, voyage optimization or weather routing has gained some recent attention as a way to drive down the fuel consumption and minimize the operating costs in shipping. Weather routing could achieve a 2-4% reduction in fuel consumption and associated GHG emissions [3]. To reap the benefits from routing, three aspects should be taken into account: the routing algorithm, the weather forecast and the ship performance models. Many research has been devoted to the first two topics, but few dive deep into the impact of the accuracy of the models predicting the power of a vessel. Most research rely on commonly used models such as sea trial curves and sea trial curves with a correction factor for waves and wind. However, the accuracy tend to be much lower in prediction the ship hydrodynamic measures of a vessel. As a result, other approaches such as machine learning models based on artificial neural networks (ANNs) in predicting the vessel’s power were developed. As did Toqua, a maritime start-up striving for the decarbonization in shipping. Two models, a pure ML model and a physics-informed ML were developed by them. In this way, the difference between varying types of ship performance can be quantified. Furthermore, the weather avoidance and the fuel efficiency of each of these mod-

els can be determined under changing weather conditions. As such in part II, the set-up of the weather routing building blocks is explained among which the FOC models and the weather routing model. Section III explains the main results involving the individual predictions of the performance models, the weather sensitivity and fuel efficiency potential of the models. Lastly, part IV summarizes the main key points of this research as well as the limitations and possible topics for future research.

II. SETUP

A. The FOC models

Four ship performance models can be distinguished in predicting the power and corresponding FOC. Two more traditional models, among which the sea trial curve and the sea trial curve with correction factor are of interest. The correction factor is applied to adjust the estimated power for waves and wind based physics-driven relations. In seeking for more accuracy in the power loss due to weather conditions, black-box models based on artificial neural networks (ANNs) have been developed by several researchers. To that end, two machine learning (ML) models have been enrolled by Toqua, a maritime start-up striving for decarbonization in shipping. The ML models developed are a pure model and a physics-informed ML model. The latter improves ANNs by also adding physical constraints to which a vessel is subject to.

The pure ML model will be referred to as ML model, the sea trial curve will be referred to as sea trial or ST model, the sea trial curve with correction factor will be referred to as sea trial + corr or ST+corr model and the physics-informed ML model will be referred to as PI-ML model.

A.1 The input parameters

The sea trial curve is an experimental model for which the laden and ballast power has been recorded in function of the speed through water (STW). The speed through water is the speed over ground adjusted for the currents. No input parameters are required to retrieve the corresponding power for a pre-defined STW. The following formula expresses the relation between both variables. However, the influence of both the current direction and speed is neglected throughout this paper. As a result, the SOG and the STW are assumed to be equal to one another.

Parameter	Range	Unit
SOG	[5,20]	[kn]
Draft	Fixed	[m]
Trim	Fixed	[m]
Wave height	[0,7.5]	[m]
Sea surface salinity	[30,40]	[PSU]
Wind speed	[0,20.7]	[m/s]
Sea surface temperature	[15,34]	[°C]
Wind direction	[0,360]	[°]
Wave direction	[0,360]	[°]
Current speed	[0,2]	[m/s]
Current direction	[0,360]	[°]
Ship heading	[0,360]	[°]
Rudder angle	[-10,10]	[°]
Speed over ground	fixed	[kn]

TABLE I: The input parameters and their corresponding value range of Toqua's ML models

Parameter	Value	ML model	PI-ML model	ST	ST + corr
Current direction	0°	✓	✓		✓
Current speed	0 m/s	✓	✓		✓
Sea temperature	23°C	✓	✓		
Trim	Fixed	✓	✓		
Draft	Fixed	✓	✓		✓
Sea surface salinity	33 PSU	✓	✓		
Heading	0°	✓	✓		✓
Rudder angle	0°	✓	✓		
SOG	12 kn	✓	✓	✓	✓
Wave direction	0°	✓	✓		✓
Wave height	0 m	✓	✓		✓
Wind speed	0 m/s	✓	✓		✓
Wind direction	0°	✓	✓		✓

TABLE II: Default values for the ship hydrodynamic models

The sea trial curve with correction factor adjust the sea trial curve according to Kreitner's method which is also explained in ISO 15016. The added resistance due to waves and wind are explained in⁴ and⁵ respectively.

As for the pure ML model and the physics-informed ML model, both require the same input parameters including ship specific, weather and voyage parameters. These input parameters and the possible ranges are displayed in table I.

An overview of the parameters included in each one of the models is given in table II as well as the default values that will be used throughout this research.

A.2 The accuracy

The accuracy of the FOC models has been validated by Toqua in terms of the mean absolute error (MAPE) and are also mentioned in their research [6].

The MAPE is calculated according to the following formula

$$MAPE = \frac{1}{n} \sum_{i=1}^n \left| \frac{y_i - \hat{y}_i}{y_i} \right| \quad (1)$$

where y_i is the actual value of the power and \hat{y}_i is the estimated value of the power.

In using the sea trial curve, the MAPE is 22.2%. Adding a correction factor lowers the MAPE to 14.3%. The physics-

d_{ij}	the distance between coordinates i and j
s_{ij}	the SOG between coordinates i and j
t_{ij}	the travel time between coordinates i and j
p_i	the main engine power traversing coordinate i
p_{ij}^{avg}	the average power between coordinates i and j
FOC_{ij}	the fuel oil consumption travelling from coordinate i to j
$SFOC$	the specific fuel oil consumption

TABLE III: The parameters of the mathematical routing model

informed model is highly accurate for which the MAPE comes down to 6.7%. The accuracy of the pure ML is similar to the physics-informed ML model. However, the data imputed in the model is quite noisy and taking into account the physics relations is essential for realistic power predictions [6].

B. The weather routing model

The routing model is an algorithm that aims to find the optimal path from start to end point subject to varying weather conditions. In routing, the goal can be diverse minimizing the FOC, travel time or the risks. In this case, the total FOC across the route will be minimized.

B.1 The model formulation

The following parameters are part of the mathematical model and are displayed in table III. Index i and j refer to the collection of geographical coordinates on the map that could possibly be traversed and range from 1 to n, where n is the total number of coordinates. The specific fuel oil consumption (SFOC) parameter is set to 170 g/kWh for the ship from which the sensor data is provided by Toqua for the purpose of this experimental research.

As the goal of the weather routing model is of to determine which geographical points should preferably be part of the final path, the decision variable is expressed in the following way. x_{ij} 1 if coordinates i and j are part of the final path, 0 otherwise.

As a result, an objective function to minimize the total FOC across a route can be set-up, expressed in formula (2). The calculation of FOC_{ij} in objective function 2 is based upon equation (4).

$$\min \sum_{i=1}^n \sum_{j=1}^n FOC_{ij} \cdot x_{ij} \quad (2)$$

$$s.t. \quad x_{ij} \in \{0, 1\} \quad (3)$$

The FOC between two points is the average power multiplied by the SFOC of the ship and the travel time between these two points. The travel time t_{ij} is equal to the distance d_{ij} divided by the speed s_{ij} . Furthermore, the average power p_{ij}^{avg} is the average between the power to transverse both coordinates. As such, p_{ij}^{avg} is equal to $\frac{p_i + p_j}{2}$. For the distance, the haversine distance is used.

$$FOC_{ij} = SFOC_{ij} \cdot p_{ij}^{avg} \cdot t_{ij} \quad (4)$$

B.2 The A-star algorithm

One of the algorithms that can be applied in weather routing is the A-star algorithm. The A-star algorithm begins with the source node s and each time adds a adjacent point of the current node to the path if the function $f = g + heuristic$ is smaller than adding another adjacent point. g is the actual cost of moving from the source node to the current node and heuristic is the estimated cost of moving from the source node to the current node. The A-star algorithm always reaches an optimal solution. An important part of the A-star algorithm is the heuristic function which distinguishes A-star from Dijkstra's algorithm. The function should be admissible in order for the algorithm to be feasible and diminish the running time. This means that $h(x) \leq g(y) + h(x, y)$ for every edge (x, y) of the graph. For the estimation of the power prediction as heuristic function, the ballast power for a predefined STW can be used. The ballast power is the power of the ship that does not carry any cargo and is therefore lower than the laden power at all time. It is also not adjusted for any weather conditions. As such added resistance is not included and the ballast power will be smaller than any power prediction for each of the four FOC models.

B.3 The simulated annealing heuristic

The simulated annealing algorithm is a meta-heuristic that optimizes an initial solution. SA begins by generating an initial random solution x_0 of the problem and deriving the associated cost $f(x_0)$. A starting temperature T_{start} is defined, which will be lowered each iteration. Thereafter, the current solution is compared to one of the neighbourhood solutions in its neighbourhood space. A neighbourhood solution $x_0 + \Delta x$ is selected at random and if the associated cost $f(x_0 + \Delta x)$ is smaller than the cost of the current solution $f(x_0)$, the current solution is replaced by the neighbourhood solution. If however the cost is larger, then the neighbourhood solution is accepted with a certain probability, namely $e^{(current\ cost - neighbour\ cost)/kT}$.

This procedure is repeated for a number of times N which is referred to as the plateau length. The plateau length can remain fixed for each run or can increase with a factor β . This procedure continues as long as the temperature T has not reached the end temperature T_{end} . The temperature is decreased according to the cooling scheme which is in this case a geomtric series. Therefore, the temperature should be lowered by a fraction α at each iteration.

The aforementioned parameters of the SA should be optimized and this has been done in the following way. A use case has been set-up for routing over the North Sea. The start point is the port of Newhaven and the end point is the port of Edinburgh. The granularity of the grid layed over the geographical area is adapted as well. A small, medium and large grid has been constructed and two time instances corresponding to the static weather conditions in the grid cells have been retrieved. As such 6 scenarios are examined to finetune the parameters. The representation of the grid sizes are shown in figure 1.

The initial solution used in the SA algorithm is the breath-first search solution. The neighbourhood operators applied are the replace, insert and delete operator in order for the path to be variable. In the path either a node can be replaced by a node,

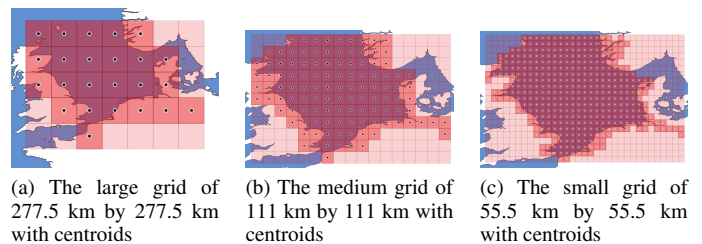


Fig. 1: The representation of different grid sizes

	Start temperature	End temperature	Plateau length	α	β	size factor
Data set I	10,000	0	8	0.9	1.3	1.0
Data set II	10,000	0	8	0.9	1.3	1.0

TABLE IV: The final input parameters for the SA algorithm for each data set

a new node can be inserted or deleted. All taking into account the adjacency of the nodes. For the other parameters, the values in table IV were the most favorable in terms of CPU-time and convergence to a low total FOC for all instances.

C. Comparison

In going forward both algorithms should be compared to one another. The fuel consumption and CPU-time for performing one iteration for both algorithms for each grid size and instance are displayed in figure 2. For this type of problem, the A-star algorithm performs better in time and FOC.

III. COMPUTATIONAL RESULTS

All results are applicable for a ship classified as a tanker. The data and models provided are customized for this type of vessel.

A. Weather definition

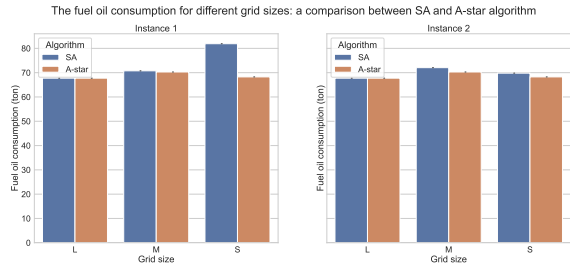
Weather at sea is determined by the wind speed and the wave height. Each combination of wind speed and wave height is associated with a Beaufort number (BN). In regards to the experiments, three types of weather can be defined: calm, medium and severe weather. In table V the weather categories adopted in this research are shown. Weather circumstances corresponding to a BN greater than 8 are not considered as these are not likely to happen in real-life.[7] The combinations of wind speed and wave height are drawn from known joint probability distributions based on historic data of the tanker.

B. Power prediction per weather category

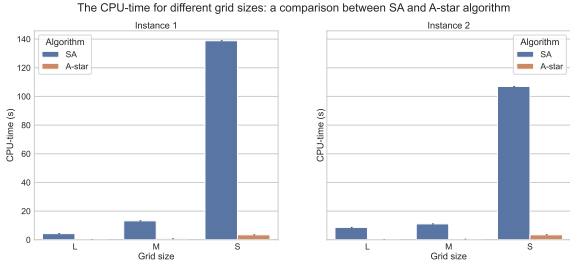
The influential parameters that should remain fixed or variable in the upcoming experiments can be determined. Based on Toqua's expertise and previous trials, the current direction and

Weather	BN	Wind speed [m/s]	Wave height [m]
Calm	[0 - 3]	[0 - 5.5]	[0 - 1.2]
Medium	[4 - 6]	[5.5 - 13.8]	[1 - 4]
Severe	[7 - 8]	[13.9 - 20.7]	[4 - 7.5]

TABLE V: Weather categories with corresponding Beaufort scale, wind speed and wave height range



(a) The fuel oil consumption for the routes constructed by A-star and SA



(b) The CPU-time for the routes constructed by A-star and SA

Fig. 2: The fuel oil consumption and CPU-time for the routes constructed by A-star and SA

speed should remain 0. Therefore, the SOG and STW are equal to one another and set to 12 kn. The trim and draft remain fixed to values specified to the vessel. The sea temperature and sea surface salinity have less effect on the power estimations and are therefore set to an average value based on historic data. As a result, only the wind speed, the wave height and the relative angle between the heading and the wind and wave directions should vary. The default values of all parameters are mentioned in table II.

The goal is to look at the individual predictions of the FOC models as well as the difference between the predictions of the models. The wind and wave direction are assumed to be equal to one another. 5 possible directions are considered 0° , 45° , 90° , 135° and 180° and 3 types of weather are considered and associated wind speed and wave directions calm, medium and severe weather. This was explained in section III-A.

In all, 15 alterations of weather and wind/wave direction on the power prediction of the four models are investigated. Within such an alteration 10,000 samples are drawn of the wind speed and wave height. The values of all other parameters are set to the default values represented in table II.

B.1 Results

The main results are displayed in figure 3 and can also be expressed in a relative percentage difference between the models. The percentage difference for one sample is calculated according to formula 5. For 10,000 samples, the mean of the 10,000 percentage differences is taken. Besides the mean, the standard deviation can also be reported. To ensure comparable results, the difference is divided by the power average over all historic

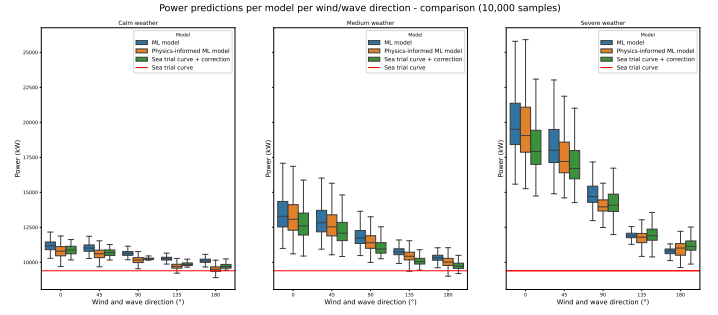


Fig. 3: Comparison of the individual power predictions of the FOC models for each weather category over 10,000 samples

data provided.

$$\% \text{ Power increase/decrease} = \frac{Power_M - Power_B}{Power_{avg}} \quad (5)$$

where $Power_M$ is the new power of the model that is compared to the benchmark model, $Power_B$ is the original power of the benchmark model and $Power_{avg}$ is the average power of the historic data.

In calm weather conditions, the power output on average of the ST+corr model is higher than the one of the PI-ML model. The relative difference ranges between 0.95% and 2.04%. Furthermore, the ML model has the highest power predictions on average. The power difference between the ML model and the PI-ML model ranges between 4.12% and 6.23%. The power difference on average increases as the angle between the heading and the wind/wave direction increases. However, for the power difference between the ML model and ST+corr model, the difference increases from 3.17% to 4.34% for a angle of 135° and thereafter slightly drops to 4.19%.

Similar to calm weather, the power output of the ML model is the highest for each wind/wave direction. However, the order of the power output of the PI-ML and ST+corr model is reversed. The average power difference ranges between 2.66% and 4.0% for the ML and PI-ML model. Likewise, the difference between ML and ST+corr model ranges from 5.77% to 8.08%. For both cases, the difference increases by angle up to 90° and slightly diminishes thereafter. The power output of the PI-ML model compared to the ST+corr model decreases along with the increase of direction. The difference ranges between 2.71% and 5.14%.

More severe weather such as 6 to 7 Beaufort (BN) translates into a changing order of magnitude between the models. Up to a angle of 90° , the power output of the ML model is higher than the other models which is also the case for calm and medium weather. However, for an angle of 135° , the ML predictions are on average smaller than the predictions of the ST+corr model. For an angle of 180° , the ML predictions are even lower than the PI-ML predictions on average. As for the PI-ML model, the power is higher than the one of the ST+corr model, but from the direction of 90° on this relation switches. Moreover, from a direction of 135° on, the prediction of the ML model is lower than the prediction of the ST+corr model. Now evaluating the power differences between the models, the relative difference between the ML model and the PI-ML model ranges between

absolute percentage values of 1.81% and 9.68%. A maximum difference of 9.68% is reached at 90° and the lowest difference of 1.81% is reached at 180°. Keeping in mind the order of magnitude of the models, the relative percentage values get a + or - sign. The power difference on average between the ST+corr predictions and the ML predictions for 0° and 45° are rather big namely 19.75% and 15.29%, but drops quickly to 6.32% for 90°. Thereafter, the order of magnitude between the two models is reversed and the difference between the predictions becomes even smaller. A similar tendency can be observed between the ST+corr and the PI-ML model. The difference drops from 17% to 6.76% from 0° to 45° and as soon as the relation between the models is reversed at 90°, the power difference between the models diminishes.

For all weather conditions, the ST model is an underestimation of the predictions. The predictions of the remaining FOC models approach the ST predictions as the angle increases. Moreover, the variation in the individual model predictions decreases along the angle, but increases as the weather becomes more severe.

C. Robustness in route optimization

The data accuracy of the FOC models can influence the route optimization. That is why robustness of the models in terms of weather sensitivity and fuel efficiency are of importance. To test the FOC models in weather routing, explained in II-A, the A-star algorithm is applied. A grid size of 55.5 km by 55.5 km is used with the same use-case described in section II-B.3. The weather conditions are static. This means that the weather parameters per grid cell do not change in time, but only in geographical sense.

Again, three weather types are considered: calm, medium and severe. Multiple homogeneous grids are set-up in order to test the models' routes. In one grid, each grid point can be seen as an individual sample or point prediction. As such, from grid point to grid point, the wind speed and wave height will differ. The grid consists of homogeneous weather conditions. Meaning that only samples are drawn within one weather category. So, if the grid consists of calm weather, each grid point entails a combination of wind speed and wave height corresponding to the joint probability distribution of calm weather. Other variables remain fixed to the default values prescribed in table II for each grid point.

The grid can be replicated with random values in each grid point several times for each weather category. In order to drawn general conclusions, a new grid will be formed 200 times per weather type. As a result, 200 different routes will be formed per model per weather type.

C.1 Weather sensitivity

For the test of weather sensitivity, the wind/wave direction remains set to 0° while the heading is changing. In this way, the relative angle between the wave/wind direction and the heading can be quantified according to formula "heading - wind/wave direction". The models' routes can be compared in terms of travel time. In figure 4, only small differences in travel time are apparent. In most cases, the length of the routes are similar, especially in medium and severe weather.

The total time consumed over a route per weather category and FOC model (200 samples)

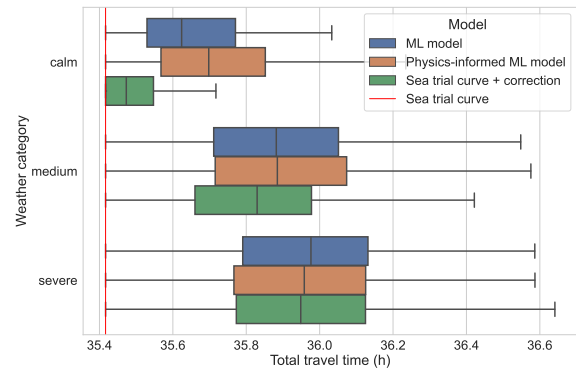


Fig. 4: Travel time comparison between weather categories and FOC models in routing

As a result, one can also quantify the overlap between the routes of two models. This is displayed in figure 5. The y-axis shows which models are compared in terms of overlap. For instance, 'ML & PI-ML' means that the pure ML model and the physics-informed ML model are compared to one another and therefore the distance between them is calculated. The x-axis entails the total distance between the subjected routes.

Remarkable is that the routes of the ML model and the physics-informed model are very similar and largely overlap in most cases for any type of weather. As such, the ML model and physics-informed model have the same results compared to the routes of the sea trial curve with or without correction. The ML and PI-ML model do not differ as much on average from the sea trial curves with correction factor in calm and medium weather, but the average distance slightly increases in severe weather as does the variation between the models' routes. As for the comparison of the sea trial curve to the other models, the boxplots indicate that the routes do not overlap on average for any type of weather, but especially for medium and severe weather. The sea trial curve follows a path corresponding the shortest distance from starting to end point without taking the weather conditions into account. Therefore, the sea trial model is not sensitive in avoiding bad weather. In this way, it is assumed that models that differ from the sea trial route are more prone to avoiding bad weather.

Furthermore, the extent to which certain FOC models avoid bad weather can also be quantified. Figure 6 shows the density plots for the wind speeds and wave heights that are crossed by each of the models' routes.

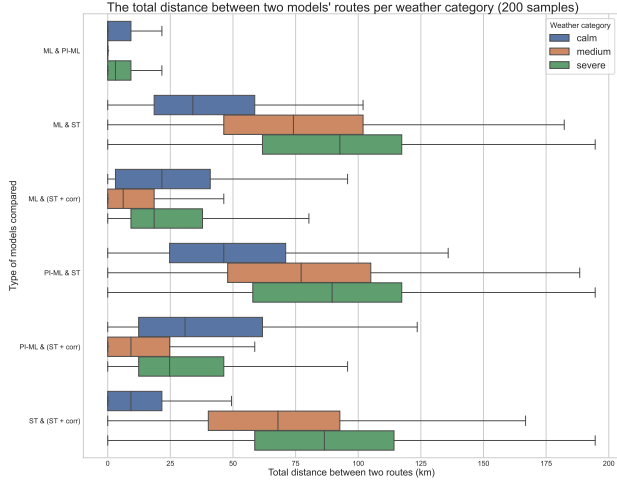
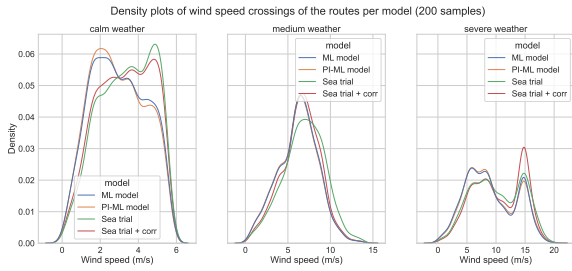
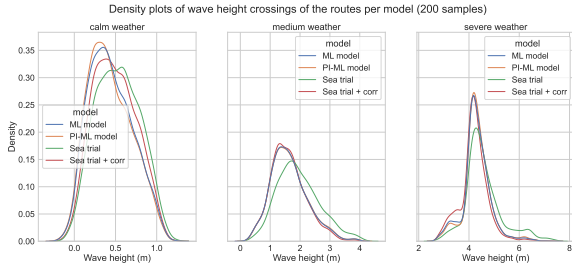


Fig. 5: Pairwise haversine distance between routes of the FOC models (200 samples)



(a) Density plot of wind speed crossings per weather category and FOC model



(b) Density plot of wave height crossings per weather category and FOC model

Fig. 6: Density plots of wind speed and wave height crossings of FOC models' routes per weather category (200 samples)

It is clear that the routes constructed by the sea trial curve pass through higher waves and wind speeds. Only in severe weather conditions, the routes of the sea trial curve with correction passes through higher wind speeds than the routes without correction.

In terms of wind speed and wave height, the ML and physics-informed ML model perform similarly. In calm weather however, the routes of physics-informed ML model have the tendency to avoid higher wind speeds and waves more.

Fuel savings (FS) and time extensions (TE) compared to the shortest route (Sea trial)	FOC model								
		Sea trial		Sea trial + corr		ML model		PI-ML model	
		FS	TE	FS	TE	FS	TE	FS	TE
Weather category	Calm	0.00%	0.00%	1.19%	0.83%	2.07%	0.94%	2.09%	1.09%
	Medium	0.00%	0.00%	4.28%	1.60%	5.48%	1.56%	5.52%	1.63%
	Severe	0.00%	0.00%	5.31%	1.46%	8.75%	1.60%	9.07%	1.46%

TABLE VI: The average fuel savings (FS) and travel time extensions (TE) of an FOC model's route compared to the shortest route (in %) - FOC recalculated by **PI-ML model** as ground truth

C.2 Fuel efficiency

Besides avoiding bad weather for safety purposes, route optimization is also concerned with fuel savings over one's route. The same experimental set-up can be used as in the sensitivity experiments. However, in this case also the wind and wave directions is randomized in each grid cell of the homogeneous grid. For each iteration, the fuel consumption of each of the models' routes can be quantified as well as the travel time. One of the FOC model should be used to recalculate the total fuel consumption over each model's route to have a comparable basis. This is considered the main challenge in calculating the return on investment (ROI) in routing, especially when the base model used is inaccurate. That is why the most accurate model, the PI-ML model is considered the ground truth. The fuel savings compared to the shortest route according to the sea trial curve are then calculated in the following way.

$$\% \text{ FOC savings} = \frac{FOC_{ST} - FOC_M}{FOC_{ST}} \quad (6)$$

where FOC_M is the total FOC of the route constructed by the model that is compared to the shortest route and FOC_{ST} is the total FOC of the shortest route according to the sea trial curve. Fuel savings however are accompanied by time extensions by not following the shortest path. The travel time extensions of the FOC model's routes compared to the routes of the shortest path are calculated in the following way.

$$\% \text{ Travel time extensions} = \frac{Time_M - Time_{ST}}{Time_{ST}} \quad (7)$$

where $Time_M$ is the total travel time of the route constructed by the model that is compared to the shortest route and $Time_{ST}$ is the total travel time of the shortest route according to the sea trial curve. Again, 200 simulations are done and the results can be averaged. The results are summarized in table VI.

In calm weather conditions, the average fuel savings of the sea trial curve with correction factor is 1.19%. This percentage doubles if routes are constructed by either the ML and PI-ML model. In essence, the savings gained from implementing one of the ML models are very similar to one another. However, a voyage's travel time does increase on average to a maximum of 1.09%. The travel time of the route's according to the shortest path is 35.67 hours. As such, an 1.09% extension translates to about 20 minutes which is a reasonable extension for the amount of fuel that can be saved.

The fuel savings increase to about 5.50% on average when

traversing medium weather opposed to calm weather for both the ML models. This is 30% gain over what can be achieved by the sea trial curve with correction factor. However, the shortest path is not followed here and that is why the travel time elongates to a maximum of 1.63%. About 35 minutes are lost in this case. Notice that the travel time is quite similar for the ML models as well as the sea trial curve with correction factor.

In severe weather conditions, the fuel savings are even more apparent, especially if the routes are constructed by the ML models. Maximum savings of about 9.07% can be reached. This translates into a 70% increase in savings over the sea trial curve with correction factor. The travel time remains equivalent to the case of medium weather and remains constant over the models' routes.

IV. CONCLUSION

In exploring the the SA algorithm opposed to the A-star algorithm, the A-star algorithm turned out to be more beneficial. Further research should be devoted to the exploration of other operators in the neighbourhood solution of the SA algorithm and the influence of the initial solution on the SA solution.

Besides the routing algorithm, the FOC models' predictions were also examined opposed to one another. For all weather types, the predictions tend to approach the sea trial curve's estimate as the relative angle between the wind/wave directions and the heading increases. The variation for each of the models also diminishes along with the increase of the angle. Furthermore, the more severe the weather becomes, the more variation constitutes among the predictions as well. One can also conclude that, for both calm and medium weather, the power predictions of the ML model are the highest on average. For severe weather, this is only true up to an angle of 90°. Moreover, in calm weather conditions the power difference between ST+corr and the PI-ML model is minimal. In medium weather conditions, this is the case for the ML and PI-ML model. For severe weather, the differences between the models' predictions are enlarging. Consequently, one should rely on the most accurate model, the PI-ML model, when dealing with routing. In the future, it could also be valuable to look at the difference in predictions of the FOC models in terms of the angle.

Mentioned earlier, route optimization can be beneficial for the safety and the fuel efficiency. Both aspects were evaluated in the second experimental. In terms of weather avoidance, the physics-informed ML model and pure ML model are very similar. They tend to better avoid bad weather opposed to the other state-to-art models under any weather circumstance. Comparing both ML models, the physics-informed ML model is slightly more weather avoidant, especially in calm weather. Some additional trials can be of use in generalizing the results in which the angle between the wind/wave direction and the heading is also randomized. Furthermore, in future research, different start and end points, different grid sizes, varying granularity and their influence of the routing algorithm as well as the FOC models could be explored.

In term of fuel efficiency, one can also conclude that the ML models account for more fuel savings opposed to the shortest route. A maximum of 9% fuel savings on average can be reached. The savings enlarge as the weather becomes more se-

vere. The travel time does extend when deviating from the shortest path to a maximum of 1.63% in medium weather conditions which corresponds to an elongation of about 35 minutes of a 35 hour voyage. The extension is apparent compared to the route of the sea trial curve. However, between the remaining models' routes, the travel time only slightly differs. Opposed to the sea trial curve with correction factor, the savings of the ML models contribute to a 70% gain in calm and severe weather and a 30% increase in medium weather. Currently, the speed is kept constant. Changing the speed to account for equal travel times for each of the models under changing weather scenarios could further enhance the fuel efficiency experiments.

In all, the ML models of Toqua are said to be bad-weather-avoidant and account for more fuel savings than frequently used performance models in the shipping industry.

REFERENCES

- (1) Zis, T. P.; Psaraftis, H. N.; Ding, L. *Ocean Engineering* **2020**, *213*, 107697.
- (2) Sirimanne, S. N.; Hoffman, J.; Juan, W.; Asariotis, R.; Assaf, M.; Ayala, G.; Benamara, H.; Chantrel, D.; Hoffmann, J.; Premti, A., et al. In *United Nations conference on trade and development, Geneva, Switzerland, 2019*.
- (3) Prpić-Oršić, J.; Vettor, R.; Faltinsen, O. M.; Guedes Soares, C. *Journal of Marine Science and Technology* **2016**, *21*, 434–457.
- (4) Conference, I. T. T. ITTC – Recommended Procedures and Guidelines <https://ittc.info/media/1936/75-04-01-012.pdf>.
- (5) For Standardization, I. O. Ships and marine technology — Measurement of changes in hull and propeller performance — Part 2:Default method <https://cdn.standards.iteh.ai/samples/63775/7de82c8a9bd4b6b8f6e275674f1d8e7/ISO-19030-2-2016.pdf>.
- (6) Colle, C.; Morobé, C. Saving AI from its Own Hype: Getting Real about the Benefits and Challenges of Machine Learning for Ship Performance Modelling Aimed at Operational Optimizations http://data.hullpic.info/HullPIC2022_Tullamore.pdf.
- (7) Mallowarachchi, V. Beaufort scale https://en.wikipedia.org/wiki/Beaufort_scale.

Contents

Overzicht	v
List of Figures	xvii
List of Tables	xx
I Introduction	1
1 General introduction	2
1.1 Research context	2
1.2 Research scope	4
1.3 Outline	5
2 Literature review	6
2.1 Introduction	6
2.2 Ship hydrodynamics	7
2.2.1 Empirical models	7
2.2.2 Physics-driven models	8
2.2.3 Machine learning models	11
2.2.4 Physics-informed machine learning models	13
2.3 Weather routing model structure	13
2.3.1 Objective function	14
2.3.2 Constraints	17
2.3.3 Geographical representation	19
2.4 Weather forecasts	21
2.5 Solution techniques	22
2.5.1 Dynamic programming	22
2.5.2 Isochrone method	24
2.5.3 Search tree algorithms	25
2.5.4 Evolutionary algorithms	27
2.6 Robustness	30

II	Experimental Setup	31
3	The fuel oil consumption models	32
3.1	Introduction	32
3.2	The state-of-art models	32
3.2.1	The sea trial curves	32
3.2.2	The sea trial curves with correction factor	33
3.3	The machine learning models of Toqua	33
3.3.1	The original ML model	33
3.3.2	The physics-informed ML model	34
3.3.3	The input parameters	34
3.4	Accuracy of the models	35
4	The weather routing model	37
4.1	The introduction	37
4.2	The model formulation	37
4.3	The weather routing algorithms	39
4.3.1	The A-star algorithm	39
4.3.2	The SA algorithm	40
5	The simulated annealing heuristic	43
5.1	Introduction	43
5.2	Scope of the problem	43
5.2.1	The models	43
5.2.2	The use case	44
5.2.3	The constraints	44
5.3	Parameters	46
5.3.1	Initial solution	46
5.3.2	Neighbourhood spaces	46
5.4	Analysis and optimization of parameters	47
5.4.1	Exploring the SA algorithm	47
5.4.2	Stop condition	49
5.4.3	The neighborhood solution	49
5.4.4	The initial solution	49
5.4.5	The starting temperature	49
5.4.6	The temperature decrement	52
5.4.7	The plateau increment	55
5.4.8	The plateau length and size factor	55
5.5	Comparison A-star and SA	55

III	Computational Experiments	60
6	Power prediction per weather category	61
6.1	Introduction	61
6.2	Data collection and models	61
6.3	General set-up	62
6.3.1	Default values for the parameters	62
6.3.2	Model assumptions	62
6.3.3	Weather definition	63
6.4	Parameter influence on the power prediction	65
6.4.1	Data description	65
6.5	The impact of weather severity and wind/wave direction	66
6.5.1	Assumptions	67
6.5.2	Experimental set-up	67
6.5.3	Results	69
7	Robustness in route optimization	77
7.1	Introduction	77
7.2	Methodology	77
7.2.1	Geographic representation	77
7.2.2	Weather forecast	78
7.2.3	Ship hydrodynamics and models	79
7.3	Weather sensitivity and fuel efficiency	79
7.4	Experimental set-up	79
7.4.1	Homogeneous weather conditions	79
7.4.2	Assumptions	81
7.4.3	Metrics	81
7.5	Weather avoidance results	83
7.5.1	Similarities in terms of travel time	83
7.5.2	Overlap between the models' routes	83
7.5.3	Weather avoidance	85
7.5.4	Bias and generalisation of the results	89
7.6	Fuel optimization results	91
IV	Conclusion	94
8	General conclusion, limitations and future research	95
V	Appendices	98
A	The simulated annealing heuristic	99

B	Power prediction per weather category	101
B.1	Impact of the weather severity	101
B.1.1	The mean of the power predictions	101
B.1.2	The standard deviation of the power predictions	102
B.1.3	The mean of the power difference	103
B.1.4	The standard deviation of the power difference	108
C	Robustness in route optimization	119
C.1	Sensitivity results: 100 samples	120
C.2	Fuel efficiency results	121
C.2.1	The fuel savings with the pure ML model as ground truth	121
C.2.2	The standard deviations of the time extensions	123
C.2.3	The standard deviations of the fuel savings	123
	Bibliography	124

List of Figures

2.1	Methodology	6
2.2	The relation between ship performance metrics (SOG = speed over ground, STW = speed through water, RPM = rounds per minute, FOC = fuel oil consumption, ETA = estimated time of arrival)	7
2.3	The hydrodynamic factors influencing the performance of a ship (Pedersen, 2014)	8
2.4	Framework for predicting the FOC by Gkerekos and Lazakis (2020)	12
2.5	The safety constraints specified by the IMO guidelines (Shao et al., 2012) . .	18
2.6	The waypoint representation according to Lin et al. (2013)	20
2.7	The grid-based representation according to Sen and Padhy (2015)	21
2.8	A-star procedure by use of way-points (Bentin et al., 2016)	26
2.9	8-way versus 16-way search in a grid (Shin et al., 2020)	27
5.1	The representation of different grid sizes	45
5.2	An initial SA simulation per instance and grid size	48
5.3	The acceptance rate of the operators in the neighbourhood solution for different grid sizes and instances	50
5.4	The expected FOC and CPU-time in function of the initial solution	51
5.5	The expected FOC and CPU-time in function of the starting temperature . .	53
5.6	The expected FOC and CPU-time in function of the temperature decrement	54
5.7	The expected FOC and CPU-time in function of the plateau increment . . .	56
5.8	The expected FOC and CPU-time in function of the temperature decrement and the size factor	57
5.9	The fuel oil consumption and CPU-time for the routes constructed by A-star and SA	59
6.1	The joint probability distributions of the wind speed and wave height for each weather category	64
6.2	The relation between wind speed and wave height	65
6.3	The relation between wind and wave direction	66
6.4	The wind and wave directions opposed to a ship heading of 0°	67

6.5	The comparison of boxplots of the power predictions per model per wind and wave direction for calm weather (10,000 samples)	70
6.6	The comparison of boxplots of the power predictions per model per wind and wave direction for medium weather (10,000 samples)	71
6.7	The comparison of boxplots of the power predictions per model per wind and wave direction for severe weather (10,000 samples)	73
6.8	Comparison of the FOC models' power prediction per wind/wave direction (10,000 samples)	75
6.9	Comparison of the FOC models' power prediction differences between two models for a wind/wave direction = 0° (10,000 samples)	76
7.1	The grid-based representation of the North Sea with start and end point . . .	78
7.2	The heatmaps for wind speed and wave height corresponding to calm weather	80
7.3	Travel time comparison between weather categories and FOC models in routing	83
7.4	Pairwise haversine distance between routes of the FOC models (200 samples)	84
7.5	Density plots of wind speed and wave height crossings of FOC models' routes per weather category (200 samples)	86
7.6	Density plot of wind speed and wave height crossings of non-overlapping grid points between routes of the ML and PI-ML models (200 samples)	87
7.7	Density plots of wind speed and wave height crossings of non-overlapping grid points between routes of the sea trial curve with correction and the ML models (200 samples)	88
7.8	Density plots of wind speed and wave height crossings of non-overlapping grid points between routes of the sea trial curve and other FOC models (200 samples)	90
7.9	Fuel consumption calculated by the PI-ML model in function of travel time for different weather categories (200 samples)	92
A.1	Routes constructed by A-star and SA for a large grid size	99
A.2	Routes constructed by A-star and SA for a medium grid size	100
A.3	Routes constructed by A-star and SA for a small grid size	100
B.1	The pairwise, relative power difference for different wind/wave directions - calm weather	110
B.2	The pairwise, relative power difference for different wind/wave directions - medium weather	113
B.3	The pairwise, relative power difference for different wind/wave directions - severe weather	116
B.4	The pairwise, relative power difference for different weather categories and different wind/wave direction - part 1	117

B.5	The pairwise, relative power difference for different weather categories and different wind/wave direction - part 2	118
C.1	Density plots of wind speed and wave height crossings of FOC models' routes per weather category (100 samples)	120
C.2	Fuel consumption calculated by the ML model in function of travel time for different weather categories (200 samples)	121

List of Tables

2.1	Overview of the objective functions concerning weather routing used in literature	14
2.2	Overview of the constraints concerning weather routing in literature	17
2.3	Geographical representation of the construction of a route and corresponding solution technique: overview of research papers	19
3.1	The input parameters and their corresponding value range of Toqua’s ML models	35
5.1	The input initial parameters for a first solution of the SA algorithm for each data set	47
5.2	The final input parameters for the SA algorithm for each data set	55
6.1	Default values for the ship hydrodynamic models	62
6.2	Weather categories with corresponding Beaufort scale, wind speed and wave height range	63
6.3	Example of the table with relative changes (in %) for comparison of the models in function of the weather severity and the wind and wave direction	69
7.1	The average fuel savings (FS) and travel time extensions (TE) of an FOC model’s route compared to the shortest route (in %) - FOC recalculated by PI-ML model as ground truth	93
B.1	The mean power prediction per model and wind/wave direction expressed in kW for calm weather (10,000 samples)	101
B.2	The mean power prediction per model and wind/wave direction expressed in kW for medium weather (10,000 samples)	101
B.3	The mean power prediction per model and wind/wave direction expressed in kW for severe weather (10,000 samples)	102
B.4	The standard deviation of the power prediction per model and wind/wave direction expressed in kW for calm weather (10,000 samples)	102
B.5	The standard deviation of the power prediction per model and wind/wave direction expressed in kW for medium weather (10,000 samples)	102

B.6	The standard deviation of the power prediction per model and wind/wave direction expressed in kW for severe weather (10,000 samples)	103
B.7	The mean, relative power difference between models for a wind and wave direction of 0° expressed in % for calm weather (10,000 samples)	103
B.8	The mean, relative power difference between models for a wind and wave direction of 45° expressed in % for calm weather (10,000 samples)	103
B.9	The mean, relative power difference between models for a wind and wave direction of 90° expressed in % for calm weather (10,000 samples)	104
B.10	The mean, relative power difference between models for a wind and wave direction of 135° expressed in % for calm weather (10,000 samples)	104
B.11	The mean, relative power difference between models for a wind and wave direction of 180° expressed in % for calm weather (10,000 samples)	104
B.12	The mean, relative power difference between models for a wind and wave direction of 0° expressed in % for medium weather (10,000 samples)	105
B.13	The mean, relative power difference between models for a wind and wave direction of 45° expressed in % for medium weather (10,000 samples)	105
B.14	The mean, relative power difference between models for a wind and wave direction of 90° expressed in % for medium weather (10,000 samples)	105
B.15	The mean, relative power difference between models for a wind and wave direction of 135° expressed in % for medium weather (10,000 samples)	106
B.16	The mean, relative power difference between models for a wind and wave direction of 180° expressed in % for medium weather (10,000 samples)	106
B.17	The mean, relative power difference between models for a wind and wave direction of 0° expressed in % for severe weather (10,000 samples)	106
B.18	The mean, relative power difference between models for a wind and wave direction of 45° expressed in % for severe weather (10,000 samples)	107
B.19	The mean, relative power difference between models for a wind and wave direction of 90° expressed in % for severe weather (10,000 samples)	107
B.20	The mean, relative power difference between models for a wind and wave direction of 135° expressed in % for severe weather (10,000 samples)	107
B.21	The mean, relative power difference between models for a wind and wave direction of 180° expressed in % for severe weather (10,000 samples)	107
B.22	The standard deviation of the relative power difference between models for a wind and wave direction of 0° expressed in % for calm weather (10,000 samples)	108
B.23	The standard deviation of the relative power difference between models for a wind and wave direction of 45° expressed in % for calm weather (10,000 samples)	108
B.24	The standard deviation of the relative power difference between models for a wind and wave direction of 90° expressed in % for calm weather (10,000 samples)	108

B.25	The standard deviation of the relative power difference between models for a wind and wave direction of 135° expressed in % for calm weather (10,000 samples)	109
B.26	The standard deviation of the relative power difference between models for a wind and wave direction of 180° expressed in % for calm weather (10,000 samples)	109
B.27	The standard deviation of the relative power difference between models for a wind and wave direction of 0° expressed in % for medium weather (10,000 samples)	111
B.28	The standard deviation of the relative power difference between models for a wind and wave direction of 45° expressed in % for medium weather (10,000 samples)	111
B.29	The standard deviation of the relative power difference between models for a wind and wave direction of 90° expressed in % for medium weather (10,000 samples)	111
B.30	The standard deviation of the relative power difference between models for a wind and wave direction of 135° expressed in % for medium weather (10,000 samples)	112
B.31	The standard deviation of the relative power difference between models for a wind and wave direction of 180° expressed in % for medium weather (10,000 samples)	112
B.32	The standard deviation of the relative power difference between models for a wind and wave direction of 0° expressed in % for severe weather (10,000 samples)	114
B.33	The standard deviation of the relative power difference between models for a wind and wave direction of 45° expressed in % for severe weather (10,000 samples)	114
B.34	The standard deviation of the relative power difference between models for a wind and wave direction of 90° expressed in % for severe weather (10,000 samples)	114
B.35	The standard deviation of the relative power difference between models for a wind and wave direction of 135° expressed in % for severe weather (10,000 samples)	115
B.36	The standard deviation of the relative power difference between models for a wind and wave direction of 180° expressed in % for severe weather (10,000 samples)	115
C.1	The average fuel savings (FS) and travel time extensions (TE) of an FOC model's route compared to the shortest route (in %) - FOC recalculated by ML model as ground truth	122
C.2	The standard deviation of the travel time extension of an FOC model's route compared to the shortest route (in %)	123

C.3	The standard deviation of the fuel savings of an FOC model's route compared to the shortest route (in %) - FOC recalculated by PI-ML model as ground truth	123
C.4	The standard deviation of the fuel savings of an FOC model's route compared to the shortest route (in %) - FOC recalculated by ML model as ground truth	123

Nomenclature

SP	Shortest Path Problem
FOC	Fuel Oil Consumption
ETA	Estimated Time of Arrival
2DDP	Two-Dimensional Dynamic Programming
3DDP	Three-Dimensional Dynamic Programming
IDP	Iterative Dynamic Programming
DP	Dynamic Programming
RPM	Rounds Per Minute
SOG	Speed Over Ground
SA	Simulated Annealing
GA	Genetic Algorithm
JGG	Just Generation Gap
RCGA	Real-Coded Genetic Algorithm
MOGA	Multi-Objective Genetic Algorithm
STW	Speed Through Water
ANN	Artificial Neural Network
ETR	Extra Tree Regressors
RFR	Random Forest Regressors
SVR	Support Vector Regressors
LR	Linear Regression
ADLM	Automated Data Logging & Monitoring
PCTC	Pure Car Truck Carrier
ATA	Actual Time of Arrival
BN	Beaufort number
SFOC	Specific Fuel Oil Consumption
PSU	Practical Salinity Units
kn	knots
3DMI	Three-Dimensional Modified Isochrone
BFS	Breath-First Search
MAPE	Mean Absolute Percentage Error
XGB	eXtreme Gradient Boosting
IMO	International Maritime Organization
UNCTAD	United Nations Conference on Trade and Development
ISO	International Organization for Standardization

Part I

Introduction

Chapter 1

General introduction

1.1 Research context

International shipping is responsible for 80-90% of the global trade and remains the most fuel- and cost-efficient mode of transport (Sirimanne et al., 2019; Zis et al., 2020). The maritime trade is expected to grow further by 2.4% annually over the upcoming 4 years according to United Nations Conference on Trade and Development (UNCTAD). 25% of vessel's operating costs are devoted to the fuel oil consumption (FOC) which correlates to the adversity of the weather along its route (Gkerekos and Lazakis, 2020). In addition, oil and chemical tankers account for 85% of the net green house gas (GHG) emissions within the shipping sector. The importance of shipping is apparent and should be evaluated in terms of sustainability, risks and costs.

Furthermore, the shipping industry has especially a significant role in climate change. On that note, the International Maritime Organization (IMO) introduced new mandatory regulations to reduce the GHG emissions from shipping. The goal is to reach in 2025 a reduction of the CO_2 emission up to 30% and in 2050 an additional reduction of 20% which is roughly equivalent to the same reduction in fuel consumption (Prpić-Oršić et al., 2016). The pressure to decarbonize asks for the use of new technology, ship designs, alternative fuels and operational adjustments (Sirimanne et al., 2019).

In light of new technology, voyage optimization or weather routing has gained some recent attention as a way to drive down the fuel consumption and minimize the operating costs in shipping. Weather routing could achieve a 2-4% reduction in fuel consumption and associated GHG emissions (Prpić-Oršić et al., 2016). Other economic drivers such as risk avoidance and the reduction of travel time could also positively be influenced by the optimization of a voyage (Zis et al., 2020).

The link between weather routing and environmental impact is clear, but the precise im-

plementation is of crucial importance in quantifying the benefits. The accuracy relies on the prediction of the ship's hydrodynamic behaviour under different weather conditions, the accuracy of the weather forecasts and the routing algorithm used (Shao et al., 2012).

Even though weather routing is an active research topic, most studies rely on first-principle approaches that are not able to precisely predict the ship performance measures such as the speed and the power of a vessel (Gkerekos and Lazakis, 2020). The need for accuracy in this area has been addressed by more recent approaches involving machine learning (ML) models, especially artificial neural networks (ANNs), to bridge this gap. Beşikçi et al. (2016); Gkerekos and Lazakis (2020); Gkerekos et al. (2019); Morobé and Van den Poel (2020); Wang et al. (2016) have already proved the usefulness of ANNs in predicting ship hydrodynamic measures.

However, how these specific ML models estimate the power and corresponding fuel consumption opposed to other state-of-the-art prediction models under varying degree of weather severity remains absent. Moreover, the benefits of using an ML model in weather routing has not yet been examined in terms of fuel savings.

To this end, Toqua, a maritime start-up striving for the decarbonization of the shipping industry, developed two ML models, a pure ML model and a physics-informed ML model. They distinguish themselves by guaranteeing a high prediction accuracy of the ship hydrodynamics. The physics-informed ML model has a mean absolute percentage error (MAPE) of only 6.7% opposed to a traditional approach, the sea trial curves (Colle and Morobé, 2022). In that way, operational optimizations such as route or speed optimization can benefit from this.

Besides the ship performance models, a broad overview of the route optimization algorithms has been developed over the years, among which the A-star and the simulated annealing algorithm. The A-star algorithm is proved to be optimal and the implementation is addressed by Bentin et al. (2016); Park and Kim (1998); Shin et al. (2020). However, one elaborates less on the implementation of SA in weather routing and the corresponding parameter tuning such as the neighbourhood operators.

Even though saving fuel is a main driver in the industry, safety and risk avoidance are of importance as well. Avoiding high waves can reduce the risk of instability of a vessel and phenomenons such as parameter rolling, surf riding and broaching can be overcome (Begovic et al., 2018). Some ship hydrodynamic models could be more sensitive to severe weather than others. Therefore, this research also attempts to investigate if ML models are more bad-weather-avoidant than the traditional approaches in route optimization.

In all, the robustness of ship performance models in route optimization is addressed in this master's dissertation comprising both the fuel efficiency and the weather sensitivity.

Robustness is mainly seen as an answer to inaccuracy in predictions. As the ML models of Toqua embody high accuracy they could contribute to the robustness in route optimization.

1.2 Research scope

Besides commonly used power prediction models such as physics-driven and empirical models explained in literature, the newly developed machine learning (ML) models of Toqua among which a pure ML model and physics-informed ML model are presented. The added value and their accuracy have already been proved by Toqua with emphasis on the use of sensor data. Current research adds to this by quantifying the over- and underestimation of the FOC predictions of more traditional models such as the sea trial curves with and without correction factor, opposed to both ML models.

Their behaviour under varying degree of weather severity is examined as well. In that way, the influence of weather conditions such as the wave height, wind speed and the angle between the heading and wind and wave direction are tested for each of the models. A distinction can be made between the individual power predictions of the models and the relative difference between predictions.

More importantly, the integration of the ML predictions in a weather routing application is applied. Both the A-star algorithm and the simulated annealing (SA) algorithm is outlined and a comparison is made between the two algorithms in terms of CPU-time and fuel consumption. For the SA algorithm, the parameter tuning is optimized and the encountered challenges are explained.

Moreover, for the purpose of finding an optimal route, a specific methodology is applied based on collective information gathering in literature. The methodology involves the structural and mathematical development of both routing algorithms as well as their link to the ship performance models.

Besides examining the predictive behaviour of different types of ship performance models, this master dissertation is the first in testing the robustness of the models. Two main research questions will be answered:

1. What type of ship performance models are more sensitive to bad weather and are therefore considered more bad weather avoidant under varying degree of weather severity?
 - (a) How do traditional approaches such as sea trial curves and sea trial curves with a correction factor behave in terms of weather sensitivity opposed to ML models?
 - (b) How does the pure ML model differ from a newly developed physics-informed ML model in terms of bad weather avoidance?

2. Does higher accuracy of the ML models translate into more fuel savings across a route and how does this effect the travel time?

Lastly, this dissertation is an excellent foundation for future research in robustness testing of weather routing due to the absence in literature and serves as a guide in the optimization of weather routing algorithms.

1.3 Outline

Current research consists of 9 chapters. The first part of this master's dissertation consists of chapters 1 and 2 and focuses mainly on providing introductory and comprehensive information about the topic. Chapter 1 includes the general introduction and explains how this master dissertation closes the gap in literature. Chapter 2 gives an overview of the existent literature concerning the link between hydrodynamic models and weather routing models as well as the possible ways to model them. Furthermore, the methodology related to the weather routing structure such as the objective function, constraints and geographical representation are presented.

The second part of this thesis is concerned with the experimental set up of the case study at hand. In chapter 3, the fuel oil consumption (FOC) models that are applied in order to model the hydrodynamic performance of a vessel will be explained. Chapter 4 complements chapter 3 by formulating the weather routing model and explaining how the resulting power prediction can be used as input for the FOC objective function of either the A-star algorithm or the simulated annealing (SA) algorithm. As the SA algorithm requires some parameter finetuning, chapter 5 is devoted to the experiments in determining the optimal values for the parameters.

In the third part, the focus lies on the computational experiments. Chapter 6 talks about the individual predictions of the FOC models independent from weather routing and the difference between them. In chapter 7, the FOC models are applied in weather routing and their robustness is tested.

In the remainder of this master dissertation the main conclusions, limitations and recommendations for future research are specified in chapter 8.

Chapter 2

Literature review

2.1 Introduction

As there are significant economic and environmental drivers such as regulatory pressure to achieve greener maritime transportation, increasing fuel prices and time restrictions, weather routing has gained great interest in literature over the years. According to Zis et al. (2020) weather routing can be defined as selecting an optimal route in a given voyage with known origin and destination port while taking into account the expected weather and sea conditions. Moreover, weather routing can be considered as a path problem for a single ship at the operational level (Zis et al., 2020).

There are several aspects related to weather routing, among which the weather routing inputs and the weather routing model. The inputs concern the type of weather forecast, the ship hydrodynamics and the models associated with it and the geographical representation. The weather routing models on the other hand are associated with the model specifications such as the objective function, constraints and the algorithm that will be applied to reach the predefined goals.

The figure below gives a short overview of the methodology commonly used in literature.

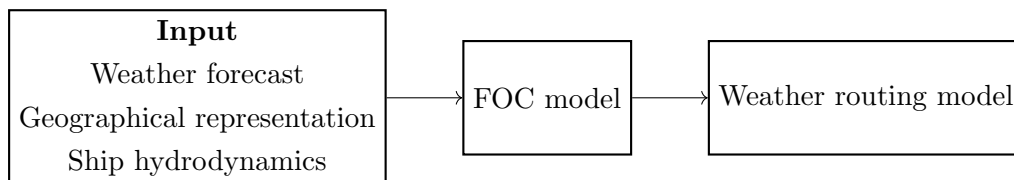


Figure 2.1: Methodology

2.2 Ship hydrodynamics

The main goal of this section is to relate the weather conditions to the performance of a ship. Weather, as well as the ship conditions, result in a certain resistance that affects the speed through water (STW) and power of a ship. Figure 2.2 gives an overview of the main metrics that are important in a ship performance model. For reference, speed over ground (SOG) is the GPS speed and if corrected for the influence of the ocean currents results in a speed through water (STW)(Yang et al., 2020). Both STW and power are the main focus in determining the objectives for a weather routing model such as the fuel oil consumption (FOC) and the estimated time of arrival (ETA), explained in section 2.3.1. The link between STW, RPM and power is often avoided in literature and therefore often a direct relation is drawn between STW and power.

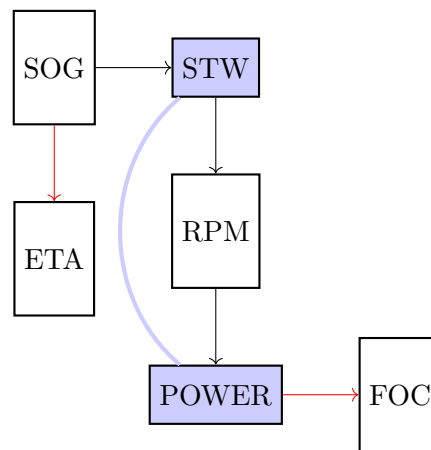


Figure 2.2: The relation between ship performance metrics (SOG = speed over ground, STW = speed through water, RPM = rounds per minute, FOC = fuel oil consumption, ETA = estimated time of arrival)

The conversion between STW and power can be estimated in multiple ways, among which empirical models, physics models and machine learning (ML) models.

2.2.1 Empirical models

Empirical models such as sea trial curves are used to draw a simple relation between the STW and power under prescribed conditions. In the majority of the cases, environmental conditions such as weather are not taken into account for the purpose of these trials.(Waters et al., 2007) In essence, the speed and corresponding power is observed and manually kept track off in order to estimate the relation between power and speed. The resulting sea trial curves for a specific ship can however be combined with a correction factor for waves and wind as to gain a more realistic prediction. A correction factor can be introduced based on Kwon’s method or Kreitner’s formula which will be explained in the next section.

2.2.2 Physics-driven models

The majority of literature relies on physical formulas such as the model of Holtrop and Mennen (1982). Building further upon this model, the research of Morobé and Van den Poel (2020) describes the main influencing factors in a condense way. As explained there, the speed through water (STW) of the ship is related to the power of the engine as follows:

$$P_d = \frac{R_T \times V}{\theta_Q} \quad (2.1)$$

where

P_d = the delivered power

R_T = the total in-service resistance

V = the speed through water

θ_Q = the quasi-propulsive efficiency

The performance measures are influenced by both the the quasi-propulsive efficiency and the total resistance which is shown in figure 2.3.

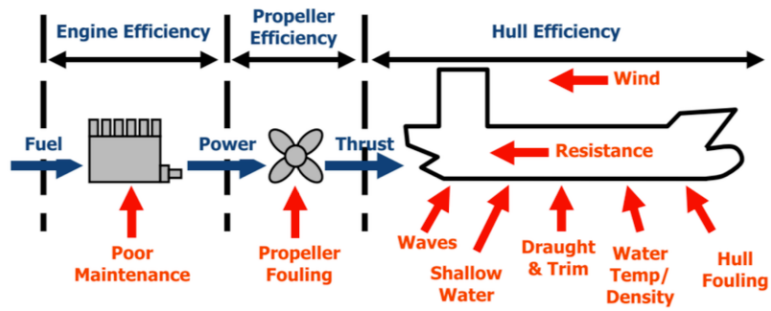


Figure 2.3: The hydrodynamic factors influencing the performance of a ship (Pedersen, 2014)

The first factor is influenced by the efficiency of the propeller of the ship and this efficiency can be subdivided into three components: the open-water efficiency, the hull efficiency and the relative rotation efficiency. The second factor, the total resistance, consists of a still-water resistance and an added resistance due to environmental factors such as wind, waves and the hull conditions (Holtrop and Mennen, 1982; Kwon, 2008; Morobé and Van den Poel, 2020). The formulas for the resistance and efficiency adopted from Morobé and Van den Poel (2020) are summarized below.

$$R_T = R_{SW} + R_{AA} + R_{AW} + R_{AH} \quad (2.2)$$

where

R_T = total resistance

R_{SW} = still-water resistance
 R_{AA} = added resistance due to wind
 R_{AW} = added resistance due to waves
 R_{AH} = added resistance due to changes in hull condition

$$\theta_Q = \theta_0 + \theta_H + \theta_{QR} \quad (2.3)$$

where

θ_Q = the quasi-propulsive efficiency

θ_0 = the open-water efficiency

θ_H = the hull efficiency

θ_{QR} = the relative rotation efficiency

The ship resistance can also be determined while taking into account the water depth. Therefore, some research rather applies a different formula for the resistance (Morobé and Van den Poel, 2020; Wang et al., 2018). The formula for the ship resistance can then be written as:

$$R_{ship} = R_{SW} + R_{wave} + R_{wind} + R_{shallow} \quad (2.4)$$

where

R_{SW} = hydrostatic or still-water resistance

R_{wave} = added resistance due to waves

R_{wind} = added resistance due to wind

$R_{shallow}$ = shallow water resistance

The specific formulas concerning the calculation of the different resistance and efficiency components are out of scope for current research purposes. The main focus of the research domain in voyage optimization is the estimation of the added resistance as this is subject to environmental factors.

Kwon's method

The added resistance due to waves and wind and the corresponding speed loss can be estimated by Kwon's method. The speed loss is also called involuntary speed reduction. One assumes that the ship is able to provide constant power output under different weather conditions (Kwon, 2008; Shao et al., 2012). The percentage loss in speed can then be expressed in the following way:

$$\frac{\Delta V}{V_1} 100\% = C_\beta C_u C_{form} \quad (2.5)$$

$$\Delta V = V_1 - V_2 \quad (2.6)$$

$$V_1 = F_n \sqrt{L_{pp}g} \quad (2.7)$$

where

ΔV = the loss of ship speed

V_1 = the ship speed in calm water

V_2 = the ship speed under selected weather conditions

C_β = the speed direction reduction coefficient

C_u = the speed reduction coefficient

C_{form} = the hull form coefficient

F_n = the Froude number

L_{pp} = the ship length between perpendiculars

g = the acceleration due to gravity

This is a simple way of calculating the speed loss without using complex hydrodynamic calculations. However, it remains a simplification and is therefore less accurate (Kwon, 2008; Shao et al., 2012).

Kreitner's formula and ISO 15016

Besides Kwon's method, Kreitner's formulas are applied in research to determine the added power instead of speed loss due to the wave and wind resistance. The formulas of the model correspond to the methodology of the ISO 15016 with the primary purpose to define procedures for the evaluation and correction of sea trials. The total power correction can then be determined by multiplying the the total wave and wind resistance by the SOG.

First off, the wave resistance formula is given below. The formula is applicable for waves up to a height of 1.5 to 2m (Conference, 2005).

$$\Delta R_{wave} = 0.64 \cdot \epsilon_w^2 \cdot B^2 \cdot C_B \cdot \rho \cdot \frac{1}{L} \quad (2.8)$$

where

ΔR_{wave} = the added wave resistance

ϵ_w = the wave height

B = the beam

C_B = the hydrodynamic drag coefficient

L = the length of the ship

ρ = the specific weight of water

Additionally, the added resistance due to wind can be calculated using formula 2.9 (for Standardization, 2016).

$$\Delta R_{wind} = 0.5 \cdot \rho_a \cdot A \cdot (v_{wr}^2 \cdot C_{rw}(\psi_{wr,ref}) - v_g^2 \cdot C_{ow}(0)) \cdot \rho \cdot 1/L \quad (2.9)$$

where

ΔR_{wind} = the added wind resistance

ρ_a = the air density

A = the transverse projected area in current loading condition

v_{wr} = the relative wind speed at reference height

$C_{rw}(\psi_{wr,ref})$ = the wind resistance coefficient, dependent on wind direction of relative wind equal to $\psi_{wr,ref}$

v_g = the ship speed over ground

$C_{ow}(0)$ = the wind resistance coefficient for head wind (0° wind direction)

2.2.3 Machine learning models

To increase the prediction accuracy of the speed, power or the resulting fuel oil consumption (FOC), recent research relies on machine learning and artificial intelligence models.

Machine learning is a branch of artificial intelligence that focuses on using data and algorithms in imitating real-life situations and relations with the purpose of improving the accuracy. Machine learning models use statistics to find patterns in large amounts of data (national laboratory, 2022).

Gkerekos et al. (2019) performed a comparative study concerning the machine learning models for predicting the fuel oil consumption. They concluded that extra tree regressors (ETRs), random forest regressors (RFRs), support vector regressors (SVRs) and artificial neural networks (ANNs) yield the best performance results. However, similar results can be obtained by applying a simple linear regression (LR) model.

Artificial neural networks (ANNs)

Due to the high accuracy, ANNs are widely adopted. Neural networks consist of an input layer, hidden layer and output layer. Wang et al. (2016) applied a wavelet neural network (WNN) to predict environmental parameters and corresponding engine speed. The predicted working condition related to the navigation environment can on their turn serve as input for a ship energy efficiency model to predict the fuel consumption. The model is based upon the theoretical formulas explained in section 2.2.2, more specifically formula 2.4. This model is embedded in a real-time dynamic optimization process in which the fuel consumption is calculated under the predicted navigation environment for different values of the main engine

Apart from ANN model, the research of Morobé and Van den Poel (2020) also applies other machine learning techniques to predict the speed through water (STW) of a vessel. The focus lies on explanatory data analysis, pre-processing, cross-validation, train-test split, the feature selection and the model building. The study affirms that ANN, but also kernel-based techniques have the best performance. The research also differentiates itself by investigating the effect of fouling on the STW. After a period of dry-docking, it is said that the vessel experiences less speed loss and thus saves fuel.

Regression models

The ship speed can also be predicted with a given revolutions per minute (RPM) through statistical analysis, developed by Mao et al. (2016). The sea parameters influencing the resistance of the ship considered here are significant wave height, average period, average wind velocity component and current velocity. A simple linear regression model, a first order autoregressive model and a mixed-effect model have been applied by Mao et al. (2016).

In the study of Shin et al. (2020), the eXtreme Gradient Boosting (XGB) regression model has been used to predict the SOG. The hyperparameters of the XGB regressor were optimized using Bayesian optimization methods with 10-fold cross validation.

2.2.4 Physics-informed machine learning models

A subcategory of machine learning are physics-informed ML models. In feeding the data to the ML models, the logical relations between parameters should be sustained. For instance, a neural network serves as a black box that links input parameters to a certain output. In order for the network to learn the input parameters training based on known data is applied. However to avoid the hassle of large data gathering and trying to improve the accuracy of the predictions even more, physics-informed machine learning comes is of use (national laboratory, 2022).

Physical relations provide an extra layer of information in order for the prediction to be better. The data is constrained to satisfy these relations (national laboratory, 2022).

2.3 Weather routing model structure

In order to construct the optimal route, the desired goal and realistic conditions should be modelled. As such, this section maps the most important objective functions and constraints applied in research. Moreover, a spectrum of solution techniques to adequately find the best possible route accounting for varying weather conditions is given.

2.3.1 Objective function

In general, ship voyage optimization focuses on different aspects when optimizing a route. The goals that reoccur in research are mitigating the risks at sea, environmental impact by minimizing the FOC and time optimization. Table 2.1 gives an overview of the research papers that focus on each of the different objectives.

Paper	Min FOC	Min risks	Min ETA	Min cost
(Delitala et al., 2010)	✓	✓	✓	✗
(Calvert et al., 1991)	✓	✗	✗	✗
(Chen, 1978)	✗	✗	✗	✓
(Shao et al., 2012)	✓	✗	✗	✗
(Bijlsma, 1975)	✓	✗	✓	✗
(Haltiner et al., 1962)	✗	✗	✓	✗
(Avgouleas, 2008)	✓	✗	✗	✗
(Sen and Padhy, 2015)	✗	✗	✓	✗
(Zhu et al., 2016)	✗	✗	✓	✗
(Takashima et al., 2009)	✓	✗	✗	✗
(Park and Kim, 2015)	✓	✗	✗	✗
(Bentin et al., 2016)	✓	✗	✗	✗
(Shin et al., 2020)	✗	✗	✓	✗
(Kosmas and Vlachos, 2012)	✗	✗	✗	✓
(Li and Qiao, 2019)	✓	✗	✓	✗
(Maki et al., 2011)	✓	✓	✗	✗
(Marie et al., 2009)	✓	✗	✓	✗
(Wang et al., 2018)	✗	✗	✓	✗
(Hinnenthal and Clauss, 2010)	✓	✗	✓	✗
(Yang et al., 2020)	✓	✗	✗	✗
(Gkerekos and Lazakis, 2020)	✓	✗	✗	✗
(Lin et al., 2013)	✓	✓	✗	✗
(Perakis and Papadakis, 1989)	✗	✗	✓	✗
(Papadakis and Perakis, 1990)	✗	✗	✓	✗
(Klompstra et al., 1992)	✓	✗	✗	✗

Table 2.1: Overview of the objective functions concerning weather routing used in literature

General costs and risks

The cost minimization expressed in the research of Chen (1978) encompasses the terminal and operating cost. The costs are based on the control vector, specifying the ship's heading and the power output, a generalized ship motion seakeeping constraint vector and the ship

coordinates for different times of arrival. Maki et al. (2011) is one of the few that includes risks more specifically parametric rolling¹ in the objective function.

Estimated time of arrival (ETA)

In most cases the fuel consumed over a route or the travel time are of interest. A common measure is the influence of the weather on the ETA. The ETA can be written as:

$$ETA = \frac{d}{SOG} \quad (2.10)$$

where

ETA = the estimated time of arrival

d = the total distance of the route sailed

SOG = the speed over ground

Due to waves and wind resistance, the STW reduces. This speed loss can be estimated by for instance Kwon's method or another technique (see section 2.2) and converted to the corresponding SOG. Consequently, if the total distance of the route is calculated, the ETA can be derived by formula 2.10. However, the STW or resulting SOG reduction can also be estimated by an ML technique similar to the approach by Shin et al. (2020) conform with the aforementioned formula.

Fuel oil consumption (FOC)

Apart from the ETA measure, several others rely on FOC as minimization objective. Again, a general measure can be set up used in most of the papers.

$$FOC = SFOC \cdot MCR\% \cdot P_{max} \cdot t_A \quad (2.11a)$$

$$SFOC = \frac{Fuel}{P_E} \quad (2.11b)$$

$$MCR\% = \frac{P_E}{MCR} \quad (2.11c)$$

where

$SFOC$ = the specific fuel oil consumption

MCR = the maximum capacity rate

¹Parametric rolling is a type of resonance between the wave frequency and the ship rolling motion (Park and Kim, 2015). The phenomenon occurs in a ship with a hull form that produces a large change in the restoring arm in waves due to their exaggerated bow flares and transom sterns. Once parametric rolling occurs, the maximum roll angle can reach 40° or more (Maki et al., 2011).

P_{max} the power output at 100% MCR

P_E = the delivered power

t_A = the travel time

In order to calculate the FOC, the specific fuel oil consumption (SFOC) of a vessel should be known. The SFOC is a measure of fuel efficiency of an engine in contrast to the power output (Zis et al., 2020). The fuel is also dependent upon the maximum capacity rate (MCR) which is said to be the maximum capacity or power a vessel's engine can handle. If the delivered power is expressed in relation to the MCR, this results in a dimensionless measure, MCR%. If the power output associated with a 100% MCR is known. In most cases, SFOC is expressed in kg/kWh and power is expressed in kW. As such, the resulting fuel consumption is determined per time unit and should be multiplied by the travel time to obtain the FOC of the total route sailed. The calculation of the travel time corresponds to the ETA formula 2.10 mentioned earlier. In all, formula 2.11a can be simplified as written here:

$$FOC = SFOC \cdot P_E \cdot t_A \quad (2.12)$$

Noticeable is that there are two possible ways in literature to calculate the FOC and indicate the influence of the weather conditions depending on whether the delivered power or SOG is kept constant.

In the first case, the FOC estimation depends on the sailing time function. Research of Bentin et al. (2016); Park and Kim (2015); Shao et al. (2012); Yang et al. (2020) for instance determine the power delivered in calm water as a relevant measure for the constant power output. Thereafter, the involuntary speed is derived by use of Kwon's method in the same way as described in section 2.3.1 for the ETA calculation. As the speed reduction is directly related to the travel time, only the t_A component expressed in formula 2.12 is affected. As a result, the FOC calculation merely comes down to an ETA minimization. The same reasoning applies when the RPM is kept at a constant rate as it directly relates to the power, seen in figure 2.3. A constant power also corresponds to a constant RPM which the research of Maki et al. (2011); Shin et al. (2020); Takashima et al. (2009) make use of to estimate the corresponding power according to the following formula (Shin et al., 2020).

$$Engine\ power = Engine\ Torque \cdot Engine\ RPM \quad (2.13)$$

Another way is to keep the SOG fixed and estimate the varying power output under different weather conditions. The power can be predicted by a machine learning technique, explained in section 2.2.3 or a physics model, explained in section 2.2.2. In the later case, the total ship resistance and the efficiency is determined based on Holtrop and Mennen (1982) methods. As such the corresponding power can be derived, according to formula 2.1. Some research that applied this approach are the one of Hinnenthal and Clauss (2010) and of Marie et al. (2009).

Multi-objectives

The weather routing models either incorporate single- or multi-objective optimization. Hinnenthal and Clauss (2010) combines both the influence of ETA as well as FOC on the routing algorithm. The goal is then to find a feasible design that is restricted by the Pareto frontier. The frontier corresponds to a set of solutions for which a single objective function cannot be further improved without deteriorating any other objective (Hinnenthal and Clauss, 2010; Marie et al., 2009).

2.3.2 Constraints

The voyage optimization models should imitate a realistic behaviour on the route to be sailed. Therefore, several constraints concerning the time of arrival, admissibility and safety are featured in literature. In that regard, table 2.2 show an overview of the constraints used and by whom. Papers mentioned before and used in this research that do not use any constraints are not included in the table below.

Paper	Time	Admissibility	Safety
(Chen, 1978)	✗	✓	✗
(Shao et al., 2012)	✓	✗	✓
(Avgouleas, 2008)	✗	✗	✓
(Park and Kim, 2015)	✗	✗	✓
(Marie et al., 2009)	✓	✗	✗
(Maki et al., 2011)	✗	✗	✓
Yang et al. (2020)	✓	✗	✓
Hinnenthal and Clauss (2010)	✓	✓	✓
Lin et al. (2013)	✓	✓	✓

Table 2.2: Overview of the constraints concerning weather routing in literature

Inadmissibility and time constraints

Chen (1978) for instance have incorporated in their multi-stage dynamic programming model constraints on inadmissible areas such as land mass, shallow water, navigation hazards etc.

A large portion of research also include time constraints. Time constraints are mostly expressed as an upper limit to the estimated time of arrival (ETA). The actual travel time (ATA) can for instance not deviate more than 30 minutes from the estimated arrival time (Marie et al., 2009) .

Safety constraints

As for the safety constraints, possible endangering phenomenons related to the ship motion are at point of interest in most papers. Shao et al. (2012) took into account safety constraints including surf-riding² and broaching-to³, instability due to high wave groups, synchronous rolling motion and parametric rolling motion. The limiting values are based on the IMO guidelines, shown in figure 2.5. Similarly, Park and Kim (2015) take into account the danger of surf-riding and parametric rolling. Again, the IMO safety guidelines were adopted.

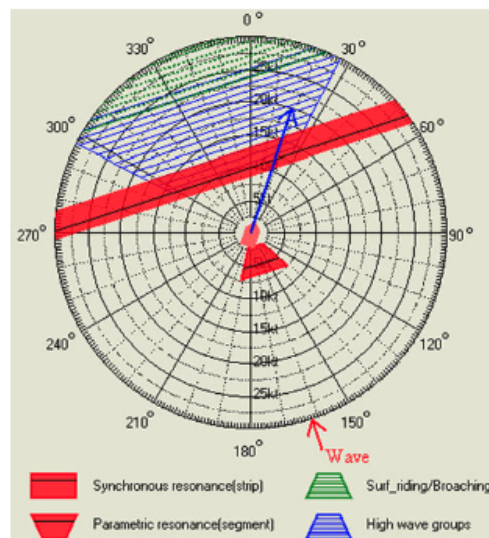


Figure 2.5: The safety constraints specified by the IMO guidelines (Shao et al., 2012)

Furthermore, the iterative dynamic programming model of Avgouleas (2008) incorporates deck wetness and slamming as safety constraints. Both phenomenons relate to the relative motion of any point on the ship. If the relative motion exceeds the freeboard⁴, deck wetness occurs. If the motion on the other hand exceeds the the draft and when the relative velocity exceeds a critical point, we are dealing with slamming. Apart from the last phenomenon, Hinnenthal and Clauss (2010) also considers constraints on the vertical and lateral accelerations, motion sickness and main engine operability. Moreover, research such as Yang et al. (2020) or Maki et al. (2011) include a maximum threshold on the STW or RPM respectively.

²The phenomenon that large following waves acting on the ship can force her to move with the same speed (Begovic et al., 2018).

³It is a phenomenon in which a ship cannot maintain a constant course despite the maximum steering effort being applied (Begovic et al., 2018).

⁴The height of a ship's side between the waterline and the deck (Avgouleas, 2008).

2.3.3 Geographical representation

An essential part of weather routing is the representation of the geographical area by coordinates to construct a feasible route. The route can either pass through waypoints along the great-circle, explained in section 2.3.3 or follow several grid points, explained in section 2.3.3. Table 2.3 indicate which papers have applied either a grid-based or waypoint solution.

Paper	Waypoints	Grid-based	Solution technique
(Delitala et al., 2010)	✓	✗	/
(Calvert et al., 1991)	✓	✗	2DDP
(Chen, 1978)	✓	✗	3DDP
(Shao et al., 2012)	✓	✗	3DDP
(Bijlsma, 1975)	✓	✗	Calculus of variations
(Haltiner et al., 1962)	✓	✗	Calculus of variations
(Avgouleas, 2008)	✓	✗	IDP
(Sen and Padhy, 2015)	✗	✓	Dijkstra
(Zhu et al., 2016)	✗	✓	Dijkstra
(Takashima et al., 2009)	✗	✓	Dijkstra
(Gkerekos and Lazakis, 2020)	✗	✓	Dijkstra
(Park and Kim, 2015)	✓	✗	A*
(Bentin et al., 2016)	✓	✗	A*
(Shin et al., 2020)	✗	✓	A*
(Kosmas and Vlachos, 2012)	✓	✗	SA
(Li and Qiao, 2019)	✓	✗	SA
(Maki et al., 2011)	✓	✗	RCGA
(Marie et al., 2009)	✗	✓	RCGA
(Wang et al., 2018)	✓	✗	MOGA
(Hinnenthal and Clauss, 2010)	✓	✗	MOGA
(Yang et al., 2020)	✓	✗	GA
(Lin et al., 2013)	✓	✗	3DMI
(Hagiwara, 1989)	✓	✗	Isochrone method
(Klompstra et al., 1992)	✓	✗	Isopone method

Table 2.3: Geographical representation of the construction of a route and corresponding solution technique: overview of research papers

Waypoint representation

In the first case, the shortest distance between the departure and destination point on the surface of the earth is drawn. This is called the great-circle route. This route is commonly considered as the reference course. However, when taking into account the weather conditions,

one can slightly differ from this course to avoid bad weather, but still maintain the shortest path. As a result, the great circle course can be divided up by several waypoints, also known as the ship's heading (Wang et al., 2020) .

The waypoint method is mainly used in dynamic programming and isochrone approaches in which each waypoint corresponds to a stage. The number of stages depends on the total distance of the route and the available computing capacity (Shao et al., 2012).

Figure 2.6 shows the correct representation of the waypoint method. The states of a stage which are applicable in the aforementioned approaches are time and geographical location. Time is not fixed for instance in 3D dynamic programming and progresses as well as the location. As such, the weather forecast will be different depending on the time travelled. Let the goal be to minimize the fuel, this is then the stage control variable. Based on the total distance from start to end point, the number of stages in which new decisions are made will be determined. In figure 2.6 11 stages with the grid locations being the states along the great circle. Per stage the state that minimizes the fuel consumption will be chosen.

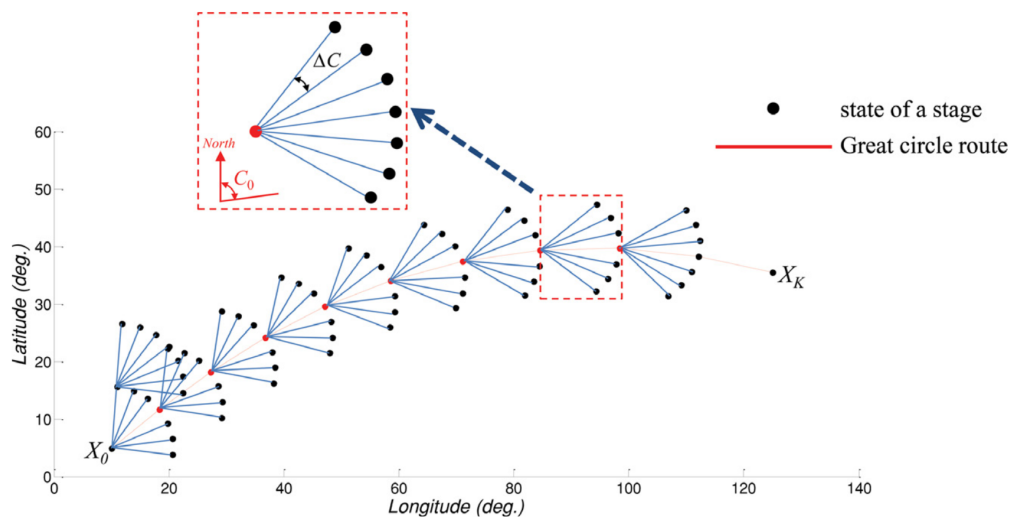


Figure 2.6: The waypoint representation according to Lin et al. (2013)

Grid-based representation

Apart from the waypoint representation, a grid-based representation is another commonly used approach to partition the geographical area. Sen and Padhy (2015) has discretized the geographical space into grids. The square grids are equal in terms of horizontal and vertical distance. The intersection of a latitude and longitude line are considered as a node. Any possible path the ship could traverse is composed of lines joining a node with its neighbouring nodes. The weights between path lines joining adjacent nodes are dependent on the objective function. An example of the grid-based representation is given in figure 2.7 (Sen and Padhy,

2015).

The aforementioned representation is known as equirectangular projection with constant latitude and longitude intervals. This is considered to be the base map. Whenever a place on the sphere is projected into a plane, distortion of the area, the angle, the direction, and the distance occurs forming dissimilar grids. Shin et al. (2020) transformed the base map into a conformal map by increasing the distance in y-direction by a scale factor based on the latitude. However, this results in numerous grids that should not be explored in the routing process. The authors therefore developed the concept of an adaptive grids for which efficient grouping is applied. Grids are grouped as the latitude and consequently the distortion increases (Shin et al., 2020).

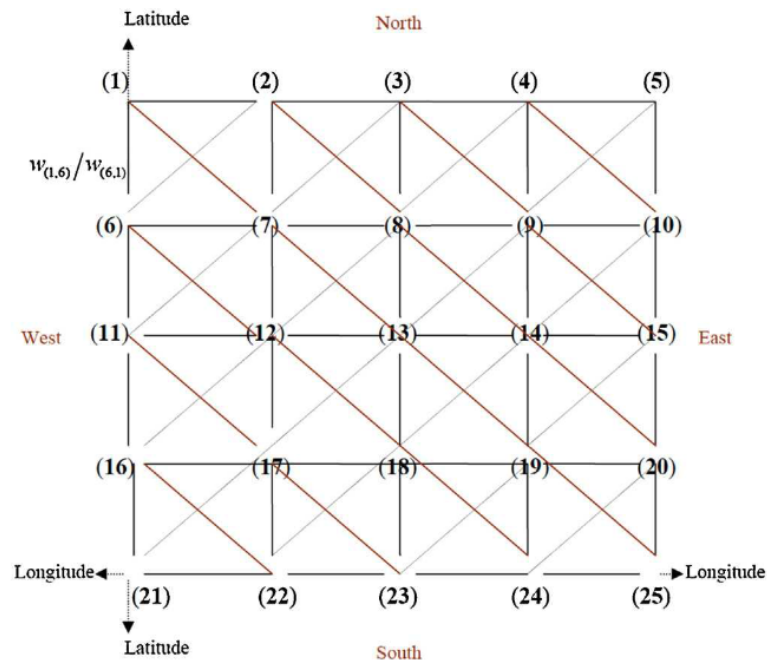


Figure 2.7: The grid-based representation according to Sen and Padhy (2015)

2.4 Weather forecasts

An accurate weather forecast is one of the inputs crucial to the prediction performed by the hydrodynamic models in route optimization. One of the main aspects is the weather forecast. However, the accuracy of the weather forecast and the influence on weather routing is out of the scope of this dissertation. Rather the distinction between static and dynamic weather grids is more important. Michalek and Balakrishnan (2009) makes a clear distinction between the two types. In case of static weather forecasts, no uncertainty intervals nor a measure of forecast accuracy is incorporated in the forecasts. Therefore, the weather forecasts do not change in time. To account for uncertainty, they developed a dynamic weather grid in which

a different time horizon for different aircraft positions are used (Michalek and Balakrishnan, 2009).

2.5 Solution techniques

A wide range of solution methods are present in finding the local or global best routes for ships. The weather routing models can be modeled as nonlinear continuous optimization problems or discrete optimization problems (Walther et al., 2016). In this section, the different solution techniques and their applications are explained.

2.5.1 Dynamic programming

Bellman (1952) introduced the theory of dynamic programming (DP) to the purpose of subdividing a given complex problem into sub-problems. Bellman's principle of optimality states that if a given decision at an initial stage is optimal, the following decisions will also be optimal.

Dynamic programming either uses a backward or forward recursive algorithm. The backward (forward) algorithm ensures the path to be optimal if and only if, for any intermediate stage, the choice for the following (previous) path is optimum for this stage (Shao et al., 2012).

Each stage is associated with a control vector in dynamic programming and represents a sub-problem. Information from a preceding stage serves as input for the determination of the control parameters of the next stage. The stage variables on the other hand should monotonically increase during a ship voyage for instance, fuel consumption, time or voyage progress. Within a stage, many states of the ship can be defined such as time and geographic location. In most cases, the states are represented by grid points.

Two-dimensional dynamic programming (2DDP)

The traditional two-dimensional dynamic programming models (2DDP) optimize the ship's heading while ship power or propeller speed rotation are kept constant. As such only the route is optimized. Calvert et al. (1991) tries to minimize for instance the fuel consumption through 2DDP. The stage variable is the voyage progress in this case, the control variable is the ship heading and the state is the position of the ship at each grid point.

Three-dimensional dynamic programming (3DDP)

The three-dimensional dynamic programming method is an extension of the 2DDP method, but besides the ship heading, the speed is also able to change in time and geographic position. In that regard, Chen (1978) developed a stochastic, dynamic minimum cost routing model performed on a Trans-Atlantic voyage using simulated data. The model is a multi-stage

decision problem in which the stage variable can either be the voyage time or a measure of voyage progress. The later takes on the form of incremental distances in the general direction of travel for instance the longitude. The focus lies on the voyage progress as state variable due to less computational effort. As a result, the state variables are the coordinates of a grid point on a predefined grid system and the time. The control variables on the other hand are the power output and the ship heading, mentioned in section 2.3.1 and are constant between two consecutive stages.

Similar to the model of Chen (1978), Shao et al. (2012) also express the power and the ship heading as control variables. The model however aims to minimize the fuel oil consumption and uses a forward algorithm instead of a backward approach. The grid points and consequently the headings are predefined. As a result, the power becomes the only control variable (Shao et al., 2012).

Calculus of variations

The approach, calculus of variations, in weather routing was first introduced by Haltiner et al. (1962) with the goal of minimizing the integral that represents the travel time between two ports. The resulting Euler differential equation can then be solved by a general relaxation technique consisting of an iterative approximation procedure. The procedure ends when the conversion indicates a minimum-time track that is sufficiently approximated. The model only takes into account the influence of the wave height and direction.

The extension of previous research is performed by Bijlsma (1975). Besides minimizing the time travelled, the fuel consumption is also kept to a minimum. The optimization problem is solved using wave charts and current data.

As Perakis and Papadakis (1989) explains calculus of variation is focused on deriving local optimality properties which are combined with global boundary conditions. The authors apply the methodology to a minimal time routing problem with time-dependency. Again, the dynamics of a vessel that travels in a 2-dimensional space are defined in minimizing the total transition time for a known visiting sequence. The control variables are therefore the power and the ship's heading. Intermediate locations represent the states and for each state the optimal departure time, depending on the speed, is determined with corresponding optimal power and heading. They proved that the power setting along the optimal trajectory always takes its upper permissible value (Perakis and Papadakis, 1989). A similar approach has been applied by Papadakis and Perakis (1990) for the minimal time routing problem within stationary and time-dependent seas. The weather factors that are taken into account are the wave direction and height.

Iterative dynamic programming (IDP)

The previous dynamic programming solutions require a fine grid to ensure convergence to a global optimum. The aforementioned problem is stated as the “the curse of dimensionality” as memory storage and computational time are considerably large. More precisely, for each stage, a complete grid of admissible states is necessary (Avgouleas, 2008).

This can be avoided by iterative dynamic programming (IDP) in which only a single grid point is used. The concept of IDP was introduced by Mekarapiruk and Luus (2000) to the purpose of increasing the odds of a global optimal solution. IDP can be used to solve optimization problems for which the state and control variables take on values from a set of real numbers. In that regard, Avgouleas (2008) developed an IDP algorithm that first makes an initial guess for the optimal control and within each iteration the control policy is improved based upon the previous one. Each iteration is similar to the general DP process and refines the granularity of the quantified allowable controls. The control variables are the speed and the ship heading and the state is the ship location on the sea surface in this case.

Isopone method

Adding another dimension of fuel to the two-dimensional plane of position and time of dynamic programming creates a three-dimensional plane of energyfronts or isopones. The isopones represent energyfronts of equal fuel consumption. The courses are again discretized along the great circle route. This method has been applied by Klompstra et al. (1992). The route is constructed in an iterative way by calculating the next isopone based on the previous one. The details of the mathematical implementation can be found in the research of Klompstra et al. (1992), but is less applied in practice opposed to the other methods explained.

2.5.2 Isochrone method

Another possible method is the isochrone method. In this method, lines associated with the same travel time and possible trajectories of the ship are derived. A set of connected points, starting from a given departure point, that a ship can traverse within a given time and going in all possible directions is said to be an isochrone. As such, the same transition time can be achieved, but the direction can be changed depending on the weather or the presence of an obstacle (Szlupczynska and Smierzchalski, 2007; Zis et al., 2020).

The isochrone method was first introduced by James (1957) and was further modified by Hagiwara (1989) among others in order to avoid the isochrone loops. A loop is caused by the non convexity of the speed characteristic for given weather data. More specifically, the area that can be crossed is partitioned when a new isochrone is generated when applying

the modified method of Hagiwara (1989). This approach can also handle narrow strait crossings. Others even include high traffic intensity areas as to avoid collision with other vessels (Szlupczynska and Smierzchalski, 2007).

Lin et al. (2013) propose a three-dimensional modified isochrone (3DMI) method. They have included a floating grid system of 3DMI's. The goal is to reach the destination while guarantying minimum fuel consumption and minimum passage time within an predefined ETA and taking constraints of safety and land avoidance into account. The main advantage is that the speed and wave heading angle varies with the geographic locations. In the same way as 3DDP method, the 3DMI method also includes stages and corresponding states. Here, the stage is the segment of a voyage route between two isochrones based on the calm-water speed assumption. A stage is comprised of potential geographical locations depending on weather and sea conditions, called the states. The control variables of each stage are the voyage progress and the fuel consumption or voyage time. In the research at hand, the fuel consumption is taken as control variable and the passage time the state of the stage.

2.5.3 Search tree algorithms

Dijkstra's algorithm

Dijkstra's algorithm is an approach that originally finds the shortest path of a problem when defined as a directed weighted graph. The graph consists of vertices, edges and weights/costs associated with the edges. The algorithm then detects the directed path with the smallest total weight. The weight is usually the distance, but in case of Sen and Padhy (2015) it represents the travel time. The travel time between two grid points is the distance divided by the reduced speed. The reduction in speed is influenced by the weather conditions or avoidance of dangerous obstacles (Walther et al., 2016).

In a similar way, Zhu et al. (2016) proposed an improved Dijkstra's algorithm. The focus lies on the storage and time reduction of the application of the algorithm.

In the research of Takashima et al. (2009), on the other hand, the fuel consumption is minimized by finding the minimum propeller revolution number for a specified voyage time. The resulting route is however a sub-optimal route.

A-star algorithm

An extension of Dijkstra's algorithm is the A-star algorithm. The goal of the algorithm is to faster calculate the optimal path by not considering existing, expensive paths. The time and space complexity can be considerably improved. The algorithm incorporates a heuristic function, $h(n)$. If the heuristic function is equal to zero, it decays into Dijkstra's algorithm. A-star selects a path that minimizes the evaluation function, $f(n) = g(n) + h(n)$. The heuristic

function, $h(n)$, estimates the cost from n to the goal and $g(n)$ represents the real cost so far to reach n . As such, the evaluation function, $f(n)$, then estimates the cost of the path that moves along n to reach the goal (Park and Kim, 2015; Shin et al., 2020).

To obtain an optimal global path, it is necessary for the heuristic function to be admissible. An admissible heuristic function is less than or equal to the real cost from a node to the destination. The algorithm also employs two sets of nodes: a closed set and an open set. The closed set encompasses all the nodes that already have been searched and the open set are nodes that still need to be searched. The algorithm is terminated if the open set is empty (Park and Kim, 2015; Shin et al., 2020).

Park and Kim (2015) apply the A-star algorithm in the first phase of the two-phase approach to find the optimal ship route while minimizing the fuel consumption. The evaluation function accounts for the speed reduction caused by the ocean environment through additional fuel consumption. Based on the resulting optimal route, the speed schedule is determined in the next phase by use of geometric programming.

Besides a two-phase approach, A-star can be applied on its own to minimize the ship propulsion energy along a path, done by Bentin et al. (2016). The path is constructed via waypoints. The energy of a route is the required energy from departure to waypoint x in addition to the estimated energy from x to the destination. Each time a follow-up waypoint is selected, the one is chosen with the lowest route energy and a set of neighbourhood waypoints is generated. The set of neighbourhood solutions is determined based on the predefined speed, travel time and the ship heading. When the selected waypoint equals the destination, the A-star algorithm ends. The procedure is shown in figure 2.8. As seen, the method opens up a sort of search tree that expands with new waypoints.

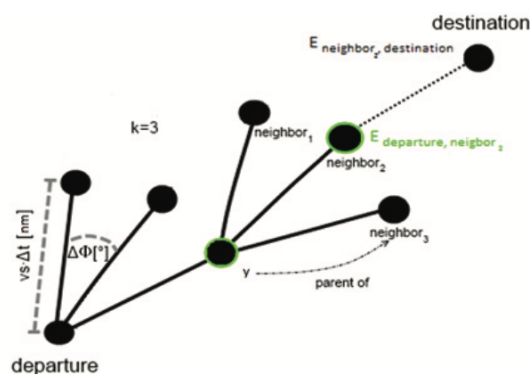


Figure 2.8: A-star procedure by use of way-points (Bentin et al., 2016)

Recently, Shin et al. (2020) have developed an improved A-star algorithm. The newly improved algorithm makes use of an adaptive grid and a low-cost heuristic to further decrease

the computational effort. The grid allows a 16-way search instead of an 8-way which renders a smoother route. This means that other adjacent grid points are also considered in addition to the grid cells in the direction of 45° as well as 26.6° presented in figure 2.9.

In addition to this method, an adaptive grid system was applied. In most cases, a equirectangular projection is used. It is a projection for a base map that forms a grid as meridional intervals of constant spacing and constant intervals of parallels. This projection is however distorted along the latitude as such the grids become disparate. This merely means that close to the polar region as the distance between meridians is narrower, resolution should be finer. As such, a larger number of grids is required and thus also a larger computational effort. An adaptive grid overcomes this problem by grouping grids together closer to the polar region to avoid exploring all grids.

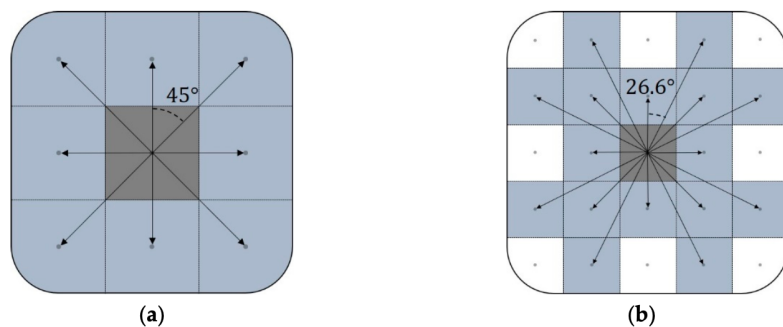


Figure 2.9: 8-way versus 16-way search in a grid (Shin et al., 2020)

Besides the adaptive grid, Shin et al. (2020) developed a low-cost heuristic method. The model tries to minimize the estimated time of arrival (ETA). In general the ETA is the distance divided by the speed over ground (SOG). For the real cost between two grid points, SOG values are predicted with machine learning models. The distance used is the haversine distance which is also used for the heuristic function. As for speed used in the heuristic function, the 99 percentile values for the SOG are used ensuring the function to be admissible. It turns out that the 16-way, adaptive grid renders more-economical paths in terms of ETA, distance and searched nodes.

2.5.4 Evolutionary algorithms

Simulated annealing (SA)

As the weather routing problem is a large scale optimization problem, this can preferably be handled by a (meta) heuristic such as simulated annealing. The heuristic is based on the method of cooling heated metal down. The metal structure is frozen when a minimal energy level is reached. In this case, the energy function is the objective function of the optimization problem.

Li and Qiao (2019) have applied the SA algorithm to optimize the route for wind-assisted ships. Both the fuel consumption as well as the voyage time are minimized. The route is constructed based on the principle of waypoints. The route between the departure and the destination point is broken up into a sequence of waypoints and these points are taken as variables in the optimization. A new route is generated by adjusting the waypoints and evaluating the new route based on the ocean wind and optimization criteria. The initial temperature has been set to 200, the end temperature to 10, The plateau length to 5000 and the reduction factor equal to 0.5. They concluded that in terms of voyage time and fuel reduction the SA algorithm performs well compared to the great circle route. The fuel consumption as optimization criteria is separately evaluated from the limited voyage time criteria. As such these are two single-objective optimizations.

Kosmas and Vlachos (2012), on the other hand, executed a multi-objective SA optimization in which a weighted combination of the voyage time and safety of the voyage are minimized. Similar to Li and Qiao (2019), the initial route is subdivided in parts based on the weather forecasts and waypoints are generated. The newly generated algorithm however sets up an initial solution that takes into account bypassing obstacles. The initial route is the line connecting the start and end point. However, in case of an obstacle, two initial routes are generated which both avoid the obstacle from a different side. As such, for n obstacles, 2^n routes are constructed and are all considered by the algorithm. Subsequently, the number of waypoints is chosen. The space interval L_d according to Kosmas and Vlachos (2012) should be close to $L_d = u * T_d$ with u the speed of the ship and T_d the drift of the environmental data in time interval. An advantageous implementation was obtained by considering different initial routes that are parallel or anti-parallel to the direction of the wave field. The application of the SA has been compared to a GA application concluding that the difference among them is not significant.

Genetic algorithm (GA)

A commonly used meta-heuristic to solve the weather routing problem is a genetic algorithm. The algorithm is based on natural selection in which only the fittest individuals are selected to reproduce offspring for the new generation. An individual is represented by a chromosome that consists of genes which are either 0 or 1. There are 5 phases in the algorithm: initial population, fitness function, selection, crossover and mutation (Mallawaarachchi, 2017).

Opposed to simulated annealing, GA generates multiple feasible initial solutions forming the initial population. Each individual in the population receives a fitness score based upon the fitness function. The fitness score determines the probability of the individual to be selected for reproduction. This is considered the selection phase. As such, two pairs of individuals, parents, with a high fitness score are matched. Thereafter, crossover is applied to the chosen

parents. A crossover point is selected at random for both parents and offspring is generated by switching the tails with a certain probability. The last step is mutation. Each gene is then altered with a certain probability to ensure diversity in the population. The algorithm terminates when the solution converges (Mallawaarachchi, 2017).

Different forms of GA as well as different operators are present in literature. For instance, Maki et al. (2011) applied a real-coded genetic algorithm (RCGA) in which the fitness function is a combination of the fuel consumption and the safety for ship routing. The main safety goal is to avoid parametric rolling. At certain angles, the ship is pushed to the other side and may cause damage to the cargo and a risky environment for the crew. Maki et al. (2011) proposed three different objective functions with different weights between safety and fuel. A real-coded genetic algorithm does not generate a bit-string to represent a solution, instead real-valued vectors are generated. For the selection phase, the algorithm relies on the just generation gap (JGG) selection model which is combined with a multi-parental crossover, *REX^{star}*.

An application of the RCGA was also performed by Wang et al. (2018) with a focus on developing a fast and efficient algorithm. The initial routes that are generated both entail the latitude and the longitude information. The paper applies three selection methods: roulette wheel selection, stochastic universal selection and tournament selection. As for the crossover method, an arithmetic operation is used to deal with the real-valued chromosomes. Moreover, a hybrid mutation method combining uniform and Gaussian mutations. Besides the essential operations, Wang et al. (2018) also incorporates a reinsert operation and migration operation. As a result, a percentage of the offspring population is inserted in the parent population according to their fitness. As for the migration operation, individuals between each subpopulation of every generation are exchanged. In that way, individuals with a high fitness can be passed over to another subpopulation to ensure spread of good individuals among populations.

Besides Maki et al. (2011), Marie et al. (2009) also optimized a multi-objective ship voyage problem for which the fuel consumption as well as the travel time are minimized using a multi-objective genetic algorithm (MOGA). They developed a new automatic meshing method. It is a way of gridding taking into account the sea-beds geography, the time dependant meteorological data and the characteristics of the vessel.

The optimization method explained by Hinnenthal and Clauss (2010) is able to find the pareto optimum routes unless the weather worsens. In that case, a minimum cost route that reaches the destination on schedule is not easily found. In these cases, the optimum becomes a trade-off between additional fuel consumption due to a longer course or fuel saving by reducing the additional resistance due to waves by avoiding strong wave fields (Hinnenthal and Clauss, 2010).

2.6 Robustness

Robustness is a concept vaguely described in literature. It is briefly mentioned in the research of Michalek and Balakrishnan (2009) which focuses on air traffic. Robust routes are here defined as routes that are not impacted by the inaccuracies of the weather forecasts. They developed an approach that classifies weather features that are highly correlated with route blockage.

Thus, robustness is more or less an answer to any kind of accuracy involving routing. If for instance the ship performance models are more accurate, a more reliable route optimization could be achieved. However, this definition remains wide in order to have some room to deviate from it.

Part II

Experimental Setup

Chapter 3

The fuel oil consumption models

3.1 Introduction

In finding the most efficient route, the goal in this research is to reduce the total fuel oil consumption (FOC) across that route. In doing so, the power should be accurately estimated taking into account the ship hydrodynamics and the weather at a certain location and time for a constant GPS speed or also called, speed over ground (SOG). As a result, the FOC can be derived according to formula 2.12. As such, the focus in this chapter lies on the variable power prediction due to environmental factors.

Four models are described that have either been used for decades or are newly developed by Toqua to ensure high accuracy in prediction power. The models are the sea trial curves with and without correction factor, the original machine learning (ML) model of Toqua and Toqua's physics-informed ML model. Even though the main service of Toqua is to promote and commercialise the latter model, the other three models were also implemented by the data science engineers for the purpose of experimental research.

3.2 The state-of-art models

The state-of-art models are the sea trial curves with and without correction factor which were already explained in sections 2.2.1 and 2.2.2 and have been widely used in the industry up to this point.

3.2.1 The sea trial curves

For the sea trial curves, the ballast and laden power are tracked for a predefined speed through water (STW) ranging from 0 to 19 knots (kn). As the SOG is always kept constant, the associated STW can be determined taking into account the current speed and direction. The dependence between SOG and STW is expressed in formula 3.1, specified by the experts

at Toqua. Other weather or ship specific parameters are not taken into account by the sea trial curves. In this way, a simple speed-power curve can be derived. The formula is based on the expertise of Toqua.

$$STW = SOG + v_{current} \cdot \cos(\phi_{heading} - \phi_{current}) \quad (3.1)$$

where

STW = the speed through water [kn]

SOG = the speed over ground [kn]

$v_{current}$ = the current speed [kn]

$\phi_{current}$ = the current direction [°]

$\phi_{heading}$ = the direction in which the heading of the vessel is pointed at [°]

3.2.2 The sea trial curves with correction factor

The implementation of the sea trial curves with a correction factor adjusts the obtained power output, resulting from the previous section, for the influence of wind and waves by either Kwon's or Kreitner's method.(see section 2.2.1) Only the latter method has been applied in this research and the values specified for the formulas stem from the ISO 15016 guidelines.(see section 2.2.2). The input parameters that the model takes into account are the current direction and speed, the draft, the heading, the SOG, the wave direction, the wave height, the wind speed and wind direction. This is a fraction of what the Toqua models use as input parameters (see table 3.1).

3.3 The machine learning models of Toqua

As the environmental pressure and awareness increases, the aforementioned models are not sufficient to accurately predict the main engine power. The impact of certain measures and solutions such as maintenance, retrofits, speed optimization and optimal routing should be quantified in a correct way. This is where the ML models of Toqua come into play.

3.3.1 The original ML model

The original machine learning model of Toqua is a neural network that accurately predicts ship hydrodynamic relations as seen in figure 2.2. The model can be categorized under predictive modelling by ANNs as explained in section 2.2.3 in order to estimate either the engine power or STW. The model however also successfully attempts to predict other relations such as predicting the RPM starting from a constant speed or the RPM to power relation. In this research, the focus lies on predicting the engine power for a constant SOG.

The power-speed relation of a ship is essential for the analysis of the current problem. In essence, the engine of a ship consumes fuel which results in a certain power output. The power in turn drives the propeller of the ship causing it to spin at a certain rounds per minute (RPM). As such, the ship can move forward at a speed through water (STW). (Morobé and Van den Poel, 2020)

In most cases, the relationship between speed and power is approximated by the speed-power curve and the RPM step is neglected. However, the interplay between speed, power and RPM is crucial. As such, this interplay is handled by the predictions of Toqua. It is the first approach that can predict the speed through water (STW) or the power of a ship in an unfouled condition with a very high accuracy. As a consequence, the power a ship should exert can be predicted at a specific point in time at any geographical nautical location. (Morobé and Van den Poel, 2020)

3.3.2 The physics-informed ML model

The physics-informed ML model of Toqua is similar to the original ML model and requires the same input parameters. The model however is also embedded with physics inherent to the voyage of a ship. For instance, the power required is lower if the wind comes from behind the ship and the ship is heading forward as the wind already pushes the ship partially forward.

3.3.3 The input parameters

The input parameters necessary to run both ML models of Toqua are ship specific parameters, weather parameters and voyage parameters.

The draft and the trim of a ship are ship specific. Depending on the ship that the model is trained for, the trim and draft will vary between 8 and 22 m and -8 and 3 m respectively. The weather parameters can be extracted for each spatial data point through the StormGlass API or can be manually set to fixed or random values, depending on the experiments to be performed. The weather parameters are the wave height, the sea surface temperature, the wind speed, the wave and wind direction, the current speed and current direction. The sea salt salinity is also of importance but cannot be retrieved from the API and should therefore be set to an average value between 30 and 40 practical salinity units (PSU) for the waters to be traversed.

The voyage parameters to be considered are the ship heading and the rudder angle, both expressed in degrees. The rudder angle can vary between -10° and 10° and the ship heading changes according to the course travelled which can vary between 0° and 360° .

The ML model calculates for each spatial coordinate the level of power at which it should operate to navigate at a constant speed. The SOG speed can take on values between 5 and 20

knots [kn]. One knot is equal to 1.852 km/h. The input parameters and their corresponding value range are summarised in table 3.1.

Parameter	Range	Unit
SOG	[5,20]	[kn]
Draft	Fixed	[m]
Trim	Fixed	[m]
Wave height	[0,7.5]	[m]
Sea surface salinity	[30,40]	[PSU]
Wind speed	[0,20.7]	[m/s]
Sea surface temperature	[15,34]	[°CC]
Wind direction	[0,360]	[°]
Wave direction	[0,360]	[°]
Current speed	[0,2]	[m/s]
Current direction	[0,360]	[°]
Ship heading	[0,360]	[°]
Rudder angle	[-10,10]	[°]
Speed over ground	fixed	[kn]

Table 3.1: The input parameters and their corresponding value range of Toqua’s ML models

3.4 Accuracy of the models

Toqua performed experimental research concerning the accuracy of the four models. Toqua has developed a new approach based on physics-informed machine learning, called ‘ship kernels’ and shows that it outperforms the other approaches in terms of accuracy while keeping it highly practical.

In calculating the accuracy, they used the mean absolute percentage error (MAPE) and used the ship’s sensor data as the true value opposed to the estimated value of the models at hand. In essence, the smaller the MAPE, the more accurate the model. The formula of the MAPE is given by equation (3.2).

$$MAPE = \frac{1}{n} \sum_{i=1}^n \left| \frac{y_i - \hat{y}_i}{y_i} \right| \quad (3.2)$$

where y_i is the actual value of the power and \hat{y}_i is the estimated value of the power. They did the test for the sea trial curve with and without correction factor, the physics-informed ML model based on sensor data and the ML model based on noon report data. In using the sea trial curve, the MAPE is 22.2%. Adding a correction factor lowers the MAPE

to 14.3%. The physics-informed model is highly accurate for which the MAPE comes down to 6.7%. The pure ML model has a similar accuracy as the PI-ML model. However, the data imputed in the model is quite noisy and taking into account the physics relations is essential for realistic power predictions. Unrealistic dependencies between parameters are in this way neglected. That is why the physics-informed model is more favourable in terms of accurate power predictions (Colle and Morobé, 2022).

Chapter 4

The weather routing model

4.1 The introduction

In this section, the weather routing model is presented. As mentioned in the literature study, the focus of the weather routing model can be diverse. The model can focus on minimizing the travel time, the fuel oil consumption (FOC) or the risks. As Toqua mainly strives for environmental purposes, the minimization of the FOC will be the main goal of the routing model.

The methods in order to obtain an optimal path subject to weather conditions such as A-star and simulated annealing (SA) will also be described in this chapter.

4.2 The model formulation

Parameters

The following parameters are part of the mathematical model. Index i and j refer to the collection of geographical coordinates on the map that could possibly be traversed and range from 1 to n , where n is the total number of coordinates. The specific fuel oil consumption (SFOC) parameter is set to 170 g/kWh for the ship from which the sensor data is provided by Toqua for the purpose of this experimental research.

d_{ij}	the distance between coordinates i and j
s_{ij}	the SOG between coordinates i and j
t_{ij}	the travel time between coordinates i and j
p_i	the main engine power traversing coordinate i
p_{ij}^{avg}	the average power between coordinates i and j
FOC_{ij}	the fuel oil consumption travelling from coordinate i to j
$SFOC$	the specific fuel oil consumption

Decision variables

The goal of a weather routing model is to determine which geographical points should preferably be part of the final path. The decision variable is expressed in the following way.

$$x_{ij} \quad 1 \text{ if coordinates } i \text{ and } j \text{ are part of the final path, } 0 \text{ otherwise}$$

Mathematical formulation

The objective of the weather routing model focuses on minimizing the fuel oil consumption which is based on formula 2.12 described in section 2.3.1.

$$\min \sum_{i=1}^n \sum_{j=1}^n FOC_{ij} \cdot x_{ij} \quad (4.1)$$

$$s.t. \quad x_{ij} \in \{0, 1\} \quad (4.2)$$

The calculation FOC_{ij} in objective function 4.1 is based upon the previously mentioned formula. As such, the FOC between two points is the average power multiplied by the SFOC of the ship and the travel time between these two points. The travel time t_{ij} is equal to the distance d_{ij} divided by the speed s_{ij} . Furthermore, the average power p_{ij}^{avg} is the average between the power to transverse both coordinates. As such, p_{ij}^{avg} is equal to $\frac{p_i + p_j}{2}$. To recap, the calculation of the FOC is expressed in the below formula.

$$FOC_{ij} = SFOC_{ij} \cdot p_{ij}^{avg} \cdot t_{ij} \quad (4.3)$$

Assumptions

Important to mention is that for the calculation of the distance d_{ij} , the Haversine distance is used. It is an accurate way to compute the distance between two points on the surface of a sphere using the longitude, latitude and the radius of the earth R ($= 6371$ km). The haversine distance is calculated according to equations 4.4 (Kettle, 2022).

$$d = R \cdot c \quad (4.4a)$$

$$c = 2 \cdot \arctan\left(\frac{\sqrt{a}}{\sqrt{1-a}}\right) \quad (4.4b)$$

$$a = \sin^2((\phi_B - \phi_A)/2) + \cos(\phi_A) \cdot \cos(\phi_B) \cdot \sin^2((\lambda_B - \lambda_A)/2) \quad (4.4c)$$

where

d = the haversine distance

ϕ_A = the latitude of point A

ϕ_B = the latitude of point B

λ_A = the longitude of point A

λ_B = the longitude of point B

R = the radius of the earth

For the research at hand, the weather conditions do not change in time for the coordinates. This means that the weather conditions are static and weather differs for one coordinate upon another coordinate in geographical sense but not in time.

4.3 The weather routing algorithms

In order to construct the optimal path, the cost objective should be evaluated in a correct and fast way. This can be attained by a suitable weather routing algorithm which can be either a search method, A-star or a meta-heuristic, simulated annealing (SA). The main difference between A-star and SA is that the latter is suitable for large-scale problems in terms of CPU time, but does not guarantee the optimal solution. A-star always ensures an optimal route in case of static weather data and is solved within a reasonable time frame if the geographical area is not too large.

4.3.1 The A-star algorithm

Algorithm 1 that stems from Shin et al. (2020), clearly shows how the A-star algorithm works. A graph G has V nodes and E edges and for each of the nodes the real cost for a path from the source node to the current node is initialized with $g(\text{node}) = \infty$. For the source node s , set $g(s)$ equal to 0 and $f(s) = g(s) + \text{heuristic}(s)$ and put s into the queue with corresponding value $f(s)$. Thereafter, node u with the minimum value in the queue is extracted and the edge-relaxation for u based on g , putting newly visited nodes into the queue is executed. The last two steps should be repeated until the target node is reached. (Shin et al., 2020)

Algorithm 1 A-star algorithm

```

1: function A*(G(V, E), W, s, t)
2:   for all  $u \in V \setminus \{s\}$  do
3:      $g[v] := \infty, pred[v] := nil$ 
4:      $g[s] := HEURISTIC(s, t)$  ▷ Heuristic function
5:      $Queue \leftarrow \{s\}, S \leftarrow \emptyset$ 
6:     while  $Queue \neq \emptyset$  do
7:        $u := ExtractMin_d(Queue)$ 
8:        $S \xleftarrow{Update} S \cup \{u\}$ 
9:       if  $u=t$  then
10:        return  $g, MAKEPATH(t, pred)$  ▷ Tracking backward
11:        for all  $e \in e_{u,v} \in E \mid u \in V, v \in adjacent[u]$  do ▷ Edge relaxation
12:          if  $g[v] > g[u] + W(e)$  then ▷  $W(e)$  is the weight of edge  $e$ 
13:             $g[v] \xleftarrow{Update} g[u] + W(e) + HEURISTIC(v, t)$ 
14:             $pred[v] \xleftarrow{Update} u$ 
15:             $Queue \xleftarrow{Update} Queue \cup \{u\}$ 
16:        return  $\emptyset$ 

```

The heuristic function

An important part of the A-star algorithm is the heuristic function which distinguishes A-star from Dijkstra's algorithm. The function should be admissible in order for the algorithm to be feasible and diminish the running time. Referring back to algorithm 1, this means that $h(x) \leq g(y) + h(x, y)$ for every edge (x,y) of the graph.

A main driver of the FOC calculation is the power prediction between two points. The ballast power according to the sea trial curves will always be smaller than any other kind of power prediction and is constant for a predefined STW. Opposed to the laden power, the ballast power is the power whenever the ship does not carry any cargo. As a result, the corresponding FOC for a ballast voyage will also be smaller than a laden voyage.

For the models used in the experiments, the power is smaller as the sea trial curves' estimations make use of the laden power rather than the ballast power. The physics models as well as the ML models intent for a certain correction due to environmental factors which in a sense adds a power difference to the ballast power.

4.3.2 The SA algorithm

The simulated annealing (SA) algorithm is displayed as algorithm 2 and the stems from the research of Rere et al. (2015). The pseudocode has been adjusted according to the current

research and can be explained as follows.

SA begins by generating an initial random solution x_0 of the problem and deriving the associated cost $f(x_0)$. A starting temperature T_{start} is defined, which will be lowered each iteration. Moreover, the Boltzmann constant k is defined, the plateau length N , the cooling function F and the plateau increment β .

Thereafter, the current solution is compared to one of the neighbourhood solutions in its neighbourhood space. A neighbourhood solution $x_0 + \Delta x$ is selected at random and if the associated cost $f(x_0 + \Delta x)$ is smaller than the cost of the current solution $f(x_0)$, the current solution is replaced by the neighbourhood solution. If however the cost is larger, then the neighbourhood solution is accepted with a certain probability, namely $e^{(current\ cost - neighbour\ cost)/kT}$. This procedure is repeated for a number of times N which is referred to as the plateau length. The plateau length can remain fixed for each run or can increase with a factor β .

Moreover, the cost minimization should be embedded in the algorithm as well and can be achieved by continuing the procedure of replacing the current solution by a solution with a lower cost as long as the temperature T has not reached the end temperature T_{end} . The temperature is decreased according to the cooling scheme.

The elements necessary to run the simulated annealing algorithm should be set to an optimal value and should therefore be determined experimentally. This will be explained in section 4.3.2.

Algorithm 2 The simulated annealing algorithm

```
1: function SA( $x_0, T_0, k, N, \beta, F$ )
2:   Generate an initial solution  $x_0$ , set the initial temperature  $T_{start}$ ,
3:   Boltzmann's constant  $k$ , plateau length  $N$ , cooling function  $F$  and
4:   plateau increment  $\beta$ 
5:   while  $T > T_{end}$  and stopping criteria is not met do
6:     for  $N$  do select a new solution:  $x_0 + \Delta x$ 
7:       if  $f(x_0 + \Delta x) > f(x_0)$  then
8:          $f_{new} = f(x_0 + \Delta x); x_0 = x_0 + \Delta x$ 
9:       else
10:         $\Delta f = f(x_0 + \Delta x) - f(x_0)$ 
11:        random  $r(0, 1)$ 
12:        if  $r > \exp(-\Delta f/kT)$  then
13:           $f_{new} = f(x_0 + \Delta x), x_0 = x_0 + \Delta x$ 
14:        else
15:           $f_{new} = f(x_0)$ 
16:         $f = f_{new}$ 
17:         $T = F(T)$  ▷ Cooling function
18:         $N = \beta \cdot N$ 
```

Chapter 5

The simulated annealing heuristic

5.1 Introduction

The simulated annealing algorithm has been briefly touched upon in chapter 4, more specifically in section 4.3.2. The description concerning the model formulation 4.2 is applicable here. Therefore, a route is constructed based on minimal fuel consumed. This entails that the power should be predicted by one of the FOC models, explained in chapter 3.

Unlike A-star, the algorithm requires some parameter tuning in order for the algorithm to work optimally and converge. In this chapter, experiments are performed in order to find the most suitable conditions and evaluate if the resulting SA is a better fit than A-star for the follow-up research surrounding weather routing. The parameters that should be tuned are the initial solution, the neighbourhood solution, the stop condition, the starting temperature, the temperature decrement and the plateau increment.

5.2 Scope of the problem

5.2.1 The models

Not all FOC models are considered in this chapter, only the original ML model is used for the prediction of the power and fine tuning of the SA algorithm. As the ML model and physics-informed ML model make use of even more parameters than the sea trial curve with or without correction, these are considered the most challenging models in prediction. The ML and physics-informed ML model are quite similar in use to one another and only differ in parameter tuning and constraints. However, as this is a black box for the user, neither for the implementation nor the prediction it will make a difference and will not influence the parameter tuning of the SA algorithm.

It is therefore fair to assume that testing the SA algorithm with only the ML model as FOC model will suffice.

5.2.2 The use case

The specific use case of weather routing applied in this dissertation concerns a route that should be constructed via the North Sea. The start point is the port of Edinburgh in England and the end point is the port of Bergen, located in Norway. The goal is to go from the start to end point consuming a minimal amount of fuel while keeping the speed at a constant pace and taking into account the weather conditions. The fuel consumption from point to point is calculated based on the power output per coordinate of the ML model.

Geographical area

The grid representation is used to divide the geographical area into smaller grid points. For the spatial coordinates, the North Sea is partitioned into equal rectangles of the same height and width. Three types of grids have been constructed, a large, medium and small grid with sizes 277.5 km by 277.5 km , 111 km by 111 km and 55.5 km by 55.5 km respectively. For each rectangle in the grid, the centroid is used as the coordinate for the weather routing data and could therefore possibly be included in the optimal path. The centroids will be referred as grid points or grid cells in the upcoming experiments.

The grids are represented in figure 5.1. Note that only the grids that overlap with the North sea and do not include land are extracted. In further experiments, the large grid size is often referred as ‘L’, the medium grid size as ‘M’ and the small grid size as ‘S’.

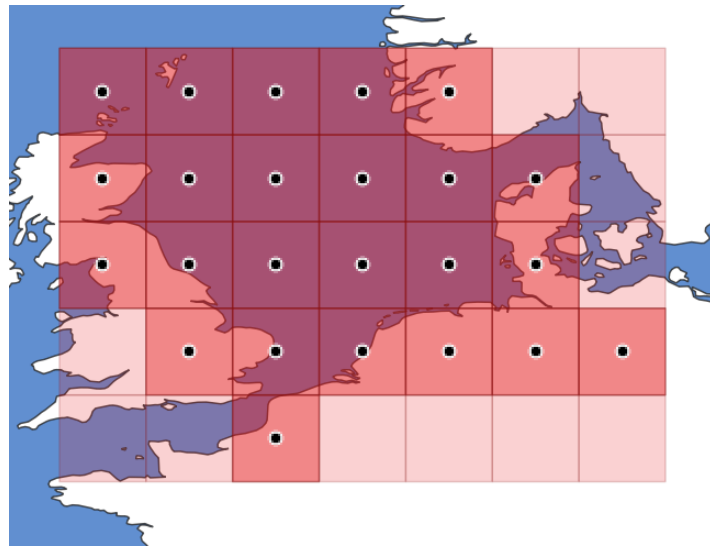
Weather conditions

For each of these coordinates in the grids, weather data is retrieved for 2 points in time. The first instance is said to be from 01/07/2021 00:00:00 and the second instance is 01/11/2021 00:00:00. As such, the solution can be compared for different weather conditions. The data set with the first instances is called data set 1 and the data set with the second time instances is called data set 2. Notice, that the conditions are retrieved for one time instance and not for example over a period of several days. The conditions do not change from time to time and are thus assumed to be static.

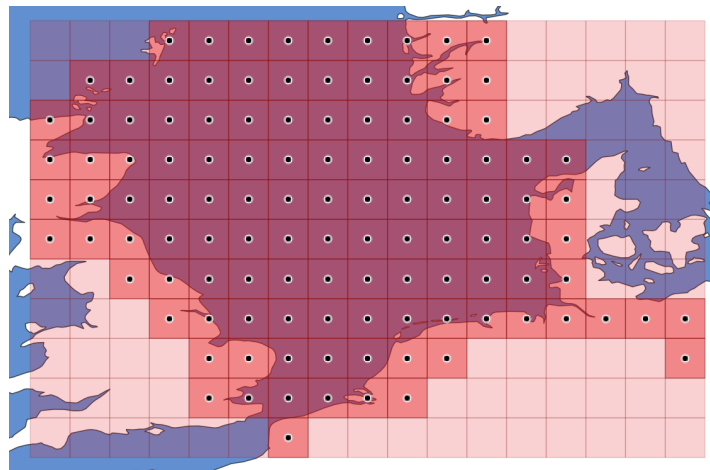
5.2.3 The constraints

Already a lot has been taken into account in the objective function of the design. The fuel consumption calculations are based on an accurate power, weather circumstance, distance etc. Therefore, spatial grid points with disadvantageous conditions such as storms will be avoided as they increase the power usage and therefore also the fuel consumption.

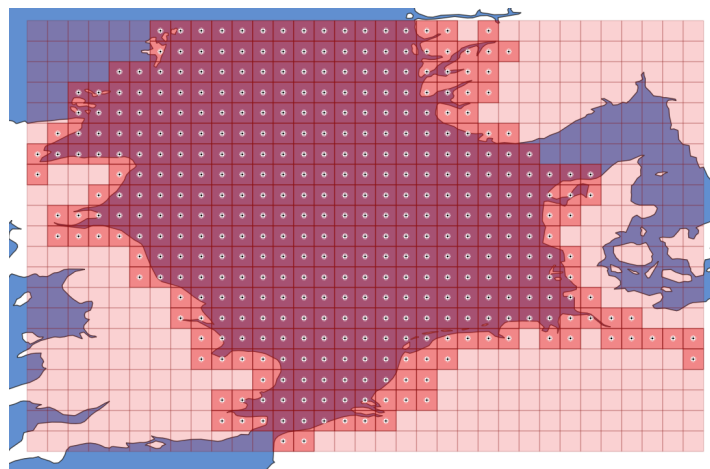
Opposed to the obstacles, the condition of a connected path by neighbouring grid points are not encompassed in the objective function. Therefore, it can be added as a soft constraint.



(a) The large grid and extracted grid of 277.5 km by 277.5 km with centroids



(b) The medium grid and extracted grid of 111 km by 111 km with centroids



(c) The small grid and extracted grid of 55.5 km by 55.5 km with centroids

Figure 5.1: The representation of different grid sizes

This can be done by adding a penalty to the objective function each time this condition is exceeded. For instance, if a path is of size 5 and the first 2 grid points are not adjacent and the last two grid points are not adjacent, a value of $2 \cdot \textit{penalty}$ is added to the total fuel consumption of the path.

The total travel time should be in accordance to the imposed arrival time. However, for simplicity reasons, this constraint is not added.

5.3 Parameters

5.3.1 Initial solution

Several initial solutions can be generated. One can opt for a random solution or rather a more specified solution. Both forms will have an impact on the running time and performance of the heuristic.

Method 1

The first method is to initialize the solution with only the start and end point included.

Method 2

Another possible initial solution could be that we start with an already near optimal solution. For instance, the result of the breath-first search algorithm for the shortest path problem. The initial solution in this case only takes the distance into account instead of the fuel consumption. In this way, a shorter initial solution can be generated.

5.3.2 Neighbourhood spaces

The hybrid neighbourhood solution used here looks at the adjacent nodes and takes four operators into account, insertion, delete, swap and replace.

One of the operators is chosen with equal probability when generating a neighbourhood solution. If two nodes are to be swapped, one must check if both nodes are adjacent nodes of one another in the grid in order to construct a connected route. The current solution should be augmented little by little that is why nodes that are next to one another in the current string can only be swapped.

If a node is deleted at a certain index, the node that originally followed up on the deleted node should be an adjacent node of the node that came before the deleted node. If this is not the case, the node is replaced by a node neighbouring the previous node.

In case of insertion, a node is added at a certain path index keeping into account that it is an adjacent node of the node prior to the added node.

The last operation is the replacement of a node. Again, it should be neighbour of the node before the node that will be replaced.

The neighbourhood algorithm also checks when adding or replacing a node that the node is not already in the current solution.

5.4 Analysis and optimization of parameters

Different values of the parameters of the SA algorithm will influence the performance of the meta heuristic. That is why the parameters that need to be determined are varied while others remain fixed. To retrieve an accurate result this is done by a Monte Carlo simulation consisting of 10 runs each. The parameters that should be tested are the following: the start temperature, the end temperature, the sizefactor, the temperature decrement α and the plateau increment β .

5.4.1 Exploring the SA algorithm

To get a grasp of how the SA algorithm works and if a near optimal solution can be returned, the algorithm is applied to the different data sets for each grid size. The arbitrary, initial input parameters are given in table 5.1. The initial solution used here is the first method that only considers the start and end node.

The figure 5.2 shows the value of the cost in terms of the number of runs. The number of runs do not include the trials performed at a specific temperature namely the plateau length N .

The results show that the solution stagnates in most cases at about 50 runs for both data sets. However, when the grid becomes more granular, more runs are needed to obtain an optimal solution. These observations are crucial to determine the stop condition in section 5.4.2. To be sure, the stop condition is set at 100 runs.

	Start temperature	End temperature	Plateau length	α	β	size factor
Data set I	10,000	0	10	0.80	1.0	1.0
Data set II	10,000	0	10	0.80	1.0	1.0

Table 5.1: The input initial parameters for a first solution of the SA algorithm for each data set

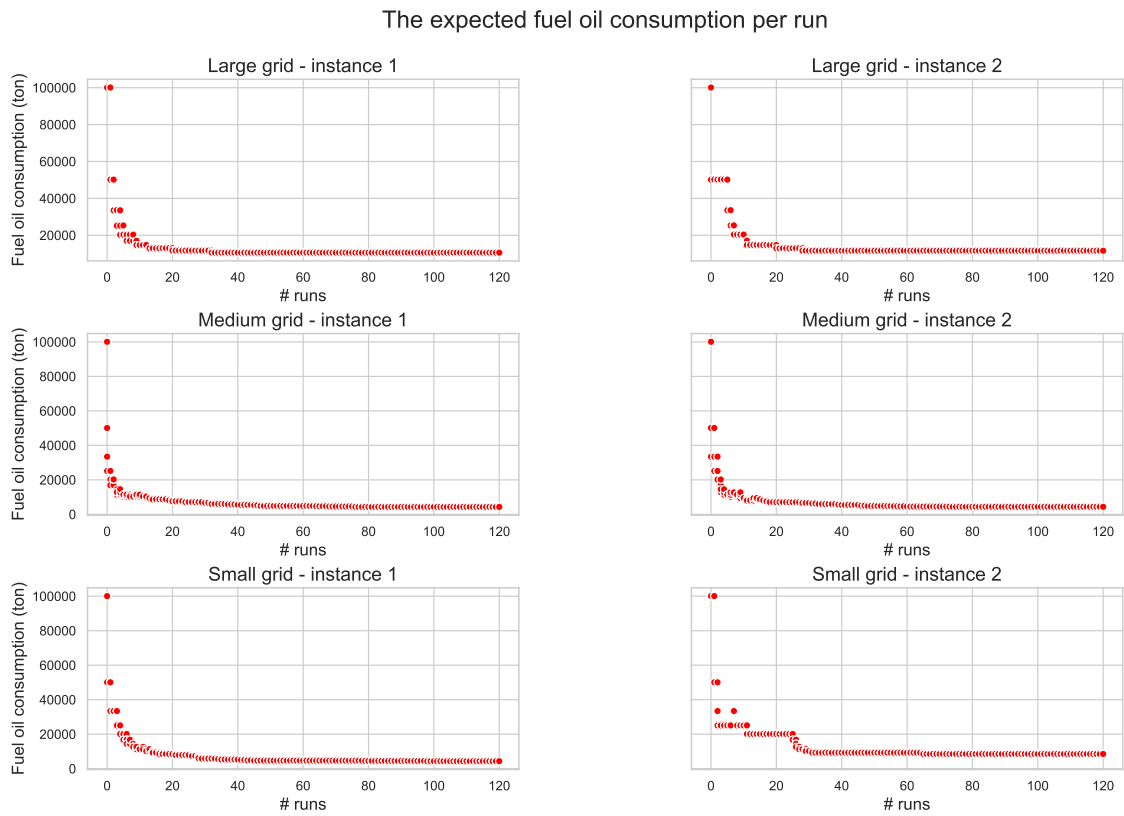


Figure 5.2: An initial SA simulation per instance and grid size

5.4.2 Stop condition

The stop condition depends on the end temperature as well as the number of runs. The end temperature is arbitrarily chosen to be 10^{-10} , but it could be that while the temperature is decreasing already an optimal solution has been found as seen in the previous section.

The SA algorithm should not stop before the temperature is decreased at least 100 times. If this threshold is reached, the SA algorithm keeps decreasing the temperature and only stops if the end temperature is reached or the same minimal fuel cost has been returned 10 times in a row. This basically means that the solution could not be improved by a neighbourhood solution anymore for the last 10 loops.

5.4.3 The neighborhood solution

Besides the stop condition, it is also valuable to look at the operators and acceptance rate in the hybrid neighbourhood solution. Based on the results of the initial runs in section 5.4.1, the acceptance rates of the operators can be retrieved and are displayed in the figure below. One can clearly see that the swap operator is of no use and should be eliminated. As such, in the follow-up experiments the swap operator is not included in the neighbourhood solution anymore.

5.4.4 The initial solution

Two methods were proposed for the initial solution. To decide which one to use in further experiments, a Monte Carlo simulation with 10 simulations is performed for each grid size and instance. The figure below shows that for each grid size, the breath-first search (BFS) solution converges to a path with lower FOC opposed to the initial solution consisting of only the start and end point. The CPU-time is slightly differs among the grid sizes and the type of solution. In all, the BSF solution will be used as initial solution for the follow-up experiments due to better conversion.

5.4.5 The starting temperature

According to Park and Kim (1998) the value of T , is set large enough to make the initial probability of accepting transitions be close to 1. A temperature that is set too high may cause a bad performance due to random selection or a long computation time. The procedure of choosing the initial temperature can be done in two ways. The initial temperature can be determined by looking at the uphill transitions or at the maximum change in objective function.

The first method consists of performing a number of trial runs of the annealing process. For each run, the objective function is calculated and the average increase in objective function

Percentage of neighbourhood operators accepted for different grid sizes and instances

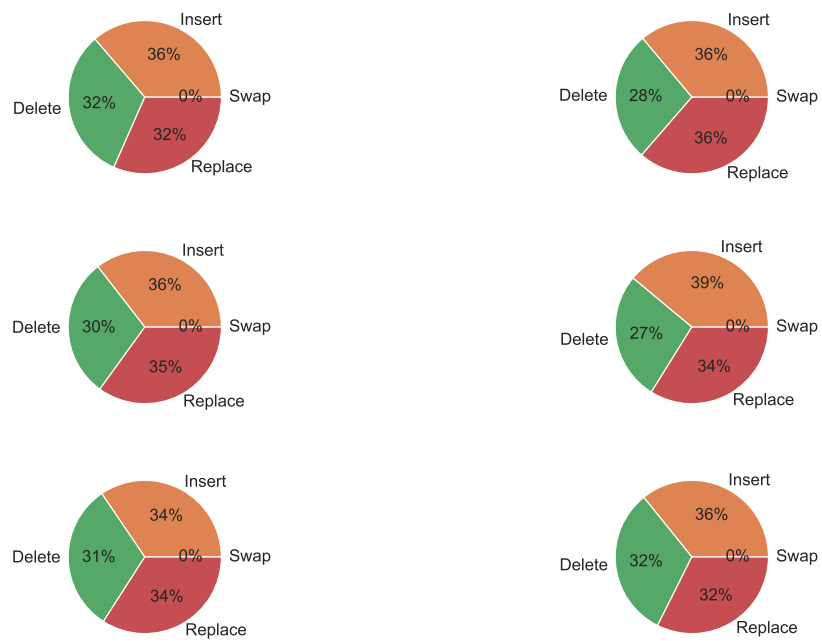
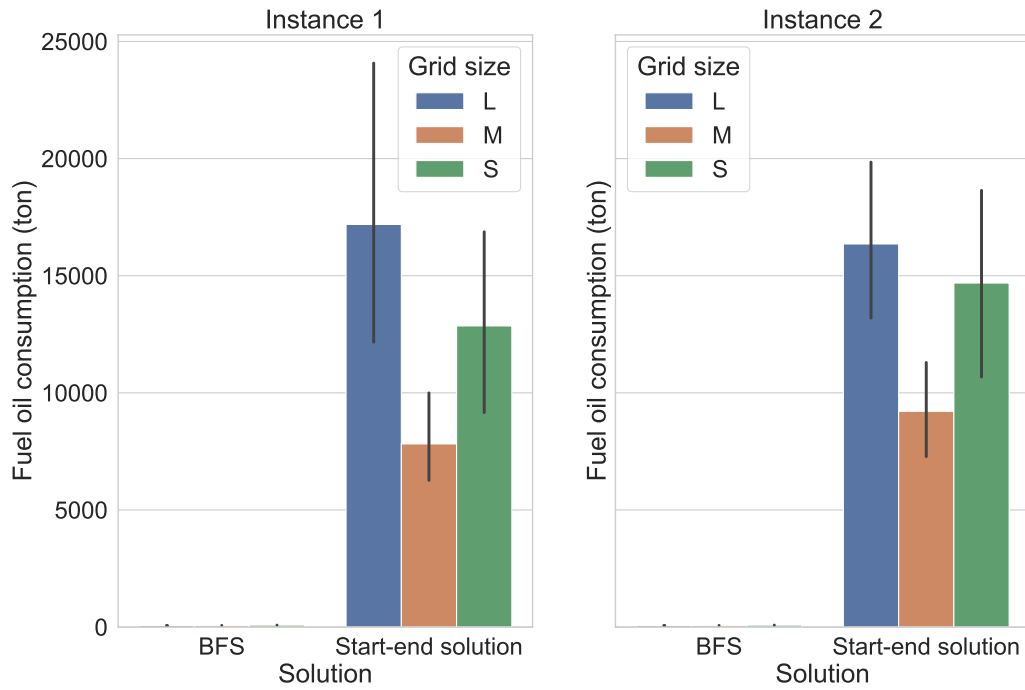


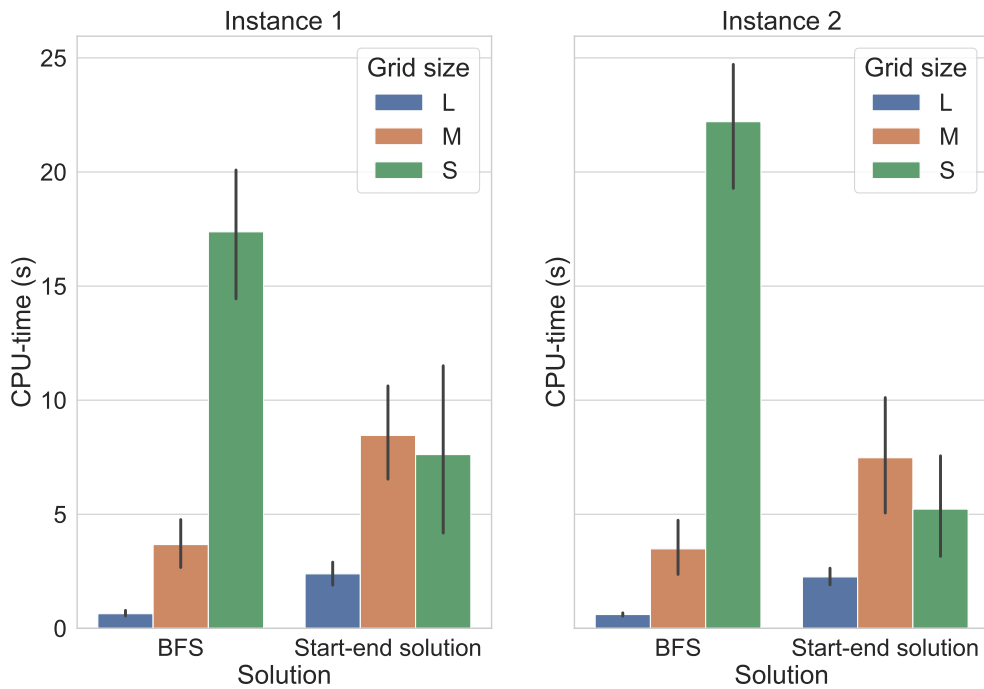
Figure 5.3: The acceptance rate of the operators in the neighbourhood solution for different grid sizes and instances

The expected fuel cost in terms of the initial probability to set the start temperature - Monte Carlo simulation (n=10)



(a) The expected FOC in function of the initial solution for different grid sizes and instances

The expected CPU-time in terms of the initial probability to set the start temperature - Monte Carlo simulation (n=10)



(b) The expected CPU-time in function of the initial solution for different grid sizes and instances

Figure 5.4: The expected FOC and CPU-time in function of the initial solution

is determined with uphill transitions only. This average number is then divided by the logarithmic value of an initial acceptance probability P according to the following formula.

$$T_{start} = -\bar{\Delta}/\ln(P) \quad (5.1)$$

However, it could also be that only the maximum transition between follow-up runs is kept track of instead of the average. This value is then again divided by a logarithmic acceptance probability. In formula (5.2), the average value is replaced by the maximum value.

$$T_{start} = -max/\ln(P) \quad (5.2)$$

This second method has been applied in current research. Looking at figure 5.5, one can generalise the results for the two data sets. Neither the CPU-time, nor the FOC changes as the probability increases. The reason is that the stop condition is already defined and the end temperature is 0. As such, the solution converges in the same time to the same solution independent of the starting temperature. The initial temperature at probability of 0.5 is used in the experiments.

5.4.6 The temperature decrement

The start temperature gradually decreases towards the end temperature. In this project, the temperature decrement is a geometric series. Therefore, at each iteration the temperature should be lowered by a fraction α in the following way: $T_{new} = \alpha T_{current}$.

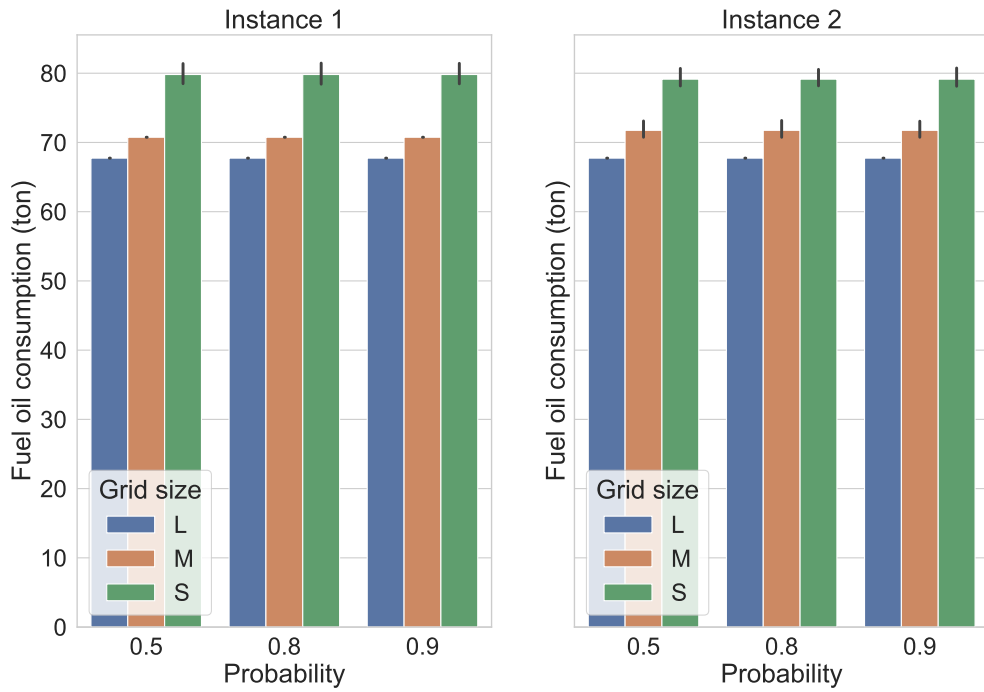
Theory states that α should range between 0.8 and 0.99. However, Johnson et al. (1989) applies even lower values of α . That is why SA is performed for the values of α equal to 0.45, 0.60, 0.80, 0.85, 0.90, 0.95, 0.97, and 0.99. The plateau increment, beta, is kept at a value of 1.

Figure 5.6 portrays the results of the SA algorithm for different values of α for data set 1 and 2. The expected fuel consumption as well as the CPU-time are reported.

Based on the results, the alpha's equal to 0.60 to 0.97 are worth investigating further in combination with varying values of beta. The current results do not give preference to one single value of alpha.

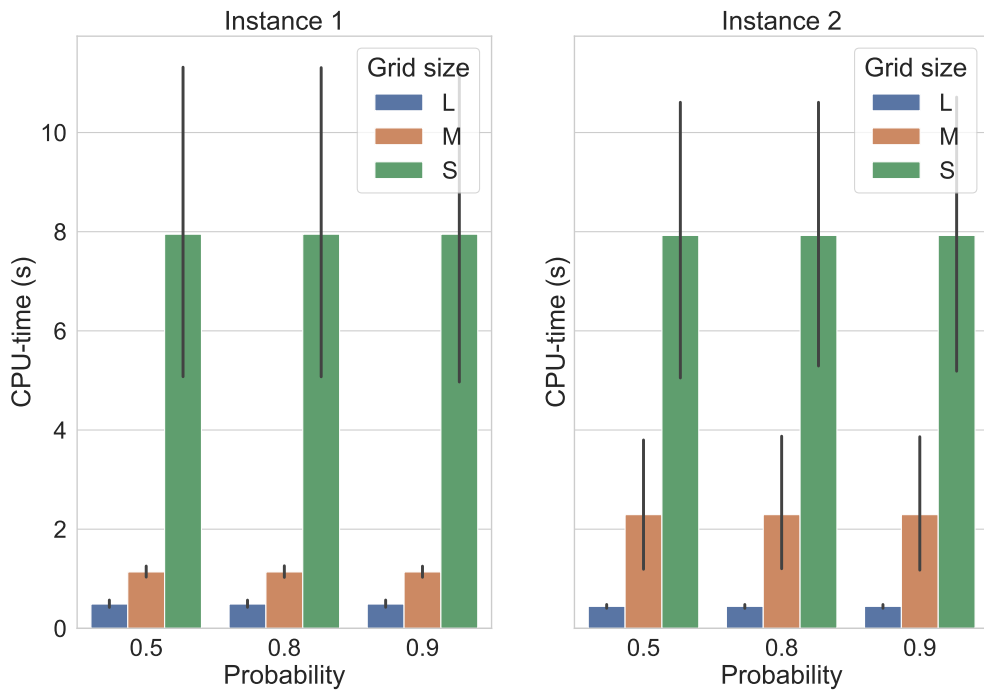
As the results are always the same for the large grid size, the tuning of the SA algorithm has little influence on the solution. The grid points are not granular enough and therefore the large grid size will not be considered in the following experiments.

The expected fuel cost in terms of the initial probability to set the start temperature - Monte Carlo simulation (n=10)



(a) The expected FOC in function of the starting temperature for different grid sizes and instances

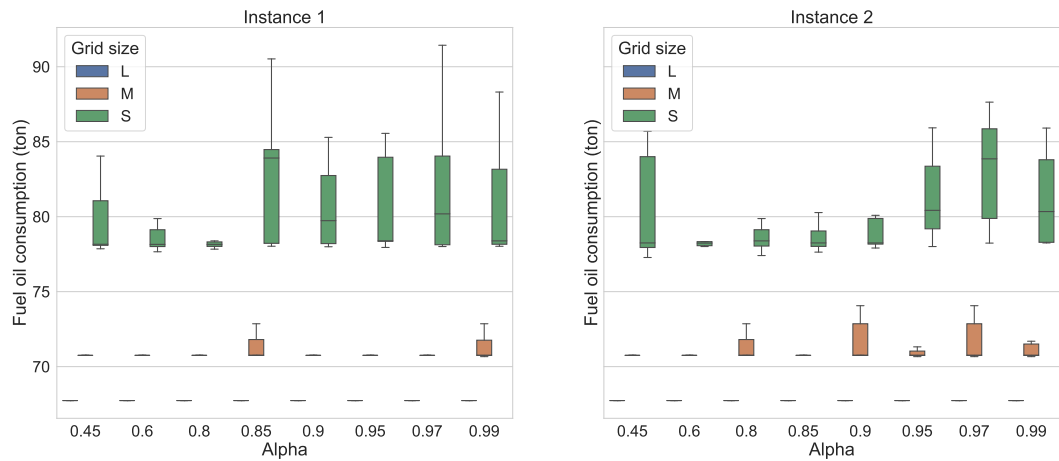
The CPU-time in terms of the initial probability to set the start temperature - Monte Carlo simulation (n=10)



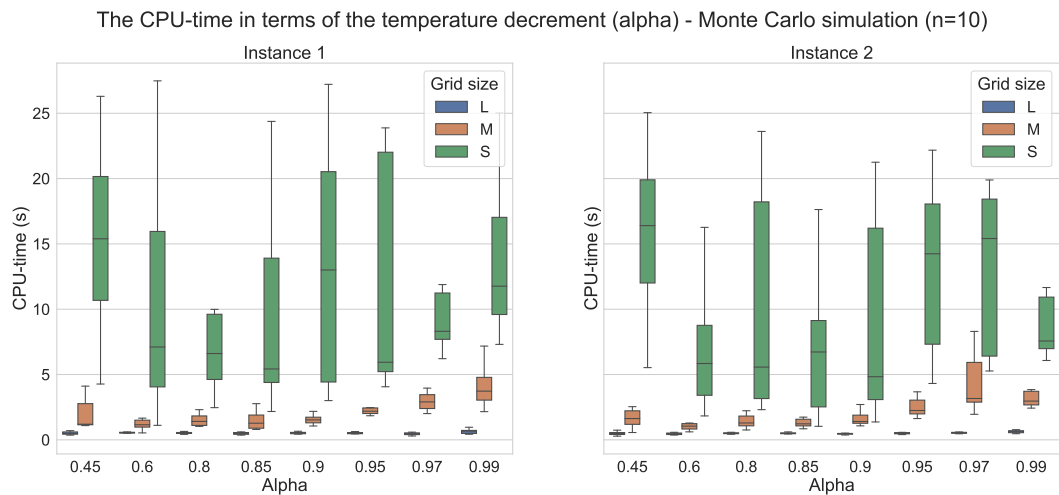
(b) The expected CPU-time in function of the starting temperature for different grid sizes and instances

Figure 5.5: The expected FOC and CPU-time in function of the starting temperature

The expected fuel oil consumption in terms of the temperature decrement (α) - Monte Carlo simulation ($n=10$)



(a) The expected FOC in function of the temperature decrement for different grid sizes and instances



(b) The expected CPU-time in function of the temperature decrement for different grid sizes and instances

Figure 5.6: The expected FOC and CPU-time in function of the temperature decrement

5.4.7 The plateau increment

The plateau length at which new neighbourhood solutions are explored at the same temperature level can either remain constant or can gradually increase for each temperature decrease. The plateau length can be increased in the following way: $N_{new} = \beta N_{current}$. Beta has been set to either 1, 1.01 or 1.03. Larger values of β are not considered due to the high computation times. The values of alpha considered here are 0.60, 0.80, 0.85, 0.90, 0.95 and 0.97.

Based on figure 5.7, one can see that the CPU-time increases as the beta and the alpha increases. The best results are achieved for an alpha equal to 0.9 and 0.95 combined with a beta equal to 1.03 for both grid types and instances. That is why these values are only considered in determining the sizefactor.

5.4.8 The plateau length and size factor

The plateau length should be set to an optimal value as well. High enough to search for all possible neighbourhood solutions, but not too high in order to minimize the CPU-time. The size factor is the factor that is multiplied by the fixed number of neighbourhoods spaces. The neighbourhoods space is set to 8 as the possibility exists that 8 adjacent grid points can be approached based on a current solution. The size factor is then set to 1, 4 and 8. Both the expected cost and the CPU-time are considered in terms of varying α , set to 0.9 or 0.95. Note that β is fixed to a value of 1.03.

As the size factor increases, the CPU-time increases as well, especially for a size factor equal to 8. A size factor of 8 does not necessarily give better results in terms of FOC. Therefore, a size factor of 8 is of the charts. For both values of alpha, size factor 1 and 4 are reasonable in terms of CPU-time and FOC.

5.5 Comparison A-star and SA

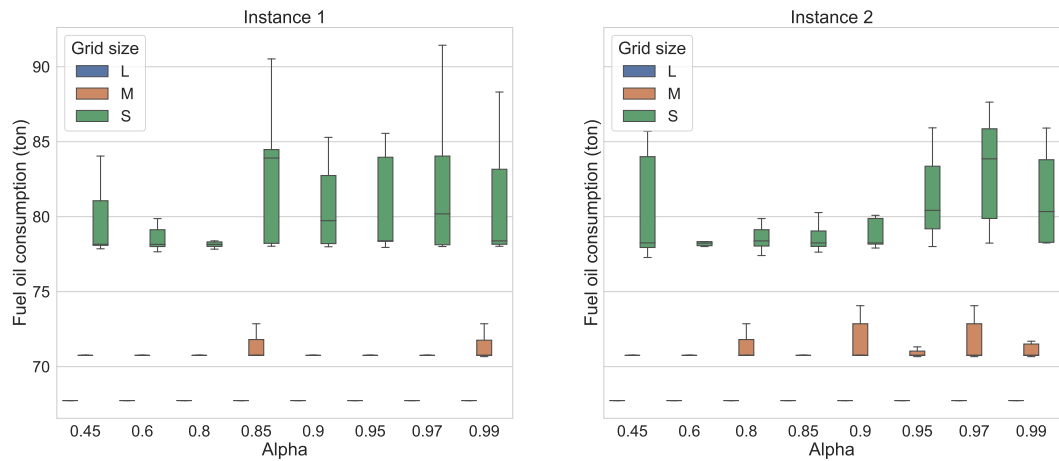
Let's compare the A-star solution with the SA solution for the following parameters for the SA algorithm. The size factor chosen here is 1 and the alpha is set to 0.9.

	Start temperature	End temperature	Plateau length	α	β	size factor
Data set I	10,000	0	8	0.9	1.3	1.0
Data set II	10,000	0	8	0.9	1.3	1.0

Table 5.2: The final input parameters for the SA algorithm for each data set

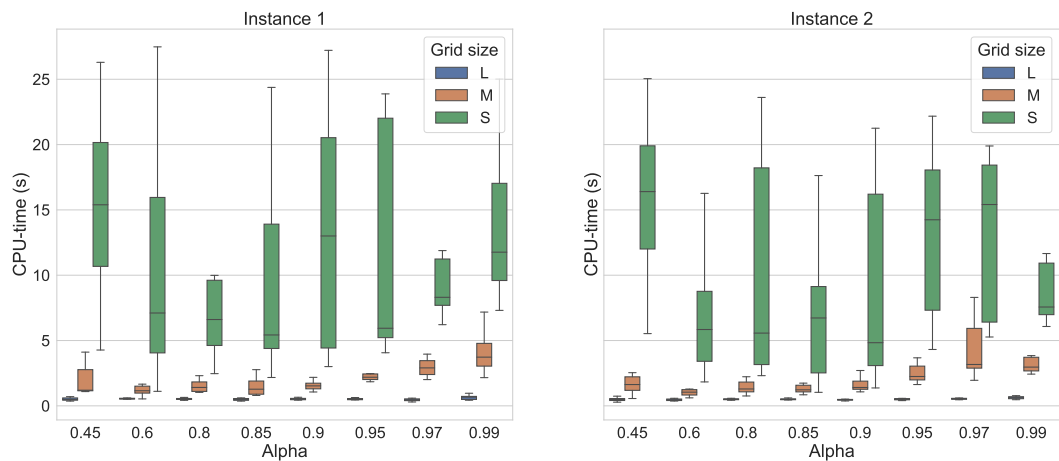
The fuel consumption and CPU-time for performing one iteration for both algorithms for each grid size and instance are displayed in figure 5.9. It is clear that for this type of problem the A-star algorithm performs better in terms of both dimensions, especially when the grid

The expected fuel oil consumption in terms of the temperature decrement (alpha) - Monte Carlo simulation (n=10)



(a) The expected FOC in function of the plateau increment for different grid sizes and instances

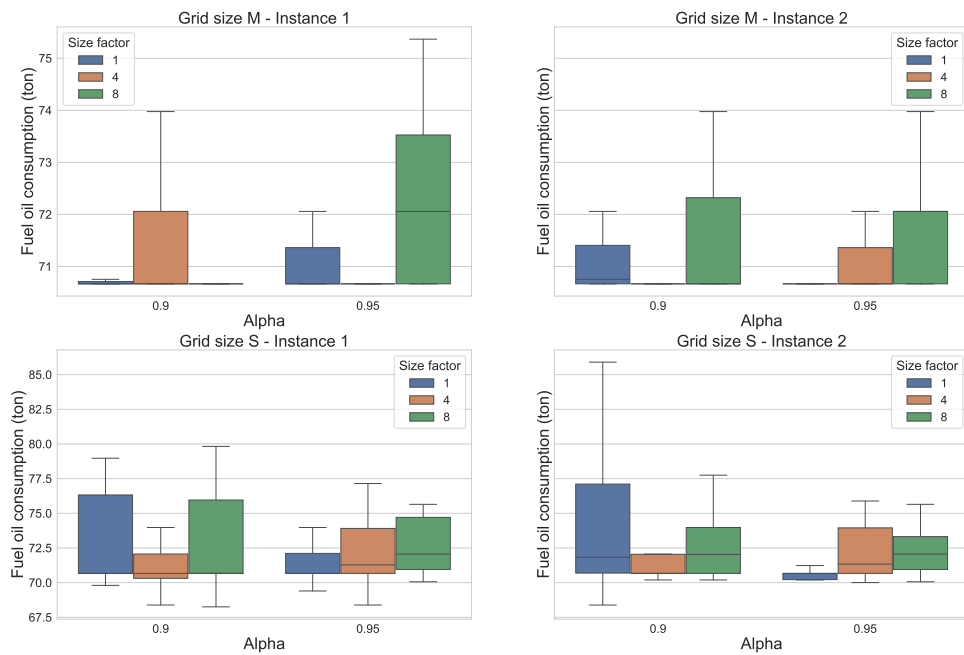
The CPU-time in terms of the temperature decrement (alpha) - Monte Carlo simulation (n=10)



(b) The expected CPU-time in function of the plateau increment decrement for different grid sizes and instances

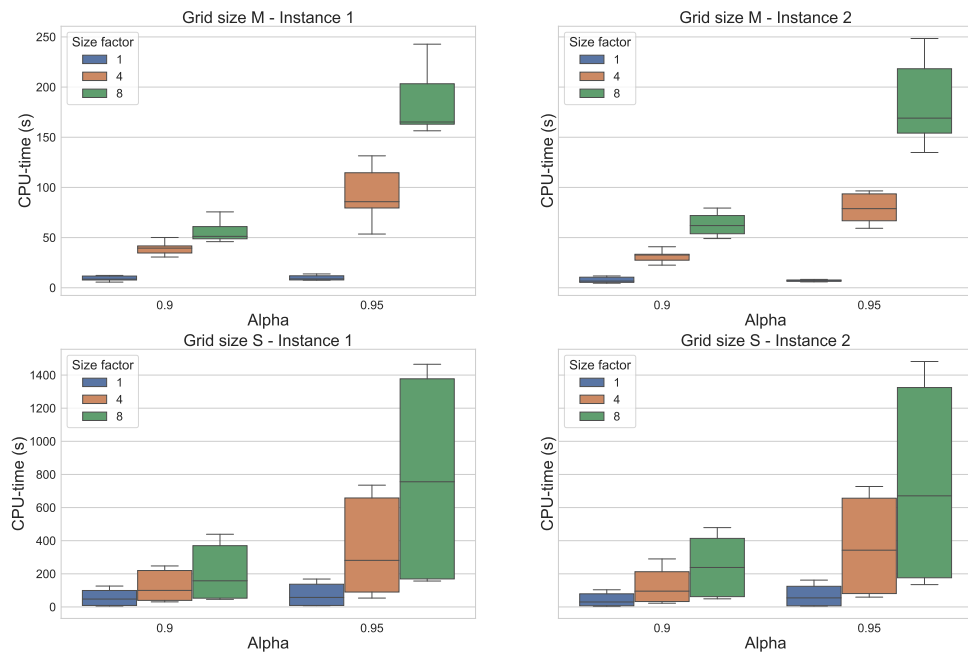
Figure 5.7: The expected FOC and CPU-time in function of the plateau increment

The expected fuel oil consumption in terms of the temperature decrement and the size factor - Monte Carlo simulation (n=10)



(a) The expected FOC in function of the temperature decrement and size factor for different grid sizes and instances

The expected CPU-time in terms of the temperature decrement and the size factor - Monte Carlo simulation (n=10)

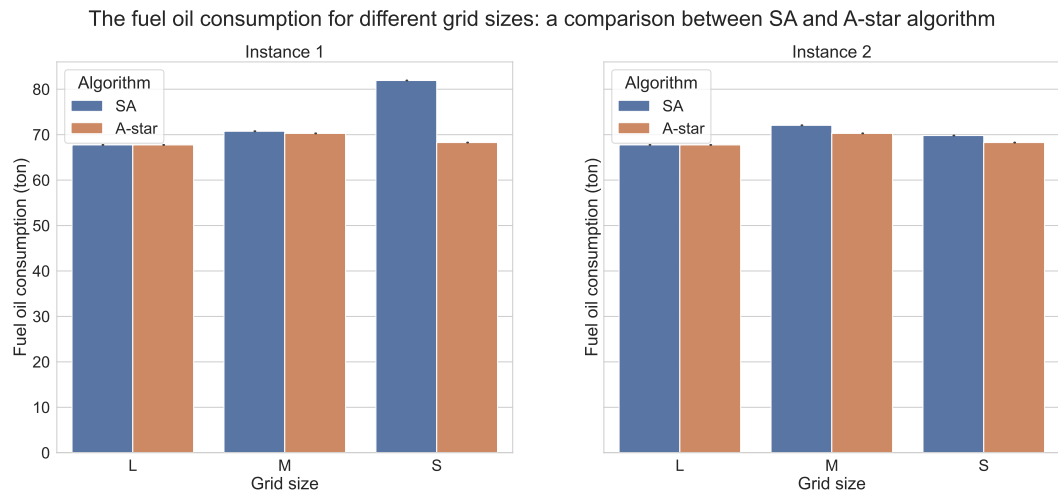


(b) The expected CPU-time in function of the temperature decrement and size factor for different grid sizes and instances

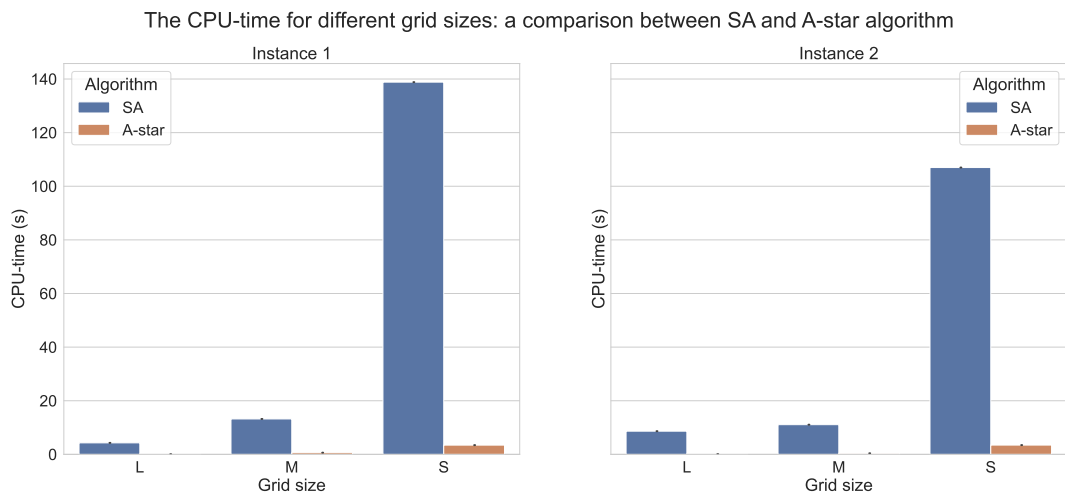
Figure 5.8: The expected FOC and CPU-time in function of the temperature decrement and the size factor

is more granular. However, it is possible that if the geographical area would be larger and the grid more granular, the SA algorithm would have been a better option. Either way, the A-star algorithm assures an optimal solution and has a lower computation time. Keeping these reasons in mind, the A-star algorithm will be applied in chapter 7 for the purpose of weather routing. The routes that were constructed and for which the metrics are derived can be found in appendix A.

Notice also that the initial solution in the SA algorithm could have a significant influence on the end result unless the algorithm runs a long time. In literature, the operators that result in a variable length of the solution are absent. In most cases, SA is applied in path planning related to the travelling salesman problem. The problem does not involve variable path length and can include neighbourhood operators such as swap, insertion, etc. It would therefore be valuable to explore the possibility of variable operators in SA for the shortest path problem.



(a) The fuel oil consumption for the routes constructed by A-star and SA



(b) The CPU-time for the routes constructed by A-star and SA

Figure 5.9: The fuel oil consumption and CPU-time for the routes constructed by A-star and SA

Part III

Computational Experiments

Chapter 6

Power prediction per weather category

6.1 Introduction

The goal of this chapter is to identify the main variables that have an influence on the power prediction for each of the four models, explained in section 3. Apart from the influential factors, the main differences between the models are also quantified. As such, an over- or underestimation of the models can be identified opposed to the most accurate model according to Toqua.

6.2 Data collection and models

The four models that are provided by Toqua were explained in chapter 3 and are based on historic information of tanker.

Apart from the four models, Toqua also provided detailed information about the historic routes sailed by the tanker dating from 2015 until 2022. Based on this information, realistic values for the weather severity can be defined and derived. This will be further explained in section 6.3.3. Moreover, the impact of some variables can be neglected and can be set to a fixed value due to minimal variability observed in the historic data as well as the minimal influence on the power prediction.

For the experiments in this section, the weather and ship conditions are set to predefined values in order to perform the experiments in a controlled way. The parameters will be set to predefined fixed values or a varying range of values.

Apart from the ship-hydrodynamic models, the weather routing model is of great importance. The algorithm applied in further experiments is the A-star algorithm (see section 4.3.1) with

the objective function, constraints and parameters explained in chapter 4.

6.3 General set-up

6.3.1 Default values for the parameters

The vessel from which information is provided, is a tanker. For each model, different input parameters are included which is indicated in table 6.1. Default values can be set for these values which remain fixed or will vary depending on the experiment.

Generally, the current direction and speed as well as the rudder angle will remain 0 with the goal of better comparison of the models recommended by the Toqua experts. As a result, the SOG will be equal to the STW at all times and for each experiment. The SOG remains 12 kn.

The other default values are in most cases set to 0 apart from the sea temperature and the sea surface salinity. These are average values derived from the historical data shown in table 6.1. The draft and the trim also remains fixed as this is ship specific.

Parameter	Value	ML model	PI-ML model	Sea trial	Sea trial + correction
Current direction	0°	✓	✓		✓
Current speed	0 m/s	✓	✓		✓
Sea temperature	23 °C	✓	✓		
Trim	Fixed	✓	✓		
Draft	Fixed	✓	✓		✓
Sea surface salinity	33 PSU	✓	✓		
Heading	0°	✓	✓		✓
Rudder angle	0 °	✓	✓		
SOG	12 kn	✓	✓	✓	✓
Wave direction	0°	✓	✓		✓
Wave height	0 m	✓	✓		✓
Wind speed	0 m/s	✓	✓		✓
Wind direction	0°	✓	✓		✓

Table 6.1: Default values for the ship hydrodynamic models

6.3.2 Model assumptions

Notice that an abbreviation for the four models is used which will reoccur throughout this research. The original ML model of Toqua is denoted as ML model, the physics-informed ML model as PI-ML model, the sea trial curves as sea trial or ST and the sea trial curves with

correction factor as sea trial + corr or ST + corr. The models are assigned a color in the upcoming figures respectively, blue, orange, red and green. As such, better visualization and comparison of different figures is possible.

6.3.3 Weather definition

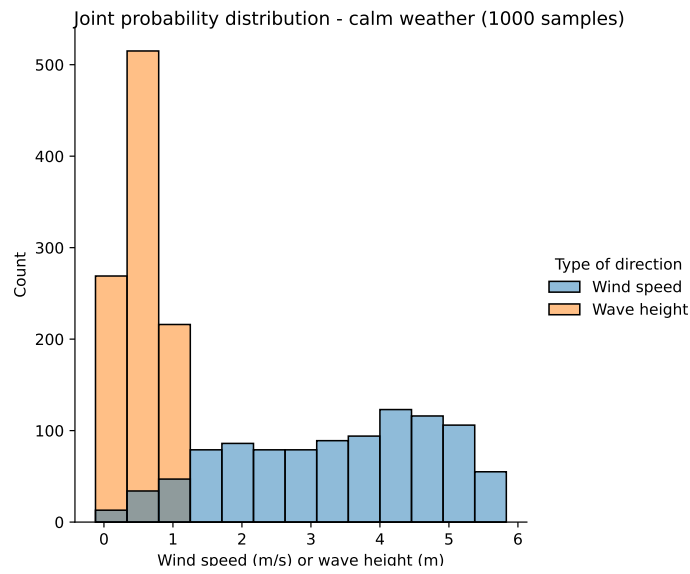
The influence of the severity of the weather on the power prediction and in turn on the routing is the main focus in this research. The severity of weather at sea is determined by the wind speed and the wave height. The wind speed and wave height combinations however are endless and therefore a clear definition should be set up to what each weather category entails.

Each combination of wind speed and wave height is associated with a Beaufort number (BN). In regards to the experiments, three types of weather can be defined: calm, medium and severe weather. In table 6.2 the weather categories adopted in this research are shown. Weather circumstances corresponding to a BN greater than 8 are not considered as these are not likely to happen in real-life. (Mallawaarachchi, 2022)

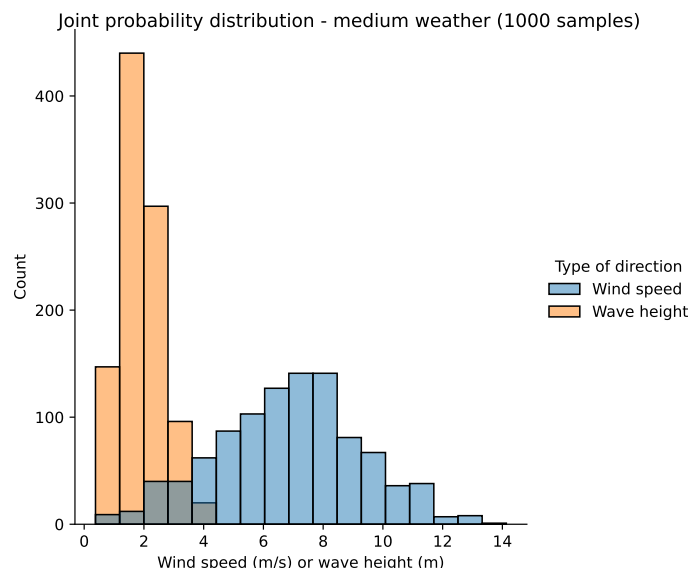
Weather	BN	Wind speed [m/s]	Wave height [m]
Calm	[0 - 3]	[0 - 5.5]	[0 - 1.2]
Medium	[4 - 6]	[5.5 - 13.8]	[1 - 4]
Severe	[7 - 8]	[13.9 - 20.7]	[4 - 7.5]

Table 6.2: Weather categories with corresponding Beaufort scale, wind speed and wave height range

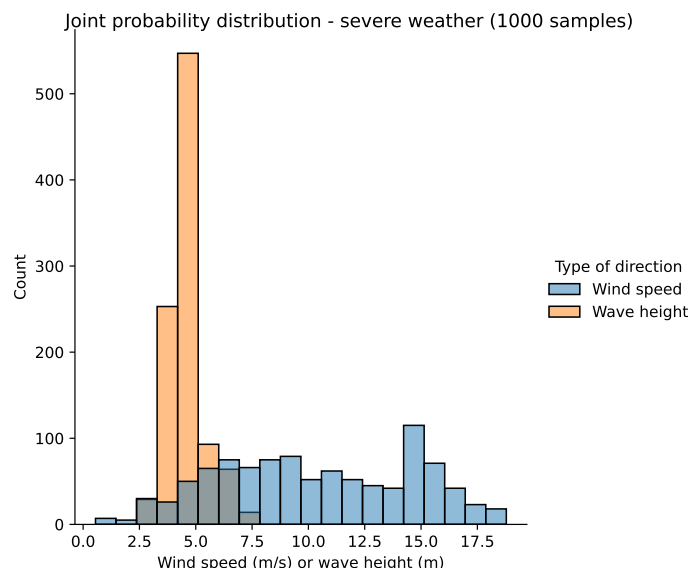
In order for the wind speed and wave height combinations to be realistic, a joint probability distribution can be formed based on the historic routes. In the historic data set, the wind speed and wave height are tracked with their corresponding Beaufort number. The following figures show for each weather category the distribution of wave height and wind speed that is associated with it. By setting up a joint probability distribution, samples of wind speed and wave height combined can be drawn.



(a) The joint probability distribution of calm weather



(b) The joint probability distribution of medium weather



(c) The joint probability distribution of severe weather

Figure 6.1: The joint probability distributions of the wind speed and wave height for each weather category

6.4 Parameter influence on the power prediction

6.4.1 Data description

For different weather severity and parameter values, the power prediction according to each model may differ. The power prediction is said to be the dependent variable and the input parameters defined in table 6.1 are the independent variables. To quantify the impact of the independent variables, one should identify which variables should remain fixed and which ones should simultaneously vary. First, the correlation between the independent variables can be quantified which can be determined based on the historic data set. If a correlation is present between two or more values, the values of the variables should vary alongside each other and the relationship between the variables should be determined.

The draft and trim are positively correlated as these are ship specific parameters and do not change over the course of a voyage. Therefore, the draft and trim will remain fixed to a value that is ship specific.

Besides the draft and trim, the wave height and wind speed are correlated as well (see figure 6.2). As said before, these parameters determine the weather severity and should therefore be variable throughout the experiments.

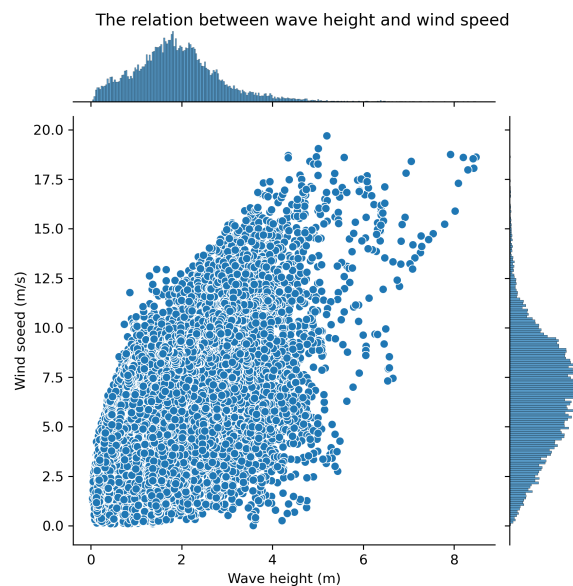


Figure 6.2: The relation between wind speed and wave height

The same can be said for the wind and wave direction. Generally, the wave and wind direction are equal to one another except for the wave direction equal to a value ranging between 150° to 250° . This relation is displayed in figure 6.3. Notice that for the wave and wind direction, the angle indicates from where the wave or wind comes. For instance, if the wind direction is

0° , the wind comes from in front of the ship. 180° indicates that the wind comes from behind the vessel.

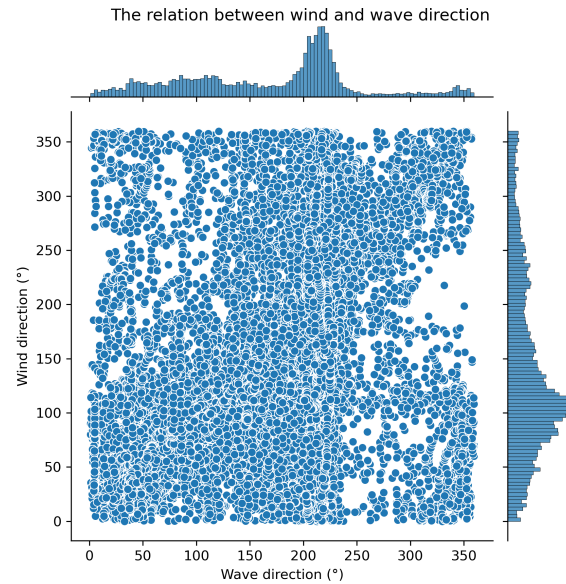


Figure 6.3: The relation between wind and wave direction

As for the sea salt salinity and the sea temperature, these parameters are also correlated, but the historic data shows that the sea salt salinity remains between 30 PSU and 40 PSU except for some outliers. The sea temperature fluctuates between 0°C and 34°C . As such, the sea salt salinity can be set to an average value of 33 PSU. The influence of the sea temperature on the power prediction is minimal and should be neglected according to Toqua for simplicity reasons. As such, the temperature is also set to an average of 23°C . For routing purposes, it is evident that the heading is variable. Aforementioned, the current speed and direction and the rudder angle should be set to 0.

6.5 The impact of weather severity and wind/wave direction

In the previous sections, the parameter settings were investigated and it was determined which variables should remain fixed or vary to fully quantify the influencing factors on the power predictions. One can therefore conclude that the parameters wind speed, wave height, wind and wave direction could have an influence on the power prediction while other values remain fixed.

Consequently, the main focus of this chapter is testing the impact of the weather severity, either calm, medium or severe weather on the power prediction in combination with a varying wind and wave direction. Not only the predictions of the individual models are of interest,

but also the differences in power between the models at hand.

6.5.1 Assumptions

The wave and wind direction are always assumed to be equal based on figure 6.3. The band between 150° and 250° for the wave direction will be neglected and should be investigated in future research. The wind speed and the wave height can be drawn from the joint probability distributions corresponding to each weather category.(see figure 6.1) For each alteration of the experiment, 10,000 samples will be taken.

Furthermore, the heading remains 0° as the course of a ship is not determined here. Merely the impact of the angle between the heading and the wind and wave direction is quantified on the power predictions. The directions refer to the angle whenever the ship is heading forward and the wind and waves exert resistance on the vessel.

6.5.2 Experimental set-up

The power can then be predicted for several cases of wind and wave direction by each of the four models. The cases that will be considered are a direction of 0° , 45° , 90° , 135° and 180° . Directions of the wind and waves from 180° to 360° will have the same effect on the power prediction as the previous cases due to symmetry reasons.

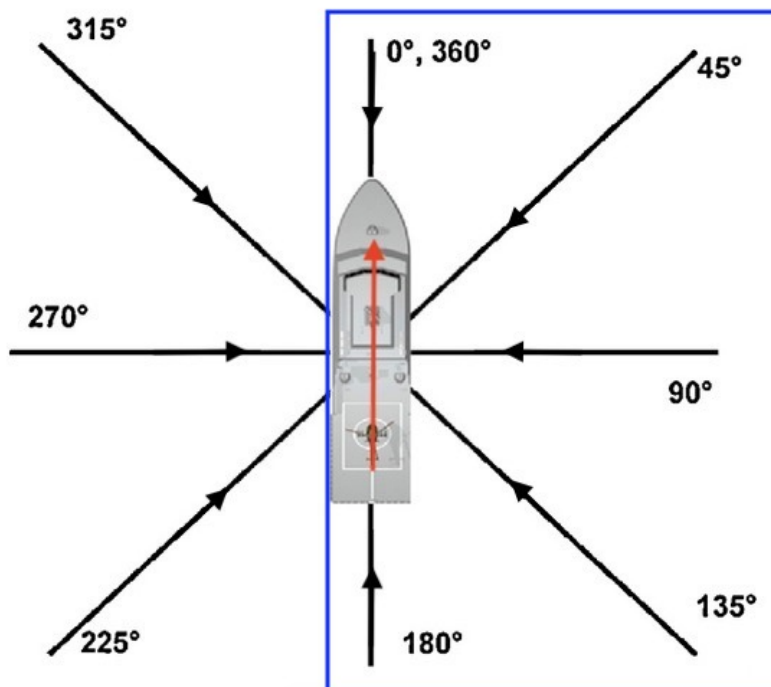


Figure 6.4: The wind and wave directions opposed to a ship heading of 0°

The wind/wave direction given, indicates from which direction the waves/wind come. The directions are pointed towards the vessel, not away from the vessel. As for the weather, the three weather categories, calm, medium and severe will be considered.

In all, 15 alterations of weather and wind/wave direction on the power prediction of the four models are investigated. Within such an alteration 10,000 samples are drawn of the wind speed and wave height. The values of all other parameters are set to the default values represented in table 6.1.

Important to mention is the interpretation of the angle between the heading and the wind/wave direction. The predictions do not only depend on the heading nor the wind/wave direction solely but rather the relative angle between them which can be computed as “heading - wind/wave direction”. So, as the heading is 0° and the wind/wave direction is for instance 45° , the relative angle will be -45° or 315° . In this case, 315° has the same effect on the power prediction as 45° because of symmetry reasons.(see figure 6.4)

Individual power predictions

Each model takes different aspects of weather into account. Therefore, the power output varies in average quantity but also in variation. Based on the samples taken per weather category, the mean power and the standard deviation of the power per model can be derived for a constant wind and wave direction. For instance, for calm weather, 10,000 samples are drawn from the joint distribution of wind speed and wave height corresponding to a BN of 0 to 3. For each of the samples, only the wind and wave direction changes from 0° to 180° while other values remain fixed. The power output is then calculated by the four models resulting in 10,000 values per model per wind/wave degree. This gives a representative overview of the models' behaviour.

All average values and standard deviations are given in the tables in appendix B.1.1 and B.1.2 per wind/wave degree, model and weather category. The results will also be represented by comparable boxplots explained in section 6.5.3.

Power difference between models

For each weather category, the average difference between models can be calculated as well and the percentage increase or decrease can be derived.

These results can also be represented by boxplots for each weather category and direction supplemented by a table of relative changes. The boxplots merely confirm the values reported in the tables and can be consulted in appendix B.1.3 and B.1.4.

An example of the structure of such a table is shown below. The values in the table comprise

average differences between the models divided by the average or standard deviation of the power of the historic routes. The differences result from 10,000 samples drawn from the joint distribution of the weather severity. As for the denominator, the average power output is only based on the samples in the historic data in an unfouled condition which comprise 10,2257 data points. An unfouled condition means that the vessels are cleaned and no unwanted bio-organisms are attached to the vessel. It is important for this experiment to only consider these data points as the models are only applicable for the power prediction of ships in an unfouled condition.

		Benchmark model - original power			
		ML model	ML-PI model	Sea trial	Sea trial + corr
New power	ML model	0.0			
	ML-PI model		0.0		
	Sea trial			0.0	
	Sea trial + corr				0.0

Table 6.3: Example of the table with relative changes (in %) for comparison of the models in function of the weather severity and the wind and wave direction

The percentage difference for one sample is calculated according to formula 6.1. For 10,000 samples, the mean of the 10,000 percentage differences is taken. Besides the mean, the standard deviation can also be reported.

$$\% \text{ Power increase or decrease} = \frac{Power_M - Power_B}{Power_{avg}} \quad (6.1)$$

where

$Power_M$ = the new power of the model that is compared to the benchmark model

$Power_B$ = the original power of the benchmark model

$Power_{avg}$ = the average power of the 10,2257 data points in the historic data.

The tables with the results can be found in appendix B.1. Again, for each weather type and wind and wave direction, the results are reported.

6.5.3 Results

In the results section both the individual predictions and the prediction differences between the models will be reported. Each time the boxplots for the individual results will be given. Other information, such as the relative difference between the models and corresponding boxplots for these results can be found in the appendix as well as the tables with all the specific values.

Calm weather

First off, the power output for a scenario of calm weather comprising 0 to 3 BN is examined.

The boxplots show that the average power of the ML model is for any wind and wave direction the highest, followed by the average power of the sea trial curve with correction factor, the physics-informed ML model and the sea trial curve. The mean and standard deviation of the individual model predictions can be found in appendix B.1.1 and B.1.2 respectively.

Power predictions per model per wind/wave direction - calm weather (10,000 samples)

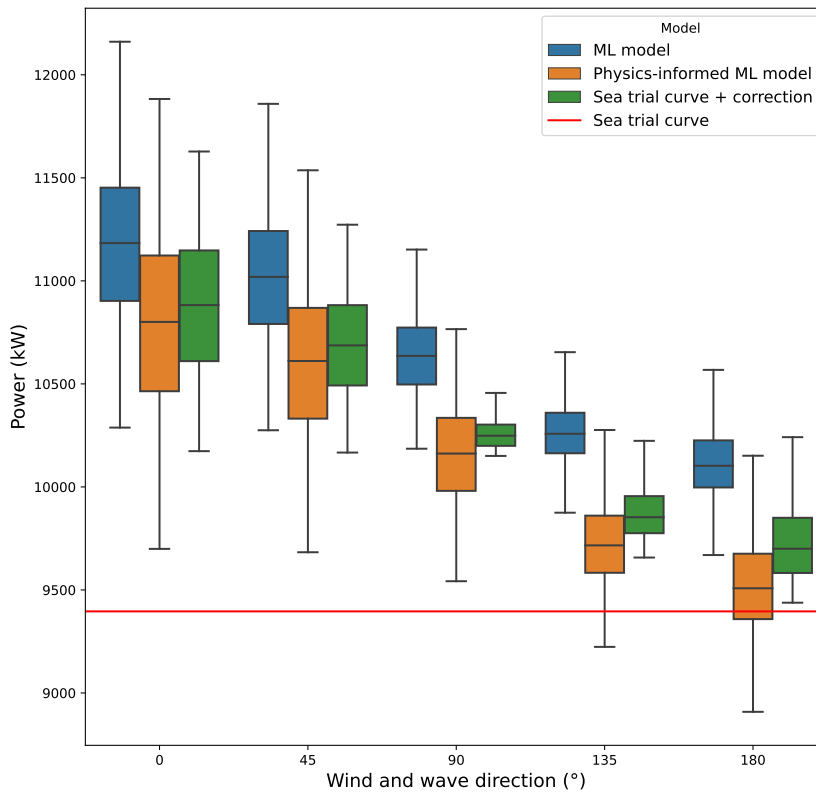


Figure 6.5: The comparison of boxplots of the power predictions per model per wind and wave direction for calm weather (10,000 samples)

The power output resulting from the sea trial curve with correction factor is higher than the one of the physics-informed model, but the difference is minimal. The difference ranges between 0.95% and 2.04%. The difference becomes slightly bigger as the wind/wave direction increases. However, research of Toqua shows that the power accuracy of the PI-ML model is bigger than the sea trial curve with correction factor and should therefore be chosen over the latter.

The power difference between the ML model and the physics-informed ML model ranges between 4.12% and 6.23% and increases while the angle increases. The same trend is partially noticeable for the difference between the power prediction of the ML model and the sea trial curve with correction factor. The power difference increases from 3.17% to 4.34% for an angle of 135° and thereafter slightly drops to 4.19%. The mean relative power differences and the

standard deviation with corresponding boxplots can be found in appendix B.1.3 and B.1.4.

As the angle increases, it applies that the power of a model opposed to the power output of the sea trial curve diminishes. Moreover, the variability in power predictions for each one of the models decreases as well as the variability in the power difference between the models. (see figure 6.5 and figure B.1) As this tendency is similar for all types of weather, this will be further explained in section 6.5.3.

Medium weather

Similar to calm weather, the power output of the ML model is the highest for each wind/wave direction. However, the order of the power output of the physics-informed model and sea trial curve with correction factor is reversed. The mean and standard deviation of the individual model predictions can be found in appendix B.1.1 and B.1.2 respectively.

Power predictions per model per wind/wave direction - medium weather (10,000 samples)

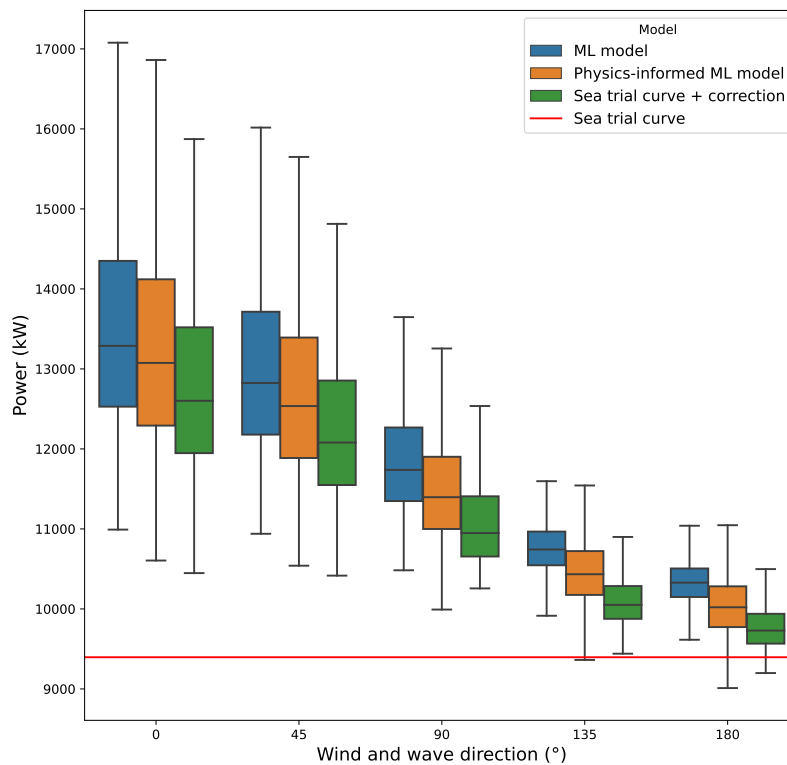


Figure 6.6: The comparison of boxplots of the power predictions per model per wind and wave direction for medium weather (10,000 samples)

The power prediction according to the physics-informed model is lower than the one of the ML model. The relative difference ranges between 2.66% and 4.0%. As the direction increases, the difference increases until a direction of 90° is reached. From that moment on, the difference

diminishes again.

Likewise, the power difference between the ML model and the sea trial curve with correction factor follows the same pattern. The difference varies between 5.77% and 8.08%.

The power output of the physics-informed ML model compared to the sea trial curve with correction factor decreases along with the increase of direction. The difference ranges between 2.71% and 5.14%. The relative difference could be said to be small again, but in terms of accuracy it is best to apply the physics-informed ML model. The mean relative power differences and the standard deviation with corresponding boxplots can be found in appendix B.1.3 and B.1.4.

Notice that the predictions of the original ML model are closer to the ones of the physics-informed ML model rather than the sea trial curve with correction factor. This is the opposite trend compared to calm weather.

As for the power prediction of sea trial curves, the predictions of the other models tend to approach the sea trial prediction whenever the direction becomes greater. Again, the variability in predictions of the models and between the models decrease along with the increase of the direction.(see figure 6.6 and figure B.2)

Severe weather

The severe weather category consists of weather corresponding to a BN of 7 and 8. In this category, the order of the predictions in terms of magnitude changes as the angle differs. Up to an angle of 90° , the power output of the ML model is higher than the other models which is also the case for calm and medium weather. However, for an angle of 135° , the ML predictions are on average smaller than the predictions of the sea trial curve with correction. For an angle of 180° , the ML predictions are even lower than the PI-ML predictions on average.

As for the physics-informed model, the power is higher than the one of the sea trial curves with correction factor, but from the direction of 90° on this relation switches. Moreover, from a direction of 135° on, the prediction of the ML model is lower than the prediction of the sea trial curve with correction factor. The mean and standard deviation of the individual model predictions can be found in appendix B.1.1 and B.1.2 respectively.

Now evaluating the power differences between the models, the relative difference between the ML model and the physics-informed ML model ranges between absolute percentage values of 1.81% and 9.68%. A maximum difference of 9.68% is reached at 90° and the lowest difference of 1.81% is reached at 180° . Keeping in mind the order of magnitude of the models, the relative percentage values get a + or - sign.

The power difference on average between the sea trial correction predictions and the ML predictions for 0° and 45° are rather big namely 19.75% and 15.29%, but drops quickly to 6.32% for 90° . Thereafter, the order of magnitude between the two models is reversed and the difference between the predictions becomes even smaller.

Power predictions per model per wind/wave direction - severe weather (10,000 samples)

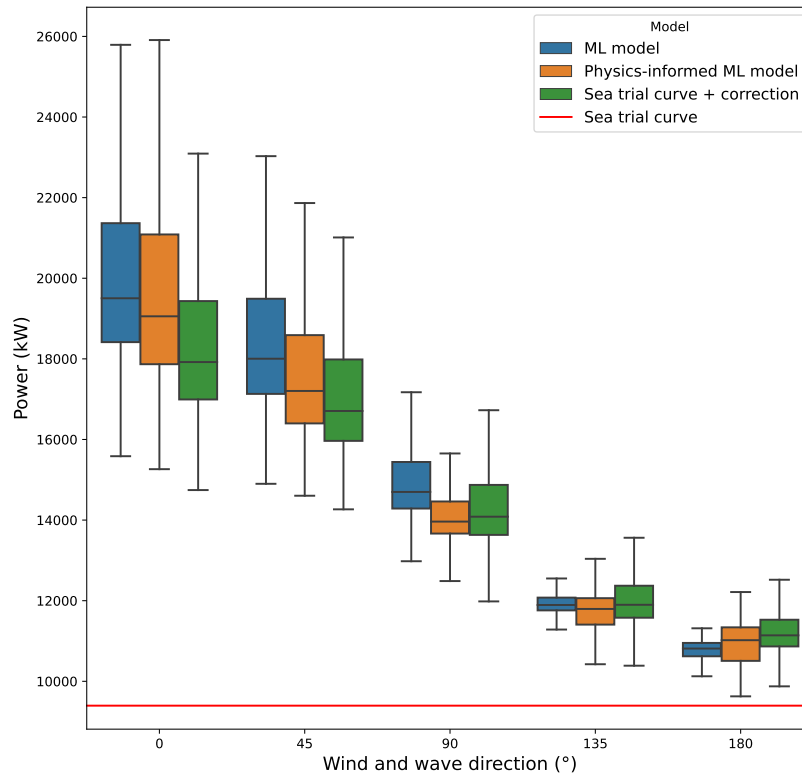


Figure 6.7: The comparison of boxplots of the power predictions per model per wind and wave direction for severe weather (10,000 samples)

A similar tendency can be observed between the sea trial curve with correction and the physics-informed ML model. The difference drops from 17% to 6.76% from 0° to 45° and as soon as the relation between the models is reversed at 90° , the power difference between the models diminishes.

The difference between the sea trial predictions and the other models are very large opposed to calm and medium weather. The difference again diminishes as the angle between the heading and the wind/wave direction increase. The variability in predictions of the models and between the models decrease along with the increase of the direction. (see figure 6.7 and figure B.3)

Comparison and variability

For each of the boxplots, the sea trial curve will be a constant line as it does not take any weather conditions into account. This is the case for all weather categories. In this case, the power output corresponding to 12 kn is 9396 kW for the sea trial curve.

Aforementioned, the model predictions of the ML model, the PI-ML model and the sea trial curve with correction tend towards the sea trial curve predictions as the relative angle between the heading and wind/wave direction increases.

However, the order of magnitude for each type of weather differs and even changes along the angle for the severe weather category. The more severe the weather becomes, the power output for each of the models will increase as well. The relative difference between the sea trial predictions and the predictions of all other models enlarges on average also for more severe weather. The same tendency cannot be observed for the mean relative difference between other types of models.

Two types of variation in the predictions can be observed, the change of variation along the weather severity and along the angle. Noticeable is that, the higher the angle between the heading and the wind/wave direction is regardless of the severity of the weather, less variation constitutes in the individual predictions of the models (see figures 6.5, 6.6 and 6.7) as well as the relative difference between the models (see figures B.1, B.2 and B.3).

The variation also enlarges as the weather worsens for both the individual predictions (see figure 6.8) and the difference between them (see figure 6.9). Only the relative differences for a wind/wave direction equal to 0° are given in figure 6.9. The figures for the other angles are given in appendix B.1.3 in figures B.4 and B.5. The same conclusions apply for the other angles.

Also notice that the difference of the models compared the sea trial curves is the largest in variation.

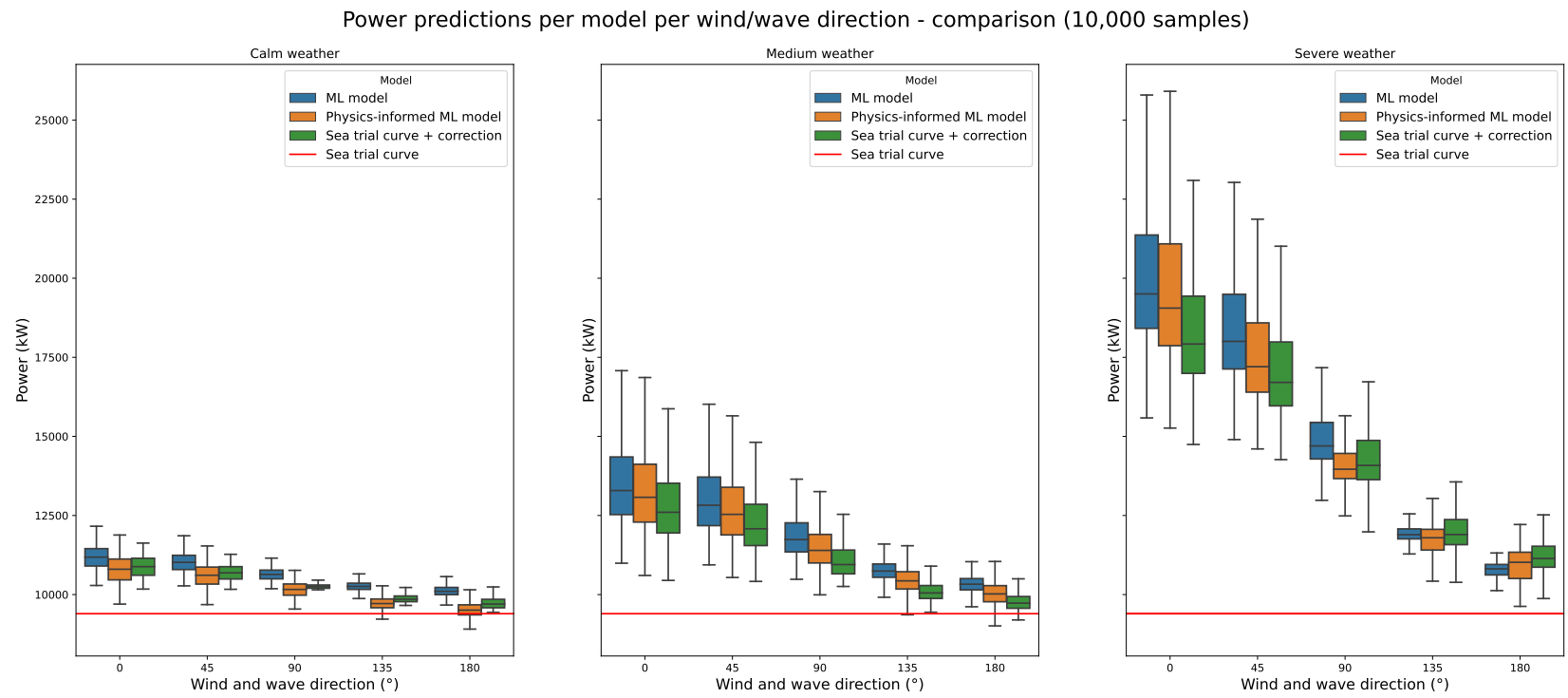


Figure 6.8: Comparison of the FOC models' power prediction per wind/wave direction (10,000 samples)

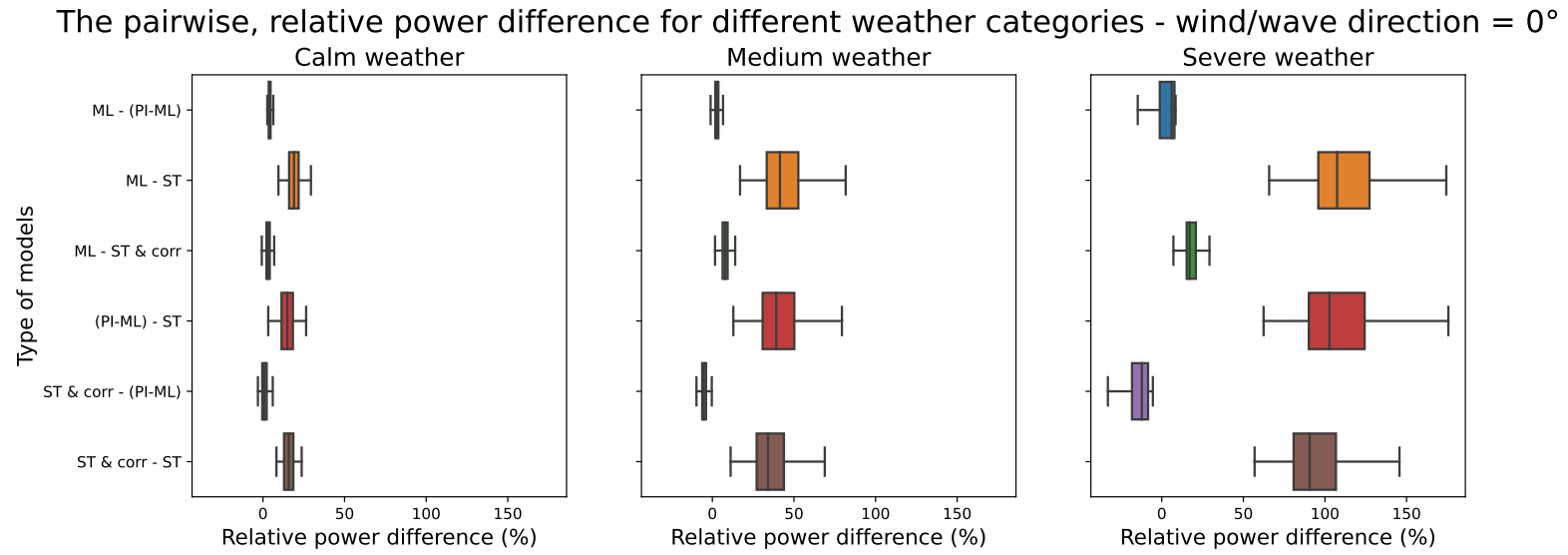


Figure 6.9: Comparison of the FOC models' power prediction differences between two models for a wind/wave direction = 0° (10,000 samples)

Chapter 7

Robustness in route optimization

7.1 Introduction

In the upcoming chapter, the sensitivity to weather severity of the FOC models will be tested in forming an optimal route, taking into account the varying weather conditions. Instead of looking at the individual power predictions of each model and the quantitative difference between them, different routes are considered in a homogeneous weather grid. Furthermore, the optimization potential of the FOC models in saving fuel in a changing weather environment will be quantified according to the most accurate model that serves as the ground truth.

7.2 Methodology

As the goal is to investigate weather routing in a controlled way, the methodology thoroughly explained in the introduction and literature study will be applied here. The methodology is displayed in figure 2.1 in chapter 2.

7.2.1 Geographic representation

The geographical area that is considered here is the same as explained in section 5 for the experiments concerning the simulated annealing heuristic. Only one grid type, the small grid, is considered with a size of 55.5 km by 55.5 km. A visualization of the geography is given below.

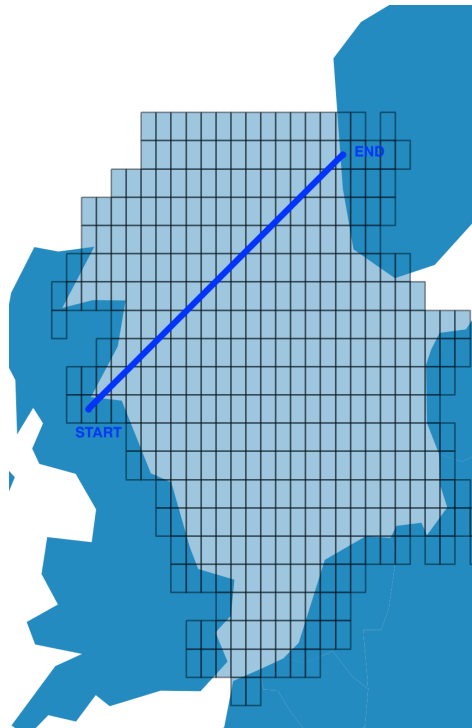


Figure 7.1: The grid-based representation of the North Sea with start and end point

The grid as a whole will be referred to as the grid and each individual small grid cell within the grid will be referred to as a grid point.

7.2.2 Weather forecast

The weather assigned to each grid point will be static and will therefore not change in time. Meaning that at time 0 the weather will be no different than at time 1, 2, 3, etc. for one particular grid point. This is important to mention because in a dynamic setting, the weather conditions are based on the time the vessel travels to reach a certain destination. However, the weather conditions do differ between grid points in a geographical sense. In grid point 1 the weather for instance will be different than in grid point 2. The goal is to mitigate the inaccuracy of weather forecasts in this way.

Again default values will be set to each grid point and some variables will vary from grid point to grid point in a randomized way. As the goal is to look at routing under different weather severity, only the wind speed and wave height will change. This will be further explained in section 7.4.

7.2.3 Ship hydrodynamics and models

The four ship hydrodynamic models as seen before are applied in this chapter and are further investigated in terms of weather routing. As such, the same input parameters as in table 6.1 are of interest here and were already examined in the previous chapter.

As for the weather routing model, the A-star algorithm is used for finding the optimal path rather than the SA algorithm. The computational run time is smaller for this type of experiments and the solution is most certainly the optimal one. In the end, the fuel oil consumption should be minimized along the trajectory.

7.3 Weather sensitivity and fuel efficiency

The goal is to prove that some type of hydrodynamic models are more sensitive in terms avoiding bad weather while forming an optimal route that minimizes the fuel oil consumption. High sensitivity in this case means that high wind speeds and large wave heights can be avoided and a safe voyage is guaranteed. This can be done by replicating a realistic weather situation over a geographical area with homogeneous weather conditions for which paths are reconstructed per model. The weather categories of interest are calm, medium and severe weather. In doing this, some metrics are set-up to evaluate the sensitivity such as the heading changes, the minimal distance between the routes etc.

Besides the sensitivity, the fuel savings can be quantified that are only devoted to the FOC models and not the routing algorithm. In both cases, it is important that some predefined conditions are met:

- A reasonable amount of randomized weather grids should be generated in order to reduce the bias of the routing algorithm, for instance 200 samples.
- The conditions should be the same for each of the ship performance models that are tested. Meaning that the routes are constructed by the base models over the same weather grid.

A slightly different set-up will be applied for the fuel efficiency quantification.

7.4 Experimental set-up

7.4.1 Homogeneous weather conditions

Similar to the previous experiments, some variables remain fixed and others should vary. As previously determined, it is only valuable to vary the wind speed, the wave height and the relative angle between the heading and wind/wave direction.

In one grid, each grid point can be seen as an individual sample or point prediction. As such, from grid point to grid point, the wind speed and wave height will differ. The grid consists of homogeneous weather conditions. Meaning that only samples are drawn within one weather category. So, if the grid consists of calm weather, each grid point entails a combination of wind speed and wave height corresponding to the joint probability distribution of calm weather (see figure 6.1a). This is illustrated in figure 7.2. It shows that each grid point is assigned a wind speed between 0 and 3 m/s combined with a wave height between 0 and 5 m. For medium or severe weather this can be done in the same way, but typically for higher values of wind speed and wave height according to joint distribution 6.1b and 6.1c respectively. Other variables remain fixed to the default values prescribed in table 6.1 for each grid point.

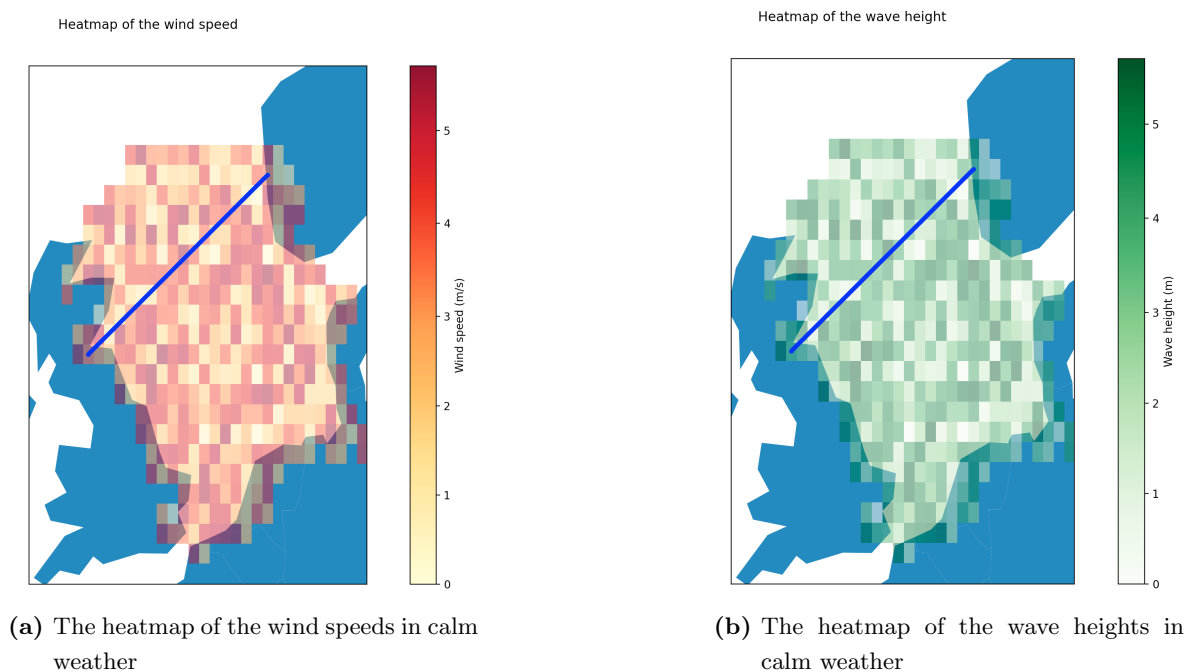


Figure 7.2: The heatmaps for wind speed and wave height corresponding to calm weather

Sensitivity

While dealing with routing, the heading does change in order to reach the destination and is therefore not set to 0° anymore. However, the wind/wave direction is kept constant to 0° for the sensitivity experiments. As such, the angle between them varies in a controlled manner. Important to mention is that again the SOG remains 12 kn at all times.

Fuel efficiency

As for the fuel efficiency experiments, the wind/wave direction also varies between 0° and 360° . Similar to the wind speed and wave height, the values for the directions are also drawn

from a known probability distributions based on the historic data provided.

For both experiments, the grid can be replicated with random values in each grid point several times for each weather category. In order to draw general conclusions, a new grid will be formed 200 times per weather type. As a result, 200 different routes will be formed per model per weather type.

7.4.2 Assumptions

As the heading is now changing, the wind/wave direction should remain constant over the grid points in order to quantify the relative angle between the heading and wind/wave direction. In the sensitivity experiment, the directions remain 0° while the heading varies. The same formula as before is applied to quantify the angle namely “heading - wind/wave direction”.

7.4.3 Metrics

In this section both metrics for the sensitivity and the fuel efficiency are defined. These metrics are evaluated per randomized weather grid for each of the ship performance models. In order to draw general conclusions, the average and the standard deviation is derived over the number of samples, for instance 200 samples. This is called a Monte Carlo simulation which is based on the theory of large numbers.

Sensitivity metrics

Different metrics can be set-up to give an informative framework on how the models operate and can be distinguished from one another in terms of routing.

First off, it is of importance to investigate if the routes formed are similar or dissimilar to one another in a single homogeneous grid. This can be done by looking at the total travel time over the trajectory.

Supplementary, if the routes are quite similar and have the same number of grid cells that are traversed, the pairwise haversine distance between each of the routes can be calculated in order to quantify the overlap between the routes.

Besides similarity, it is valuable to look at the heavy weather avoidance as a sign of sensitivity of the FOC models. Some models might be better in avoiding areas of higher wind speeds and wave heights. One possible way could be to set up a density plot or histogram in which the number of traversals by a certain model through a particular values of wind speed/wave height is tracked. If a model only traverses low wind speeds and wave height, the model is good at avoiding worse weather.

The average heading changes over one route can also be a possible indication of the model trying to avoid severe weather. More heading changes means bypassing grid cells that are not favourable for the fuel minimization over a route.

Fuel efficiency metrics

In order to quantify and compare the fuel savings over a specific route constructed by the performance models, one should identify a ground truth. As said, there are four FOC models to be tested, the sea trial curve, the sea trial curve with correction factor, the pure ML model and the physics-informed ML model. One of these models should be used to recalculate the total fuel consumption over each model's route to have a comparable basis. This is considered the main challenge in calculating the return on investment (ROI) in routing, especially when the base model used is inaccurate.

The best way forward is to choose the most accurate model to recalculate the fuel consumption. Explained in section 3.4, the accuracy of the pure ML model and the physics-informed model are close to one another and is considerably higher than the traditional methods. Therefore, both ML models will be used as ground truth and the results will be averaged over 200 scenarios. The results of the ML as ground truth are displayed in appendix C.2.1. The fuel savings compared to the shortest route according to the sea trial curve are then calculated in the following way.

$$\% \text{ FOC savings} = \frac{FOC_{ST} - FOC_M}{FOC_{ST}} \quad (7.1)$$

where

FOC_M = the total FOC of the route constructed by the model that is compared to the shortest route

FOC_{ST} = the total FOC of the shortest route according to the sea trial curve

Another challenge in striving for comparability and quantifying the savings to its full extent is that favourably all scenarios should have the same departure and arrival times. To account for the same travel time, the SOG should be varied. This is not the case in this master's dissertation and should be further explored in future research. The fuel consumption is therefore still compared to the travel time over one's route. The fuel savings should take into account the time savings or extensions. The travel time extensions of the FOC model's routes compared to the routes of the shortest path are calculated in the following way.

$$\% \text{ Travel time extensions} = \frac{Time_M - Time_{ST}}{Time_{ST}} \quad (7.2)$$

where

$Time_M$ = the total travel time of the route constructed by the model that is compared to

the shortest route

$Time_{ST}$ = the total travel time of the shortest route according to the sea trial curve

7.5 Weather avoidance results

7.5.1 Similarities in terms of travel time

For each type of weather, 200 different homogeneous grids have been replicated. The similarity between the routes formed per model and weather type are given in figure 7.3. In terms of total travel time, the routes do not differ significantly neither between the models nor between the different weather categories. This means that the routes have more or less the same length and only slightly differ if certain types of weather are avoided.

The total time consumed over a route per weather category and FOC model (200 samples)

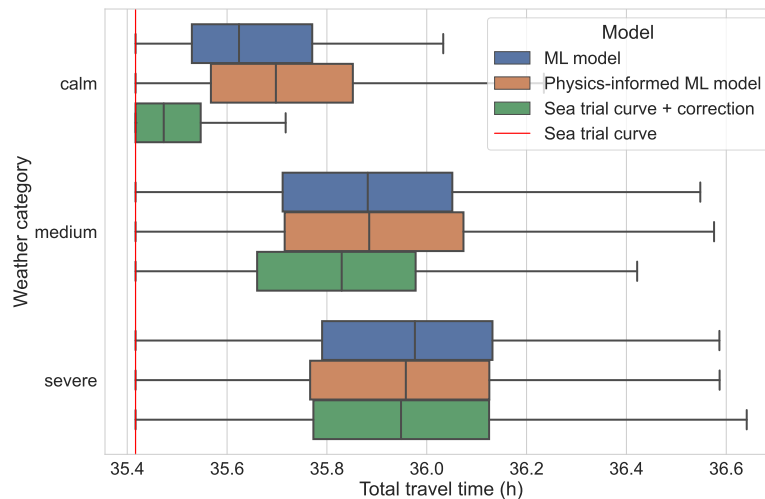


Figure 7.3: Travel time comparison between weather categories and FOC models in routing

7.5.2 Overlap between the models' routes

As the routes constructed by each model do not differ as much in length per weather category, it is valuable to look at the pairwise distance between these routes. Meaning that the total distance traversed over one trajectory per model is not evaluated, but rather the distance between the routes of the models is quantified. In this way, if the measure is close to zero, the routes for a certain simulation overlap. The distance measure used is the haversine distance and 200 simulations are evaluated per weather category.

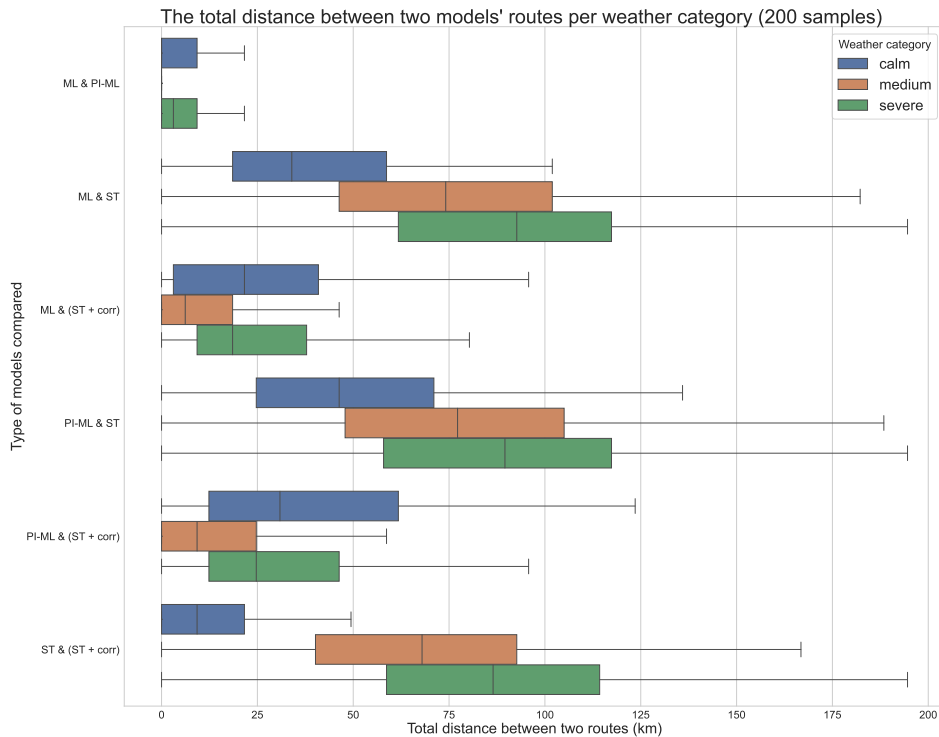


Figure 7.4: Pairwise haversine distance between routes of the FOC models (200 samples)

In figure 7.4 the total distance obtained between the routes of two models over 200 samples per weather category is shown. In figure 7.4 the total distance obtained between the routes of two models over 200 samples per weather category is shown. The y-axis shows which models are compared in terms of overlap. For instance, ‘ML & PI-ML’ means that the pure ML model and the physics-informed ML model are compared to one another and therefore the distance between them is calculated. The x-axis entails the total distance between the subjected routes.

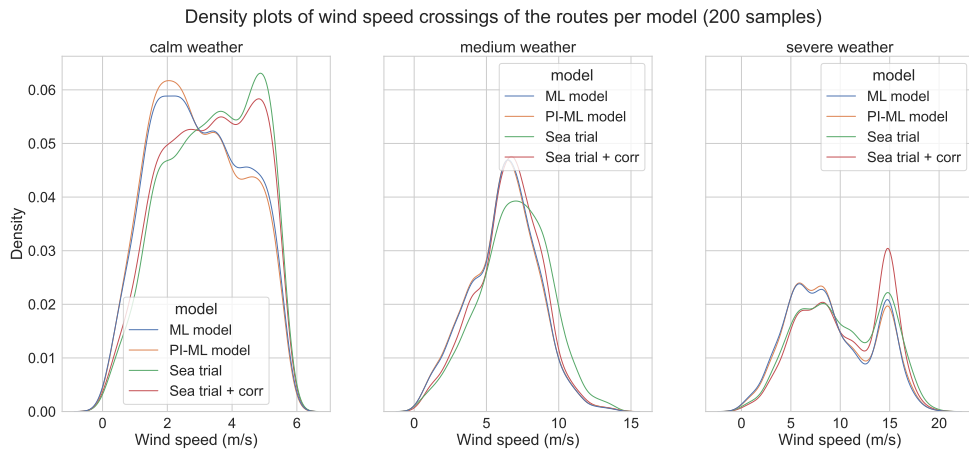
Remarkable is that the routes of the ML model and the physics-informed model are very similar and largely overlap in most cases for any type of weather. As such, the ML model and physics-informed model have the same results compared to the routes of the sea trial curve with or without correction.

The ML and PI-ML model do not differ as much on average from the sea trial curves with correction factor in calm and medium weather, but the average distance slightly increases in severe weather as does the variation between the models’ routes.

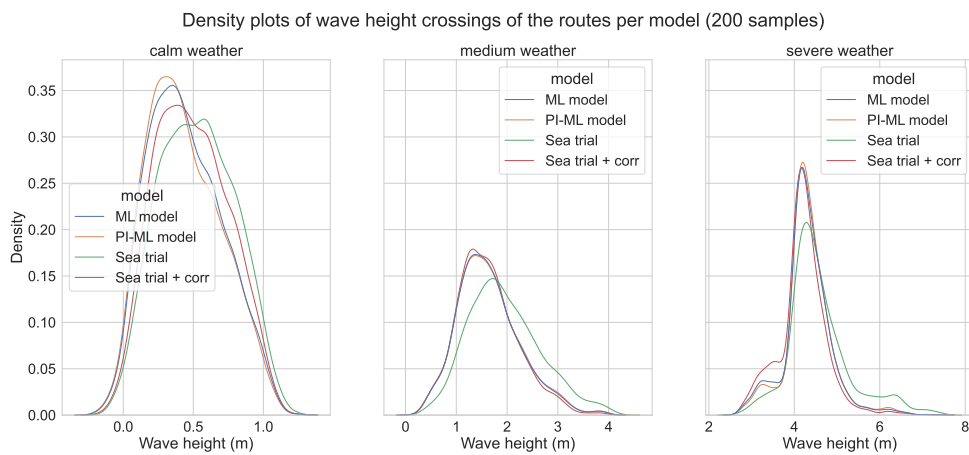
As for the comparison of the sea trial curve to the other models, the boxplots indicate that the routes do not overlap on average for any type of weather, but especially for medium and severe weather. The sea trial curve follows a path corresponding the shortest distance from starting to end point without taking the weather conditions into account. Therefore, the sea trial model is not sensitive in avoiding bad weather. In this way, it is assumed that models that differ from the sea trial route are more prone to avoiding bad weather.

7.5.3 Weather avoidance

After defining which models' routes are similar in terms of overlap and total time travelled, one can also look at the extent of weather avoidance of the models. That is why a density plot is made for the wind speed and the wave heights that are crossed by each models' route over 200 simulations. This is again done for each weather category.



(a) Density plot of wind speed crossings per weather category and FOC model



(b) Density plot of wave height crossings per weather category and FOC model

Figure 7.5: Density plots of wind speed and wave height crossings of FOC models' routes per weather category (200 samples)

It is clear that the routes constructed by the sea trial curve pass through higher waves and wind speeds. Only in severe weather conditions, the routes of the sea trial curve with correction passes through higher wind speeds than the routes without correction.

In terms of wind speed and wave height, the ML and physics-informed ML model perform similarly. In calm weather however, the routes of physics-informed ML model have the tendency to avoid higher wind speeds and waves more.

Difference between ML and PI-ML model

One can also take a closer look at the difference between the routes of only two models. For instance, the routes of ML and physics-informed ML model. In most cases, the routes overlap,

but if only the weather conditions are considered whenever they differ a new, more detailed density plot can be made.

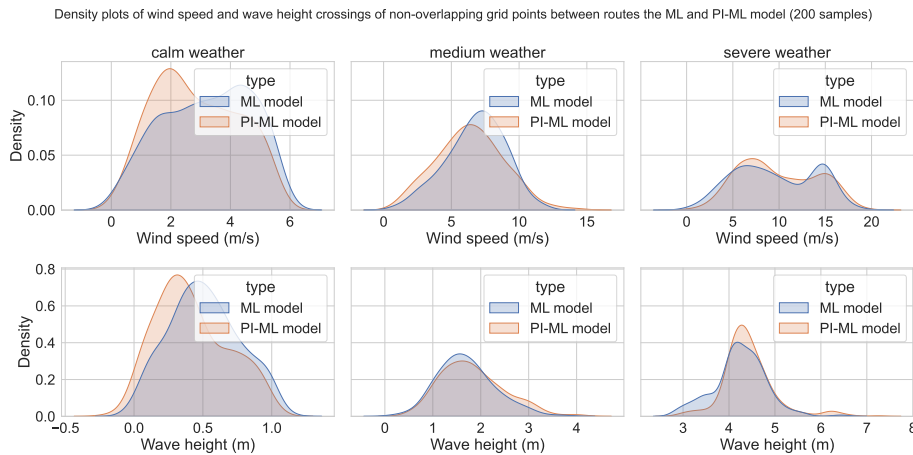


Figure 7.6: Density plot of wind speed and wave height crossings of non-overlapping grid points between routes of the ML and PI-ML models (200 samples)

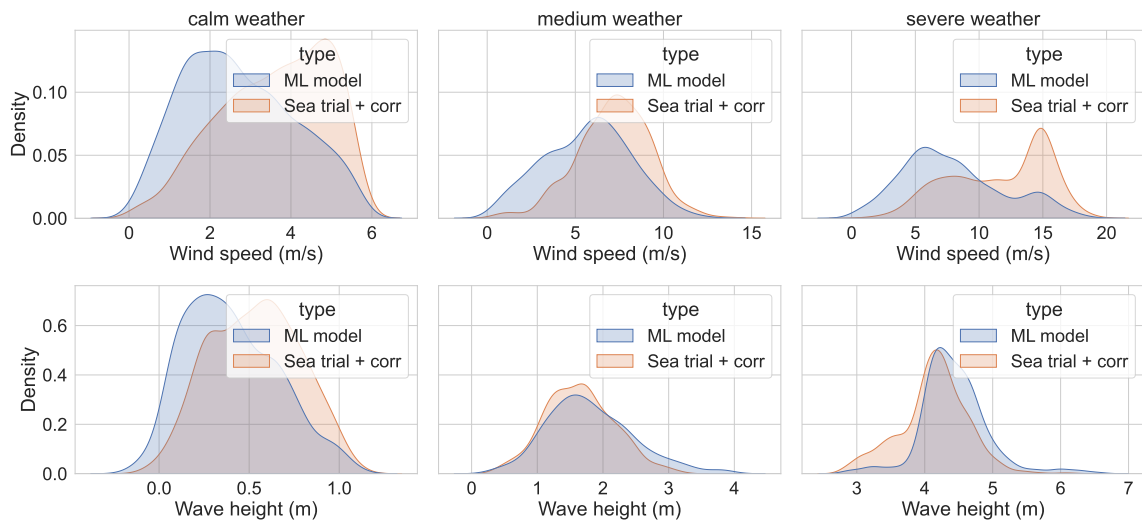
Figure 7.6 only considers the wind speeds and wave heights of the grid points that are crossed by the PI-ML and ML model whenever they do not overlap. The results show that the physics-informed model is more bad weather avoidant in calm weather. In medium and severe weather conditions, the models perform quite similar. In all, they appear to have a similar functional dependency on the weather conditions.

Comparison of the models to the sea trial curve

The aforementioned conclusions are confirmed by figure C.2c. The ML and PI-ML model avoid worse weather more rather than the sea trial curve.

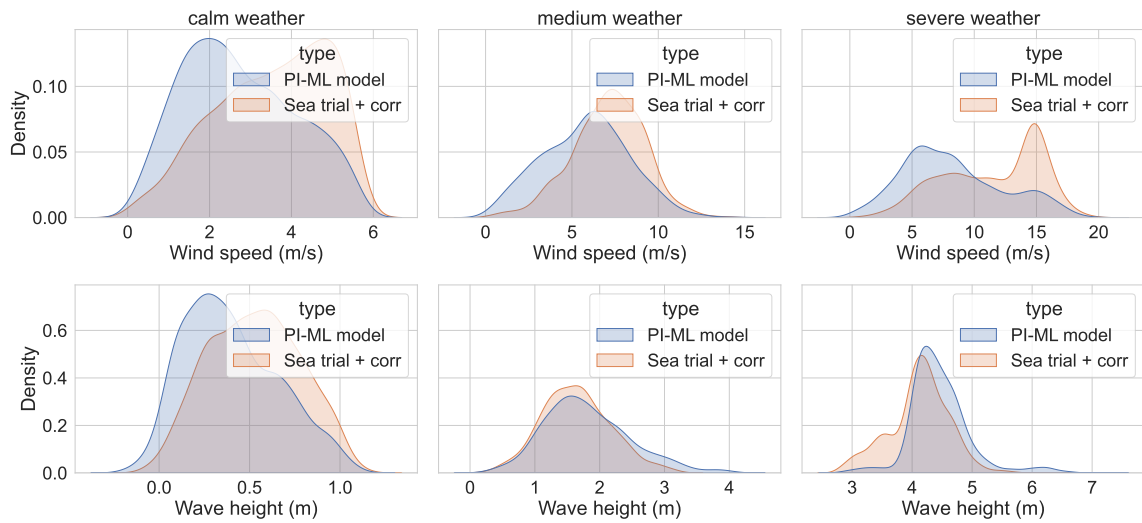
In case of the sea trial curve with correction factor, only the sea trial is preferred in severe weather conditions.

Density plots of wind speed and wave height crossings of non-overlapping grid points between routes the ML model and sea trial + corr (200 samples)



(a) Density plot of wind speed and wave height crossings of non-overlapping grid points between routes of the ML model and sea trial curve with correction

Density plots of wind speed and wave height crossings of non-overlapping grid points between routes the PI-ML model and sea trial + corr (200 samples)



(b) Density plot of wind speed and wave height crossings of non-overlapping grid points between routes of the PI-ML model and sea trial curve with correction

Figure 7.7: Density plots of wind speed and wave height crossings of non-overlapping grid points between routes of the sea trial curve with correction and the ML models (200 samples)

Difference between ML, PI-ML model and the sea trial curve with correction factor

In comparison to the sea trial curve with correction factor, the PI-ML and ML model perform in a similar way. Under each type of weather, the ML model and PI-ML model are more robust against bad weather. In severe weather conditions, the ML models cross slightly higher waves, but this is compensated by crossing lower wind speeds.

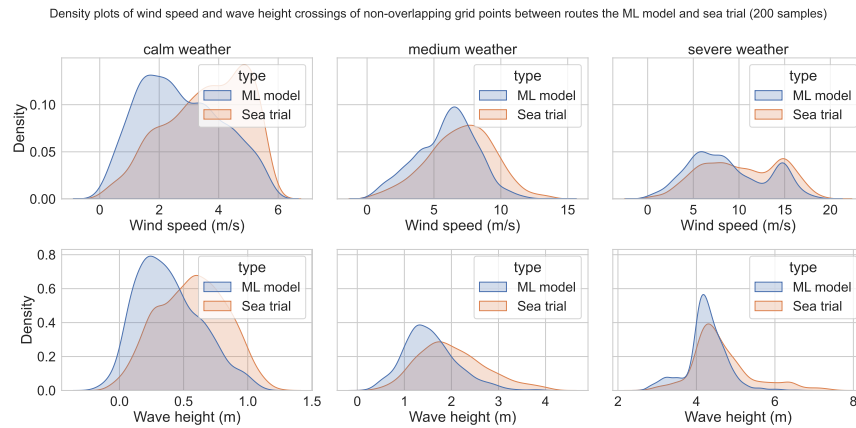
7.5.4 Bias and generalisation of the results

There is a certain bias when comparing the FOC models in terms of avoiding more or less bad weather. The results largely depend on the A-star algorithm as well. In the case that two FOC models are compared to one another, they might deviate or overlap as the power prediction and resulting fuel calculation differs. Individual power predictions and the difference between the models were already examined in chapter 6. In the current chapter however the difference between the models are more or less obsolete and rather the difference between individual predictions of the same model are of importance. Meaning that one should look at how the power in one grid point relates to the power in another grid point predicted by one and the same model.

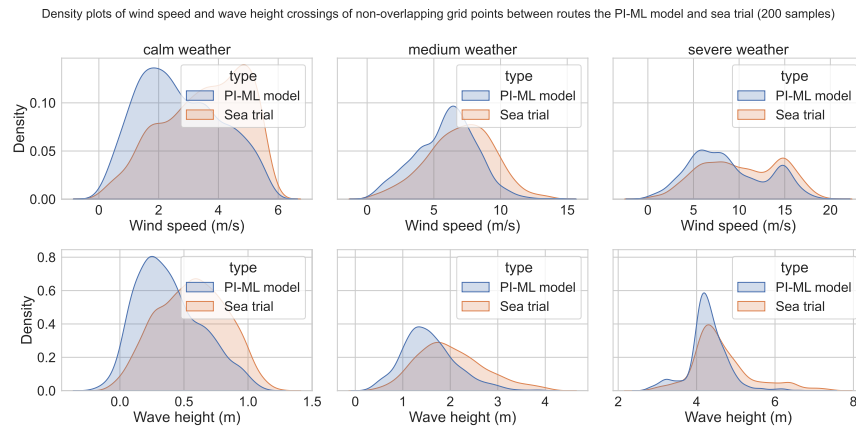
This is essential for the functioning of the A-star algorithm. If the power prediction in one point is much larger than the prediction in an adjacent grid point, this location will not be crossed by the model's route.

The bias in comparing two models in routing establishes itself when a certain model deviates from the route of another model. Whenever they do not overlap, the A-star algorithm considers other neighbouring grid points for which the other model has likely no access to if the deviation is large. If then the neighbouring grid points have more favourable weather conditions, it would seem that the model is more weather avoidant.

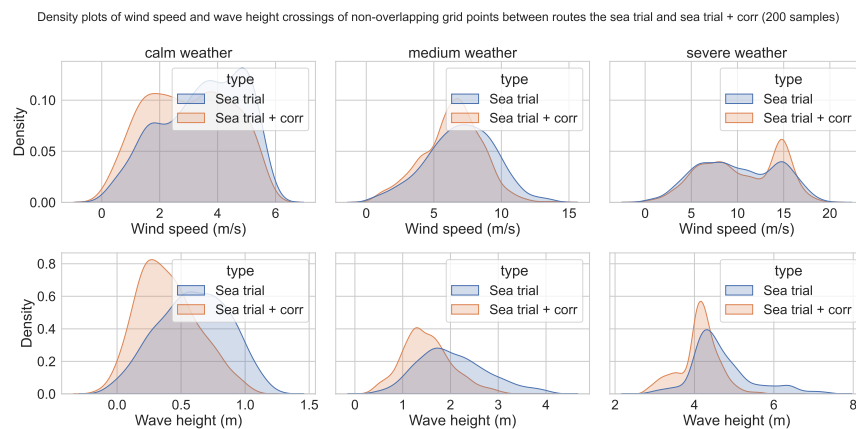
The bias can be mitigated by constructing a grid with random weather conditions and creating a large amount of similar situations, for instance 200 homogeneous grids. This has been applied in the experiments above. In order for the results to be generalized, the experiments were done for 100 homogeneous grids and 200 homogeneous grids. If the results are the same, the bias of the A-star algorithm can be neglected and a reasonable amount of samples have been taken. The results for 100 homogeneous grids can be found in appendix C. Indeed, the results for twice the size of samples are the same.



(a) Density plot of wind speed and wave height crossings of non-overlapping grid points between routes of the ML model and sea trial curve



(b) Density plot of wind speed and wave height crossings of non-overlapping grid points between routes of the PI-ML model and sea trial curve



(c) Density plot of wind speed and wave height crossings of non-overlapping grid points between routes of the sea trial curve with and without correction

Figure 7.8: Density plots of wind speed and wave height crossings of non-overlapping grid points between routes of the sea trial curve and other FOC models (200 samples)

7.6 Fuel optimization results

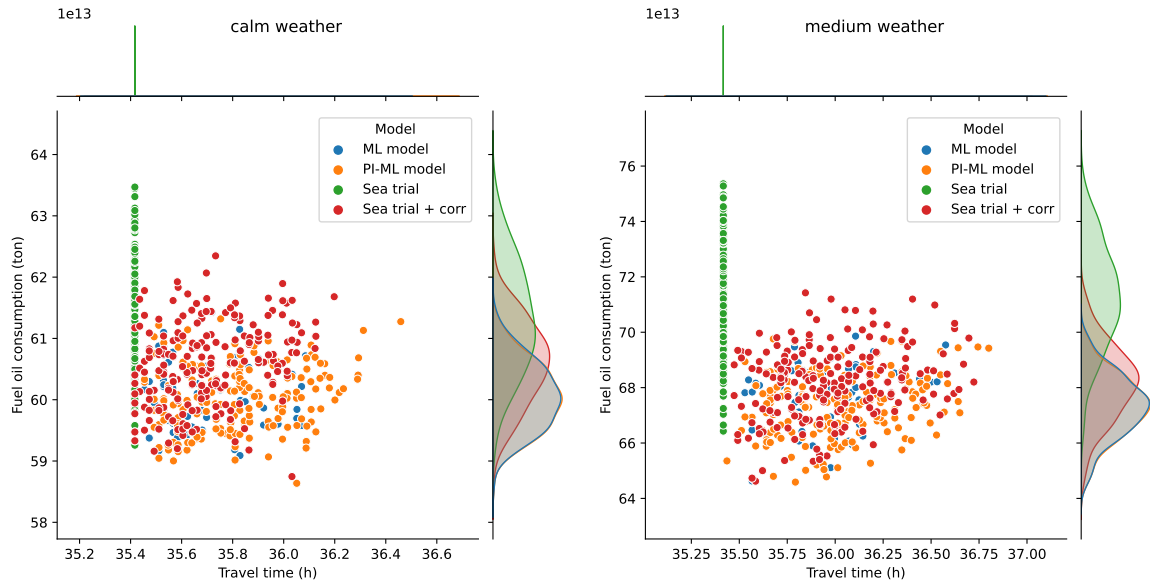
The main goal, besides safety, of optimizing a voyage is minimizing the fuel consumption. According to the methodology stated above, the fuel savings over a route can be quantified. Figure C.2 visually displays the fuel consumption of the routes constructed by each of the FOC models in function of the travel time. The recalculation of the FOC is done here by the physics-informed ML model as ground truth. The results with the ML model as ground truth can be found in appendix C.2.1. Combined with table C.1, the average fuel savings and travel time extensions compared to the shortest route, one can draw the following conclusions.

In calm weather conditions, the average fuel savings of the sea trial curve with correction factor is 1.19%. This percentage doubles if routes are constructed by either the ML and PI-ML model. In essence, the savings gained from implementing one of the ML models are very similar to one another. However, a voyage's travel time does increase on average to a maximum of 1.09%. The travel time of the route's according to the shortest path is 35.67 hours. As such, an 1.09% extension translates to about 20 minutes which is a reasonable extension for the amount of fuel that can be saved.

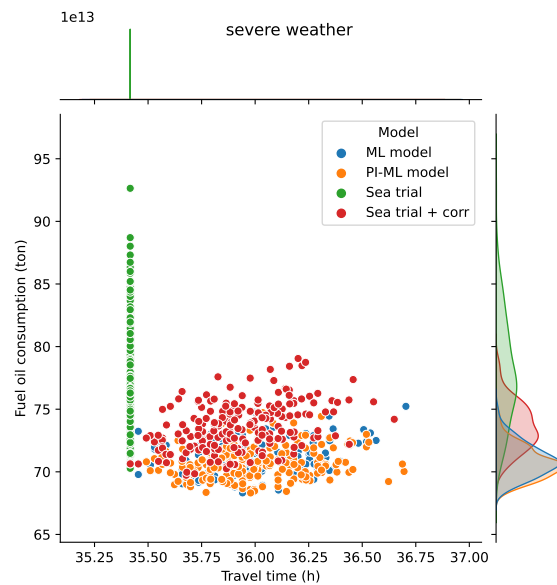
The fuel savings increase to about 5.50% on average when traversing medium weather opposed to calm weather for both the ML models. This is 30% gain over what can be achieved by the sea trial curve with correction factor. However, the shortest path is not followed here and that is why the travel time elongates to a maximum of 1.63%. About 35 minutes are lost in this case. Notice that the travel time is quite similar for the ML models as well as the sea trial curve with correction factor.

In severe weather conditions, the fuel savings are even more apparent, especially if the routes are constructed by the ML models. Maximum savings of about 9.07% can be reached. This translates into a 70% increase in savings over the sea trial curve with correction factor. The travel time remains equivalent to the case of medium weather and remains constant over the models' routes.

Mentioned above are the average values. The standard deviations of the fuel savings and the time extensions are mentioned in appendix C.2.3 and C.2.2. The results with the pure ML model as ground truth are quite similar and are explained in appendix C.2.1.



(a) Fuel consumption in function of travel time - calm weather (b) Fuel consumption in function of travel time - medium weather



(c) Fuel consumption in function of travel time - severe weather

Figure 7.9: Fuel consumption calculated by the PI-ML model in function of travel time for different weather categories (200 samples)

Fuel savings (FS) and time extensions (TE) compared to the shortest route (Sea trial)		FOC model							
		Sea trial		Sea trial + corr		ML model		PI-ML model	
		FS	TE	FS	TE	FS	TE	FS	TE
Weather category	Calm	0.00%	0.00%	1.19%	0.83%	2.07%	0.94%	2.09%	1.09%
	Medium	0.00%	0.00%	4.28%	1.60%	5.48%	1.56%	5.52%	1.63%
	Severe	0.00%	0.00%	5.31%	1.46%	8.75%	1.60%	9.07%	1.46%

Table 7.1: The average fuel savings (FS) and travel time extensions (TE) of an FOC model's route compared to the shortest route (in %) - FOC recalculated by **PI-ML model** as ground truth

Part IV

Conclusion

Chapter 8

General conclusion, limitations and future research

In this chapter, the main conclusions and limitations of this master's dissertation are summarized and future research is proposed. This dissertation was concerned with three parts, the routing algorithm and corresponding methodology, the individual power predictions of the FOC models and lastly the robustness in weather routing of these models. The FOC models considered were the sea trial curve, the sea trial curve with correction factor, the pure ML model and the physics-informed ML model. Both ML models were provided by Toqua and are proved to be the most accurate in predicting the power of a vessel under various weather conditions.

Due to the environmental impact of the shipping industry, the objective of routing was to minimize the FOC over one's route. In comparing the A-star algorithm and the optimized simulated annealing (SA) algorithm, the A-star algorithm was preferred in terms of CPU-time and convergence to the optimal solution with corresponding lower FOC. The main challenge in fine tuning the SA parameters turned out to be defining the correct neighbourhood solution and corresponding operators. As SA is often applied in the travelling salesman problem, few operators that account for a variable path length are known. More research should be devoted to the neighbourhood operators that can be included. In addition, the initial solution turned out to have an influence on the neighbourhood operators as well, but this influence has not been quantified. Therefore, analysing more types of initial solutions and their influence on the final optimization can also be a subject of future research. Some research did encounter these types of issues by relying on the genetic algorithm (GA) heuristic. That is why, besides further optimizing the SA solution, this dissertation can also be complemented by analyzing and optimizing an GA for this case study and comparing this solution to the SA solution.

Apart from the routing algorithm, the FOC models were examined in depth as well. To the purpose of evaluating the FOC models in differing weather conditions, three weather buckets

were set-up: calm, medium and severe weather. How more traditional models such as the sea trial curve and sea trial curve with correction factor operate under varying conditions opposed to the ML models were evaluated. Additionally, the most influential factors on the predictions were determined. The factors that could have a possible impact on the estimations turned out to be the wind speed, the wave height and the relative angle between the heading and the wind/wave direction. As such, 15 scenarios were set-up combining varying wind/wave angles ranging from 0° to 180° and the three weather types to examine the individual predictions of the FOC models.

For all weather types, the predictions tend to approach the sea trial curve's estimate as the relative angle between the wind/wave directions and the heading increases. The variation for each of the models also diminishes along with the increase of the angle. Furthermore, the more severe the weather becomes, the more variation constitutes among the predictions as well. One can also conclude that, for both calm and medium weather, the power predictions of the ML model are the highest on average. For severe weather, this is only true up to an angle of 90° . Moreover, in calm weather conditions the power difference between sea trial curve with correction factor and the physics-informed ML (PI-ML) model is minimal. In medium weather conditions, this is the case for the ML and PI-ML model. For severe weather, the differences between the models' predictions are larger. Consequently, one should rely on the most accurate model, the PI-ML model, when dealing with routing.

In the future, it could also be valuable to look at the difference in predictions of the FOC models in terms of the angle. For instance, how large is the drop in power on average between an angle of 0° and 45° for each of the models? This is valuable as weather routing algorithms such as A-star are concerned with the minimal difference in predictions of the models itself. If going in a 45° direction is the same for one FOC model opposed to another, they are more likely to follow the same route. However, it will still depend largely on the similarity in weather sensitivity as well.

Mentioned earlier, route optimization can be beneficial for the safety and the fuel efficiency. Both aspects were evaluated in the second experimental part of this thesis. In terms of weather avoidance, the physics-informed ML model and pure ML model are very similar. They tend to better at bad weather avoidance compared to the other state-to-art models under any weather circumstance. Comparing both ML models, the physics-informed ML model is slightly more weather avoidant, especially in calm weather. Some additional trials can be of use in generalizing the results in which the angle between the wind/wave direction and the heading is also randomized. In the current experimental set-up, the angle remains either 0° , 45° , 90° or 180° . Adding to this, the effect of the granularity of the grid and the size of the geographical area should be accounted for. In future research, different start and end points, different grid sizes, varying granularity and their influence of the routing algorithm as

well as the FOC models could be explored.

In term of fuel efficiency, one can also conclude that the ML models account for more fuel savings compared to the shortest route. A maximum of 9% fuel savings on average can be reached. The savings enlarge as the weather becomes more severe. The travel time does extend when deviating from the shortest path to a maximum of 1.63% in medium weather conditions which corresponds to an elongation of about 35 minutes on a 35 hour voyage. The extension is significant compared to travel time of the sea trial curve's route. However, between the remaining models' routes, the travel time only slightly differs. Opposed to the sea trial curve with correction factor, the savings of the ML models contribute to a 70% gain in calm and severe weather and a 30% increase in medium weather. In the future, the experiments can also be performed for a Beaufort number ranging from 0 to 7 without distinction between weather types. In this case, one should pay attention to the randomization to resemble the reality which should be accompanied by a great number of samples. Currently, the speed is kept constant. Changing the speed to account for equal travel times for each of the models under changing weather scenarios could further enhance the fuel efficiency experiments. Even more realistic savings can be quantified in this way. In this master's dissertation, dynamic weather forecasts were not considered. In exploring, dynamic rather than static weather conditions, the D-star algorithm can be applied and examined in order to quantify an optimal solution.

In all, the ML models of Toqua are said to be bad-weather-avoidant and account for more fuel savings than frequently used performance models in the shipping industry. ML models based on ANNs were already proven to be highly accurate in predicting ship performance measures, but they turned out to be also the most robust in weather routing. This master's dissertation served as a comprehensive framework in comparing different performance models and emphasis lies on making an informed decision in using these models in routing.

Part V

Appendices

Appendix A

The simulated annealing heuristic

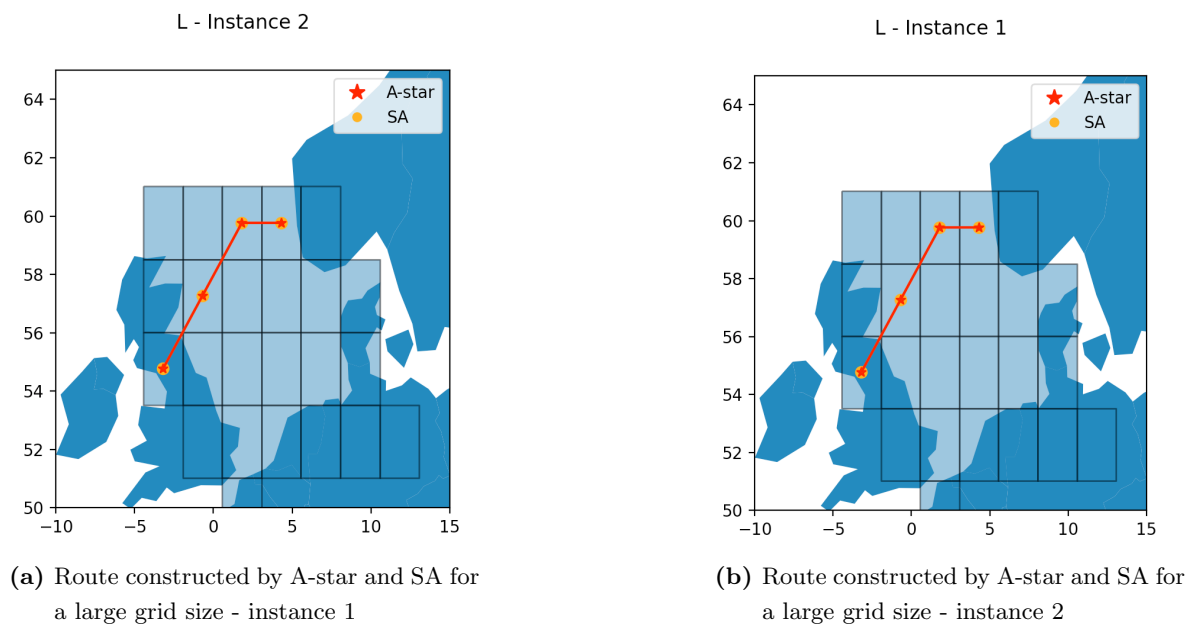


Figure A.1: Routes constructed by A-star and SA for a large grid size

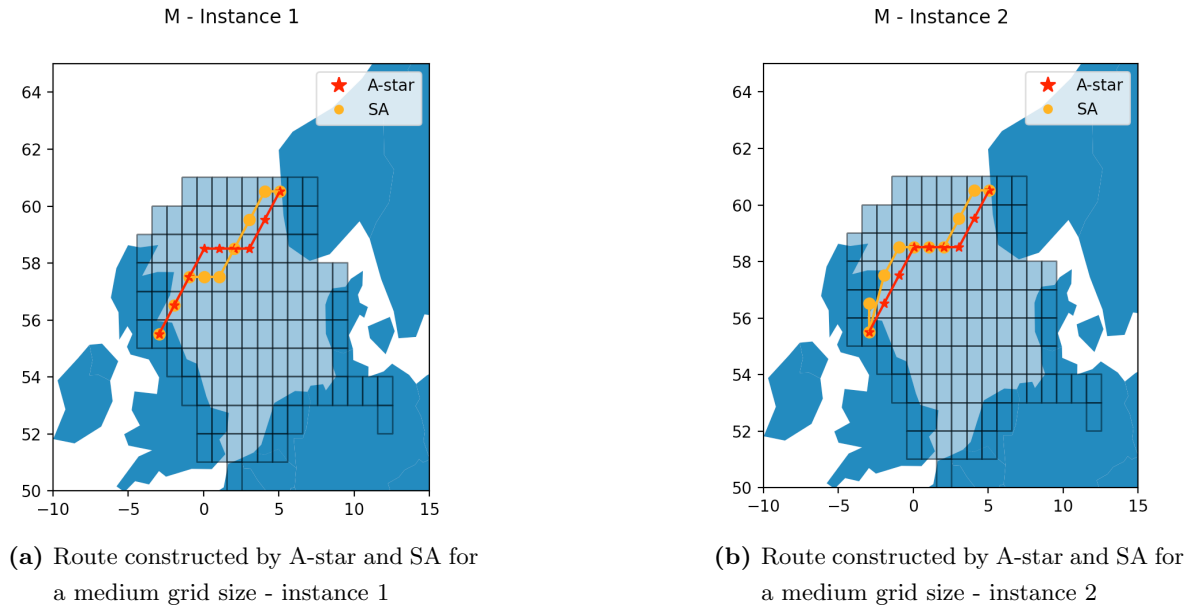


Figure A.2: Routes constructed by A-star and SA for a medium grid size

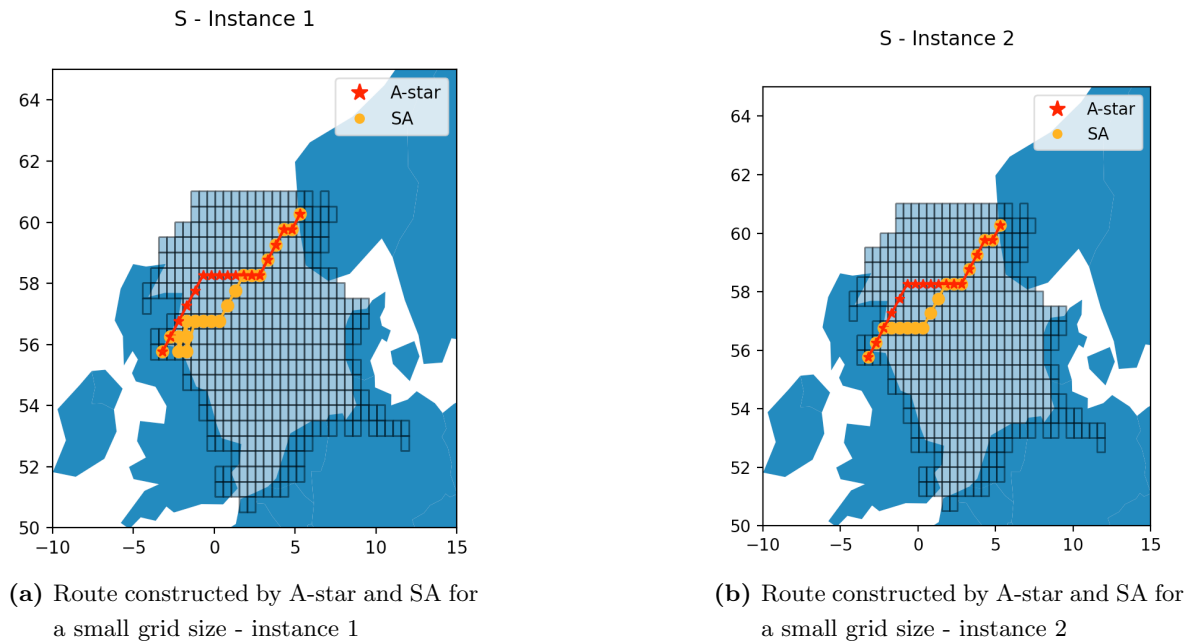


Figure A.3: Routes constructed by A-star and SA for a small grid size

Appendix B

Power prediction per weather category

B.1 Impact of the weather severity

B.1.1 The mean of the power predictions

Calm weather

		Wind/wave direction				
		0°	45°	90°	135°	180°
Model	ML model	11176.41	11016.65	10638.2	10269.89	10120.27
	PI-ML model	10787.55	10596.92	10158.99	9734.67	9534.65
	Sea trial	9396	9396	9396	9396	9396
	Sea trial + corr	10878.42	10686.76	10255.72	9872.17	9727.0

Table B.1: The mean power prediction per model and wind/wave direction expressed in kW for calm weather (10,000 samples)

Medium weather

		Wind/wave direction				
		0°	45°	90°	135°	180°
Model	ML model	13587.39	13068.03	11875.29	10766.26	10330.6
	PI-ML model	113335.36	12741.12	11499.37	10464.57	10043.13
	Sea trial	9396	9396	9396	9396	9396
	Sea trial + corr	12853.76	12309.49	11117.05	10127.84	9788.71

Table B.2: The mean power prediction per model and wind/wave direction expressed in kW for medium weather (10,000 samples)

Severe weather

		Wind/wave direction				
		0°	45°	90°	135°	180°
Model	ML model	20532.42	18818.37	15098.14	11930.7	10769.45
	PI-ML model	20282.69	18023.3	14187.65	11726.69	10933.31
	Sea trial	9396	9396	9396	9396	9396
	Sea trial + corr	18679.21	17381.04	14496.54	12063.17	11272.96

Table B.3: The mean power prediction per model and wind/wave direction expressed in kW for severe weather (10,000 samples)

B.1.2 The standard deviation of the power predictions**Calm weather**

		Wind/wave direction				
		0°	45°	90°	135°	180°
Model	ML model	363.44	302.51	178.29	144.47	170.84
	PI-ML model	432.09	359.32	226.95	200.5	242.44
	Sea trial	0	0	0	0	0
	Sea trial + corr	320.68	236.19	67.85	119.87	170.2

Table B.4: The standard deviation of the power prediction per model and wind/wave direction expressed in kW for calm weather (10,000 samples)

Medium weather

		Wind/wave direction				
		0°	45°	90°	135°	180°
Model	ML model	1429.2	1200.91	709.34	342.73	278.01
	PI-ML model	1417.61	1145.62	674.82	441.81	424.49
	Sea trial	0	0	0	0	0
	Sea trial + corr	1242.39	1037.56	628.23	371.71	313.02

Table B.5: The standard deviation of the power prediction per model and wind/wave direction expressed in kW for medium weather (10,000 samples)

Severe weather

		Wind/wave direction				
		0°	45°	90°	135°	180°
Model	ML model	3375.86	2688.03	1319.17	377.45	264.36
	PI-ML model	3910.45	2598.06	842.18	526.54	577.06
	Sea trial	0	0	0	0	0
	Sea trial + corr	2571.6	2193.0	1445.08	918.24	718.07

Table B.6: The standard deviation of the power prediction per model and wind/wave direction expressed in kW for severe weather (10,000 samples)

B.1.3 The mean of the power difference**Calm weather**

		Benchmark model - original power			
		ML model	PI-ML model	Sea trial	Sea trial + corr
New power	ML model	0.0	4.12	19.01	3.17
	PI-ML model	-4.12	0.0	14.89	-0.95
	Sea trial	-19.01	-14.89	0.0	-15.84
	Sea trial + corr	-3.17	0.95	15.84	0.0

Table B.7: The mean, relative power difference between models for a wind and wave direction of 0° expressed in % for calm weather (10,000 samples)

		Benchmark model - original power			
		ML model	PI-ML model	Sea trial	Sea trial + corr
New power	ML model	0.0	4.45	17.3	3.51
	PI-ML model	-4.45	0.0	12.84	-0.94
	Sea trial	-17.3	-12.84	0.0	-13.78
	Sea trial + corr	-3.51	0.94	13.78	0.0

Table B.8: The mean, relative power difference between models for a wind and wave direction of 45° expressed in % for calm weather (10,000 samples)

		Benchmark model - original power			
		ML model	PI-ML model	Sea trial	Sea trial + corr
New power	ML model	0.0	5.09	13.23	4.08
	PI-ML model	-5.09	0.0	8.14	-1.01
	Sea trial	-13.23	-8.14	0.0	-9.16
	Sea trial + corr	-4.08	1.01	9.16	0.0

Table B.9: The mean, relative power difference between models for a wind and wave direction of 90° expressed in % for calm weather (10,000 samples)

		Benchmark model - original power			
		ML model	PI-ML model	Sea trial	Sea trial + corr
New power	ML model	0.0	5.69	9.28	4.24
	PI-ML model	-5.69	0.0	3.59	-1.45
	Sea trial	-9.28	-3.59	0.0	-5.04
	Sea trial + corr	-4.24	1.45	5.04	0.0

Table B.10: The mean, relative power difference between models for a wind and wave direction of 135° expressed in % for calm weather (10,000 samples)

		Benchmark model - original power			
		ML model	PI-ML model	Sea trial	Sea trial + corr
New power	ML model	0.0	6.23	7.68	4.19
	PI-ML model	-6.23	0.0	1.44	-2.04
	Sea trial	-7.68	-1.44	0.0	-3.48
	Sea trial + corr	-4.19	2.04	3.48	0.0

Table B.11: The mean, relative power difference between models for a wind and wave direction of 180° expressed in % for calm weather (10,000 samples)

Medium weather

		Benchmark model - original power			
		ML model	PI-ML model	Sea trial	Sea trial + corr
New power	ML model	0.0	2.66	44.7	7.8
	PI-ML model	-2.66	0.0	42.03	5.14
	Sea trial	-44.7	-42.03	0.0	-36.89
	Sea trial + corr	-7.8	-5.14	36.89	0.0

Table B.12: The mean, relative power difference between models for a wind and wave direction of 0° expressed in % for medium weather (10,000 samples)

		Benchmark model - original power			
		ML model	PI-ML model	Sea trial	Sea trial + corr
New power	ML model	0.0	3.47	39.15	8.08
	PI-ML model	-3.47	0.0	35.68	4.61
	Sea trial	-39.15	-35.68	0.0	-31.07
	Sea trial + corr	-8.08	-4.61	31.07	0.0

Table B.13: The mean, relative power difference between models for a wind and wave direction of 45° expressed in % for medium weather (10,000 samples)

		Benchmark model - original power			
		ML model	PI-ML model	Sea trial	Sea trial + corr
New power	ML model	0.0	4.0	26.41	8.09
	PI-ML model	-4.0	0.0	22.4	4.08
	Sea trial	-26.41	-22.4	0.0	-18.32
	Sea trial + corr	-8.09	-4.08	18.32	0.0

Table B.14: The mean, relative power difference between models for a wind and wave direction of 90° expressed in % for medium weather (10,000 samples)

		Benchmark model - original power			
		ML model	PI-ML model	Sea trial	Sea trial + corr
New power	ML model	0.0	3.21	14.56	6.81
	PI-ML model	-3.21	0.0	11.35	3.59
	Sea trial	-14.56	-11.35	0.0	-7.75
	Sea trial + corr	-6.81	-3.59	7.75	0.0

Table B.15: The mean, relative power difference between models for a wind and wave direction of 135° expressed in % for medium weather (10,000 samples)

		Benchmark model - original power			
		ML model	PI-ML model	Sea trial	Sea trial + corr
New power	ML model	0.0	3.06	9.91	5.77
	PI-ML model	-3.06	0.0	6.85	2.71
	Sea trial	-9.91	-6.85	0.0	-4.13
	Sea trial + corr	-5.77	-2.71	4.13	0.0

Table B.16: The mean, relative power difference between models for a wind and wave direction of 180° expressed in % for medium weather (10,000 samples)

Severe weather

		Benchmark model - original power			
		ML model	PI-ML model	Sea trial	Sea trial + corr
New power	ML model	0.0	2.77	118.62	19.76
	PI-ML model	-2.77	0.0	115.85	17.0
	Sea trial	-118.62	-115.85	0.0	-98.85
	Sea trial + corr	-19.76	-17.0	98.85	0.0

Table B.17: The mean, relative power difference between models for a wind and wave direction of 0° expressed in % for severe weather (10,000 samples)

		Benchmark model - original power			
		ML model	PI-ML model	Sea trial	Sea trial + corr
New power	ML model	0.0	8.54	100.37	15.29
	PI-ML model	-8.54	0.0	91.83	6.76
	Sea trial	-100.37	-91.83	0.0	-85.08
	Sea trial + corr	-15.29	-6.76	85.08	0.0

Table B.18: The mean, relative power difference between models for a wind and wave direction of 45° expressed in % for severe weather (10,000 samples)

		Benchmark model - original power			
		ML model	PI-ML model	Sea trial	Sea trial + corr
New power	ML model	0.0	9.68	60.77	6.32
	PI-ML model	-9.68	0.0	51.09	-3.36
	Sea trial	-60.77	-51.09	0.0	-54.45
	Sea trial + corr	-6.32	3.36	54.45	0.0

Table B.19: The mean, relative power difference between models for a wind and wave direction of 90° expressed in % for severe weather (10,000 samples)

		Benchmark model - original power			
		ML model	PI-ML model	Sea trial	Sea trial + corr
New power	ML model	0.0	2.11	27.05	-1.51
	PI-ML model	-2.11	0.0	24.94	-3.62
	Sea trial	-27.05	-24.94	0.0	-28.55
	Sea trial + corr	1.51	3.62	28.55	0.0

Table B.20: The mean, relative power difference between models for a wind and wave direction of 135° expressed in % for severe weather (10,000 samples)

		Benchmark model - original power			
		ML model	PI-ML model	Sea trial	Sea trial + corr
New power	ML model	0.0	-1.81	14.69	-5.43
	PI-ML model	1.81	0.0	16.5	-3.61
	Sea trial	-14.69	-16.5	0.0	-20.11
	Sea trial + corr	5.43	3.61	20.11	0.0

Table B.21: The mean, relative power difference between models for a wind and wave direction of 180° expressed in % for severe weather (10,000 samples)

B.1.4 The standard deviation of the power difference

Calm weather

		Benchmark model - original power			
		ML model	PI-ML model	Sea trial	Sea trial + corr
New power	ML model	0.0	0.88	3.33	1.08
	PI-ML model	0.88	0.0	4.19	1.66
	Sea trial	3.33	4.19	0.0	3.22
	Sea trial + corr	1.08	1.66	3.22	0.0

Table B.22: The standard deviation of the relative power difference between models for a wind and wave direction of 0° expressed in % for calm weather (10,000 samples)

		Benchmark model - original power			
		ML model	PI-ML model	Sea trial	Sea trial + corr
New power	ML model	0.0	0.74	2.75	1.06
	PI-ML model	0.74	0.0	3.46	1.68
	Sea trial	2.75	3.46	0.0	2.33
	Sea trial + corr	1.06	1.68	2.33	0.0

Table B.23: The standard deviation of the relative power difference between models for a wind and wave direction of 45° expressed in % for calm weather (10,000 samples)

		Benchmark model - original power			
		ML model	PI-ML model	Sea trial	Sea trial + corr
New power	ML model	0.0	0.61	1.62	1.11
	PI-ML model	0.61	0.0	2.21	1.71
	Sea trial	1.62	2.21	0.0	0.55
	Sea trial + corr	1.11	1.71	0.55	0.0

Table B.24: The standard deviation of the relative power difference between models for a wind and wave direction of 90° expressed in % for calm weather (10,000 samples)

		Benchmark model - original power			
		ML model	PI-ML model	Sea trial	Sea trial + corr
New power	ML model	0.0	0.63	1.56	1.12
	PI-ML model	0.63	0.0	2.15	1.68
	Sea trial	1.56	2.15	0.0	1.28
	Sea trial + corr	1.12	1.68	1.28	0.0

Table B.25: The standard deviation of the relative power difference between models for a wind and wave direction of 135° expressed in % for calm weather (10,000 samples)

		Benchmark model - original power			
		ML model	PI-ML model	Sea trial	Sea trial + corr
New power	ML model	0.0	0.76	1.9	1.09
	PI-ML model	0.76	0.0	2.64	1.63
	Sea trial	1.9	2.64	0.0	1.81
	Sea trial + corr	1.09	1.63	1.81	0.0

Table B.26: The standard deviation of the relative power difference between models for a wind and wave direction of 180° expressed in % for calm weather (10,000 samples)

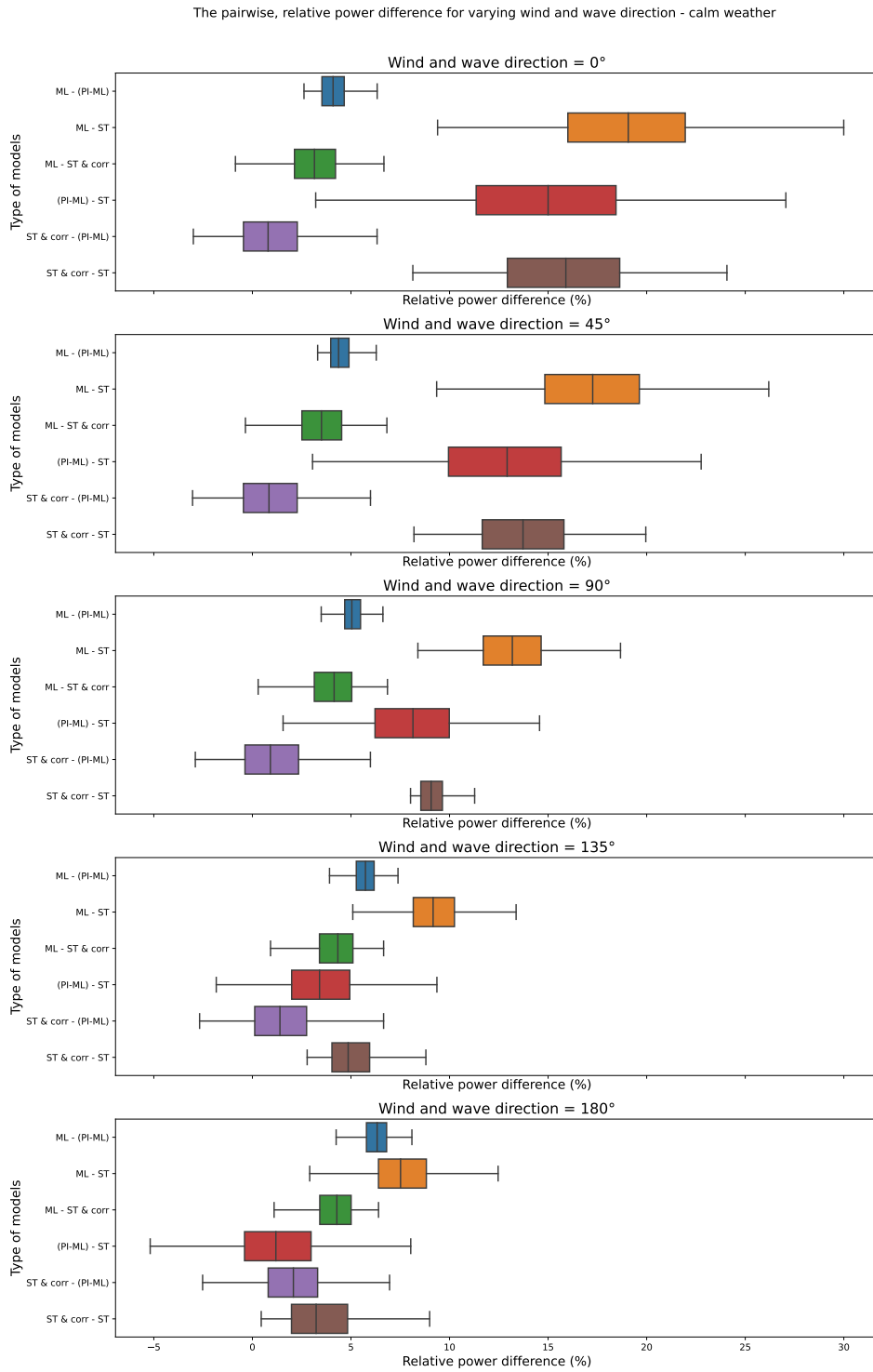


Figure B.1: The pairwise, relative power difference for different wind/wave directions - calm weather

Medium weather

		Benchmark model - original power			
		ML model	PI-ML model	Sea trial	Sea trial + corr
New power	ML model	0.0	1.76	8.29	1.35
	PI-ML model	1.76	0.0	9.89	1.48
	Sea trial	8.29	9.89	0.0	9.0
	Sea trial + corr	1.35	1.48	9.0	0.0

Table B.27: The standard deviation of the relative power difference between models for a wind and wave direction of 0° expressed in % for medium weather (10,000 samples)

		Benchmark model - original power			
		ML model	PI-ML model	Sea trial	Sea trial + corr
New power	ML model	0.0	1.09	7.16	1.03
	PI-ML model	1.09	0.0	8.09	1.37
	Sea trial	7.16	8.09	0.0	7.35
	Sea trial + corr	1.03	1.37	7.35	0.0

Table B.28: The standard deviation of the relative power difference between models for a wind and wave direction of 45° expressed in % for medium weather (10,000 samples)

		Benchmark model - original power			
		ML model	PI-ML model	Sea trial	Sea trial + corr
New power	ML model	0.0	0.85	4.91	1.08
	PI-ML model	0.85	0.0	5.35	1.32
	Sea trial	4.91	5.35	0.0	4.68
	Sea trial + corr	1.08	1.32	4.68	0.0

Table B.29: The standard deviation of the relative power difference between models for a wind and wave direction of 90° expressed in % for medium weather (10,000 samples)

		Benchmark model - original power			
		ML model	PI-ML model	Sea trial	Sea trial + corr
New power	ML model	0.0	1.09	3.88	0.98
	PI-ML model	1.09	0.0	4.85	1.37
	Sea trial	3.88	4.85	0.0	4.14
	Sea trial + corr	0.98	1.37	4.14	0.0

Table B.30: The standard deviation of the relative power difference between models for a wind and wave direction of 135° expressed in % for medium weather (10,000 samples)

		Benchmark model - original power			
		ML model	PI-ML model	Sea trial	Sea trial + corr
New power	ML model	0.0	1.42	3.96	1.2
	PI-ML model	1.42	0.0	5.25	1.62
	Sea trial	3.96	5.25	0.0	4.29
	Sea trial + corr	1.2	1.62	4.29	0.0

Table B.31: The standard deviation of the relative power difference between models for a wind and wave direction of 180° expressed in % for medium weather (10,000 samples)

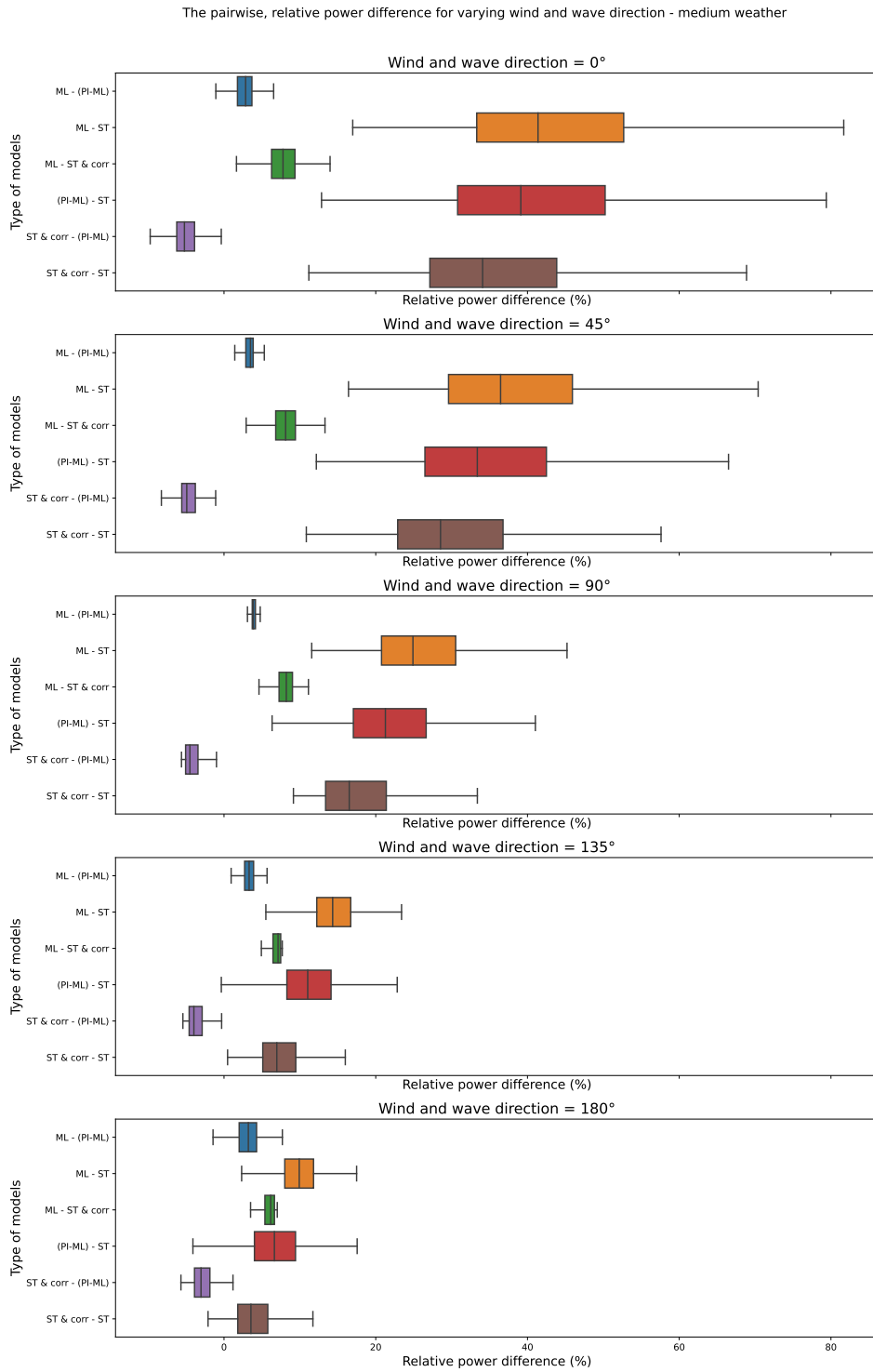


Figure B.2: The pairwise, relative power difference for different wind/wave directions - medium weather

Severe weather

		Benchmark model - original power			
		ML model	PI-ML model	Sea trial	Sea trial + corr
New power	ML model	0.0	3.9	14.42	5.06
	PI-ML model	3.9	0.0	16.43	6.79
	Sea trial	14.42	16.43	0.0	17.65
	Sea trial + corr	5.06	6.79	17.65	0.0

Table B.32: The standard deviation of the relative power difference between models for a wind and wave direction of 0° expressed in % for severe weather (10,000 samples)

		Benchmark model - original power			
		ML model	PI-ML model	Sea trial	Sea trial + corr
New power	ML model	0.0	2.34	11.99	5.05
	PI-ML model	2.34	0.0	11.33	6.56
	Sea trial	11.99	11.33	0.0	14.67
	Sea trial + corr	5.05	6.56	14.67	0.0

Table B.33: The standard deviation of the relative power difference between models for a wind and wave direction of 45° expressed in % for severe weather (10,000 samples)

		Benchmark model - original power			
		ML model	PI-ML model	Sea trial	Sea trial + corr
New power	ML model	0.0	3.9	7.0	5.67
	PI-ML model	3.9	0.0	4.01	6.71
	Sea trial	7.0	4.01	0.0	10.6
	Sea trial + corr	5.67	6.71	10.6	0.0

Table B.34: The standard deviation of the relative power difference between models for a wind and wave direction of 90° expressed in % for severe weather (10,000 samples)

		Benchmark model - original power			
		ML model	PI-ML model	Sea trial	Sea trial + corr
New power	ML model	0.0	4.14	4.63	5.75
	PI-ML model	4.14	0.0	5.84	7.0
	Sea trial	4.63	5.84	0.0	10.24
	Sea trial + corr	5.75	7.0	10.24	0.0

Table B.35: The standard deviation of the relative power difference between models for a wind and wave direction of 135° expressed in % for severe weather (10,000 samples)

		Benchmark model - original power			
		ML model	PI-ML model	Sea trial	Sea trial + corr
New power	ML model	0.0	3.61	5.01	5.98
	PI-ML model	3.61	0.0	7.1	7.73
	Sea trial	5.01	7.1	0.0	10.24
	Sea trial + corr	5.98	7.73	10.24	0.0

Table B.36: The standard deviation of the relative power difference between models for a wind and wave direction of 180° expressed in % for severe weather (10,000 samples)

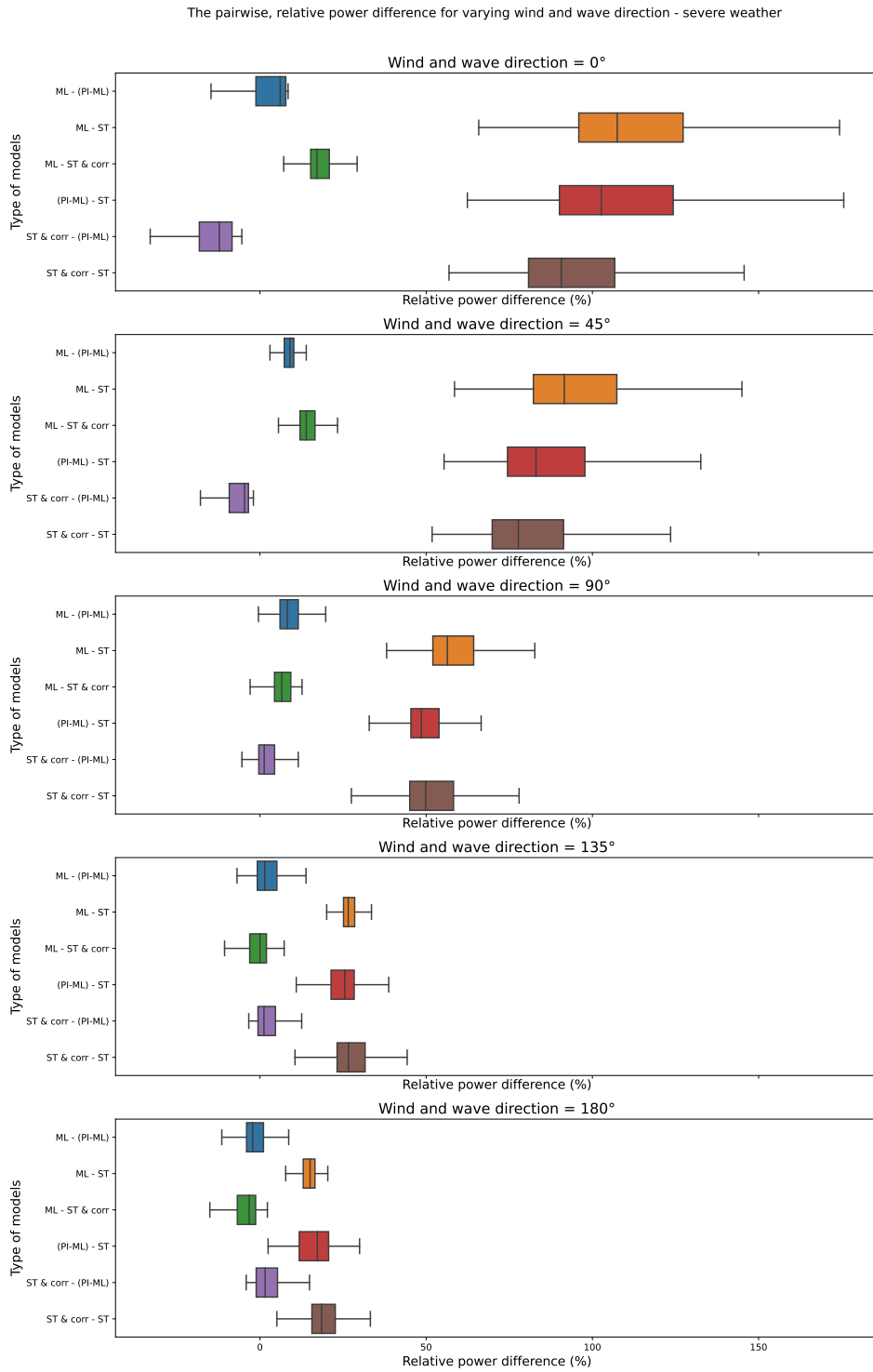
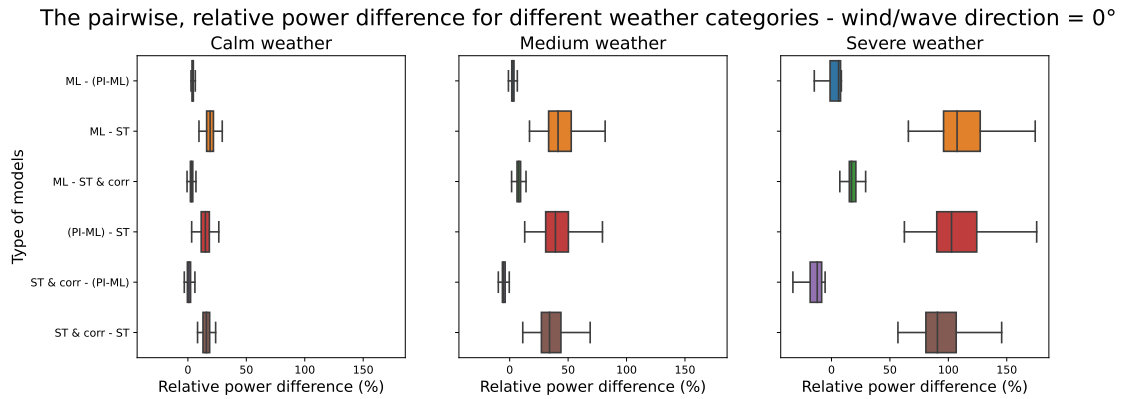
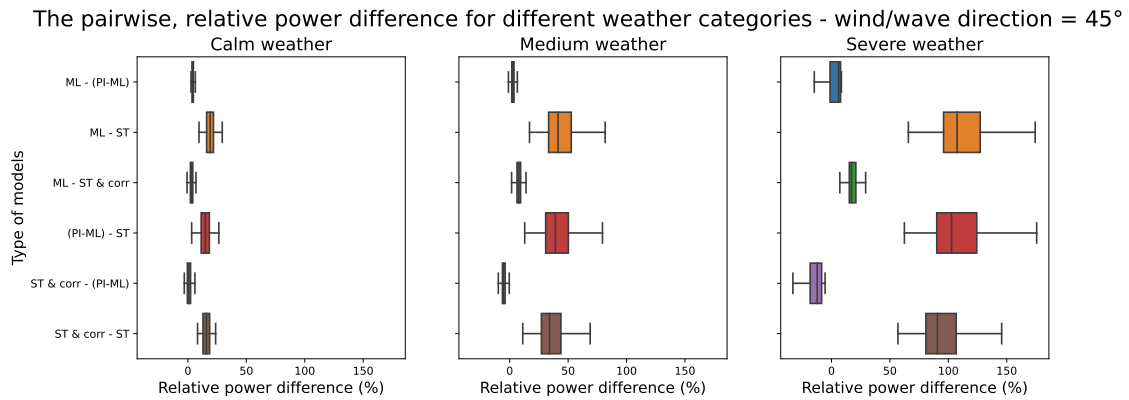


Figure B.3: The pairwise, relative power difference for different wind/wave directions - severe weather

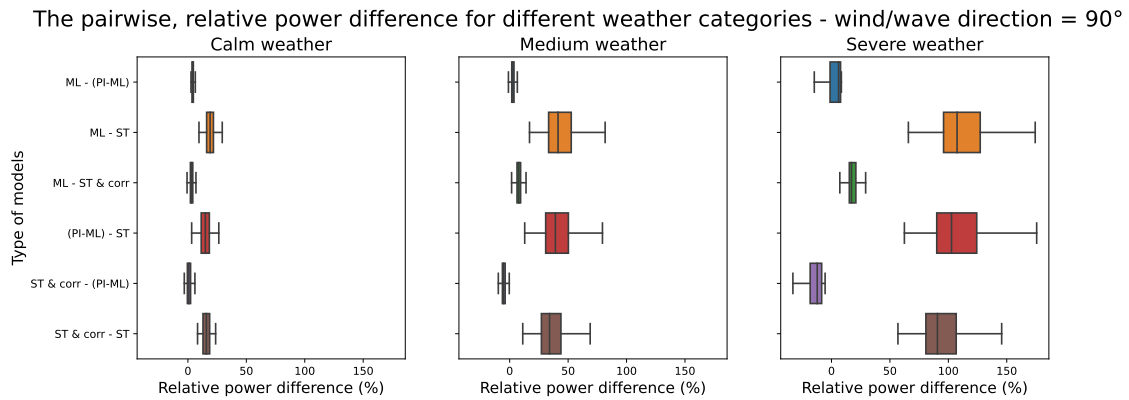
Visualization variation between power difference per wind/wave direction



(a) The pairwise, relative power difference for different weather categories - wind/wave direction = 0°

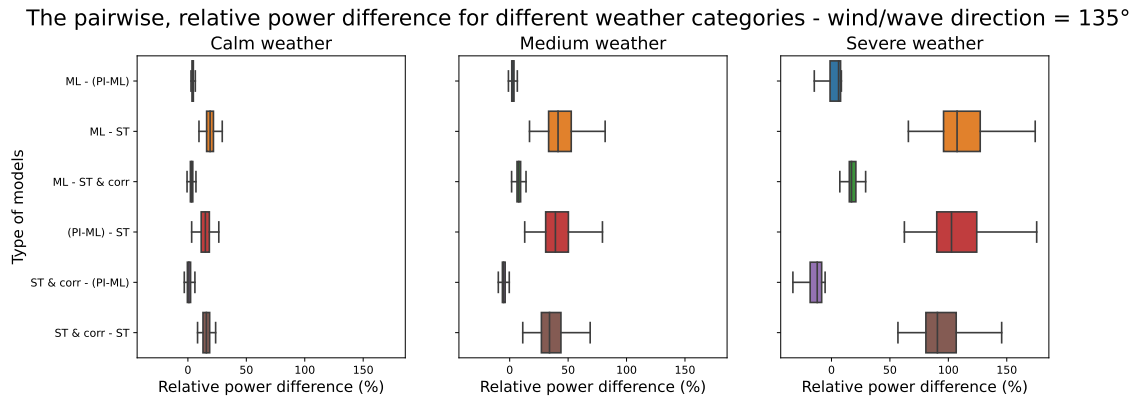


(b) The pairwise, relative power difference for different weather categories - wind/wave direction = 45°

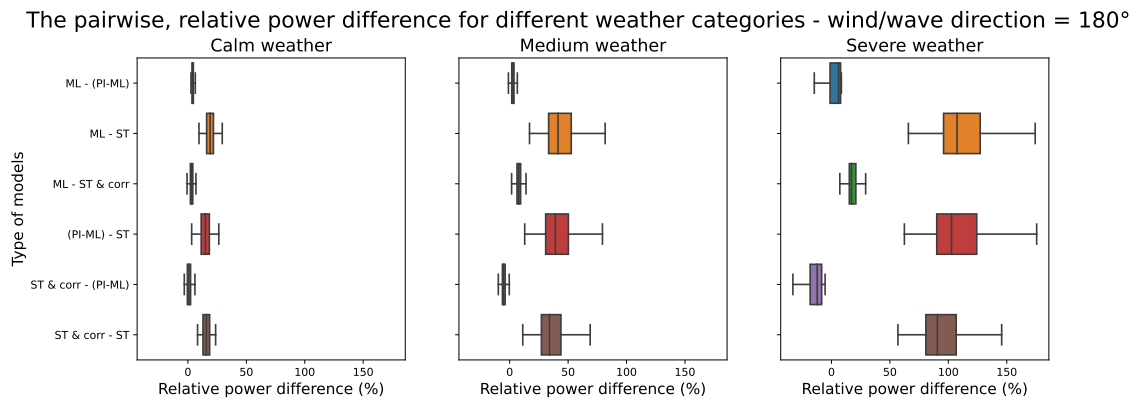


(c) The pairwise, relative power difference for different weather categories - wind/wave direction = 90°

Figure B.4: The pairwise, relative power difference for different weather categories and different wind/wave direction - part 1



(a) The pairwise, relative power difference for different weather categories - wind/wave direction = 135°



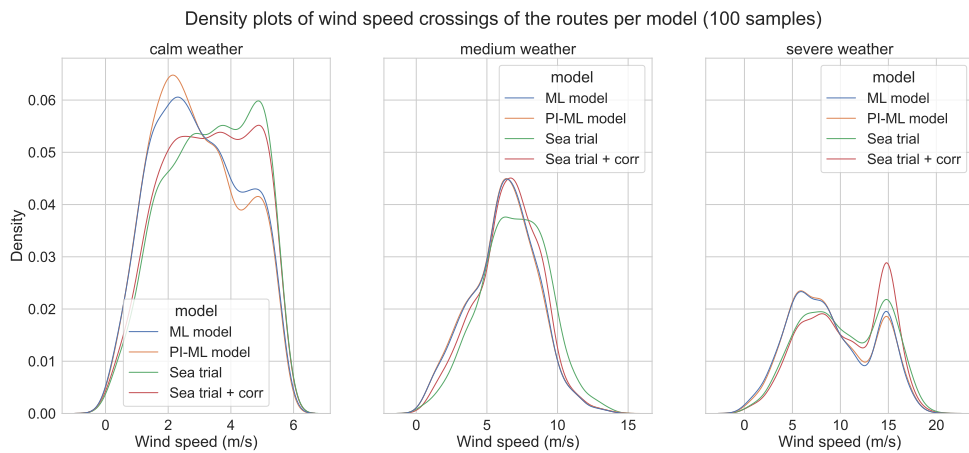
(b) The pairwise, relative power difference for different weather categories - wind/wave direction = 180°

Figure B.5: The pairwise, relative power difference for different weather categories and different wind/wave direction - part 2

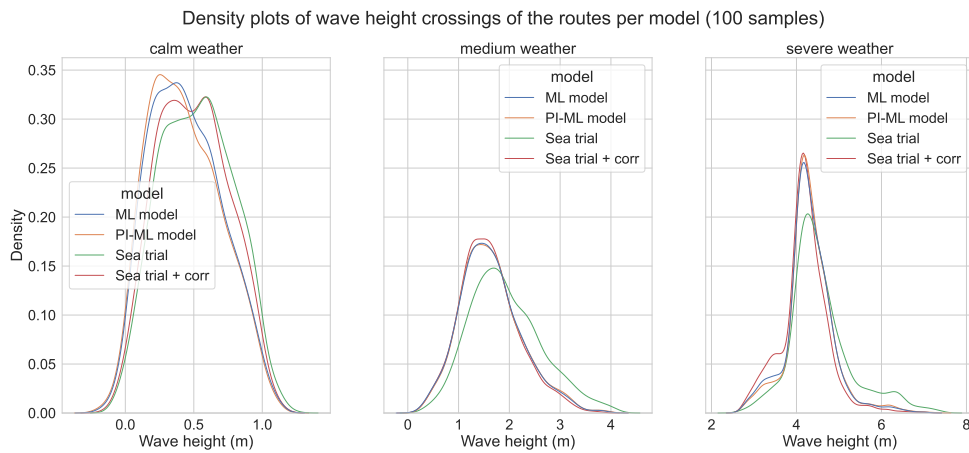
Appendix C

Robustness in route optimization

C.1 Sensitivity results: 100 samples



(a) Density plot of wind speed crossings per weather category and FOC model



(b) Density plot of wave height crossings per weather category and FOC model

Figure C.1: Density plots of wind speed and wave height crossings of FOC models' routes per weather category (100 samples)

C.2 Fuel efficiency results

C.2.1 The fuel savings with the pure ML model as ground truth

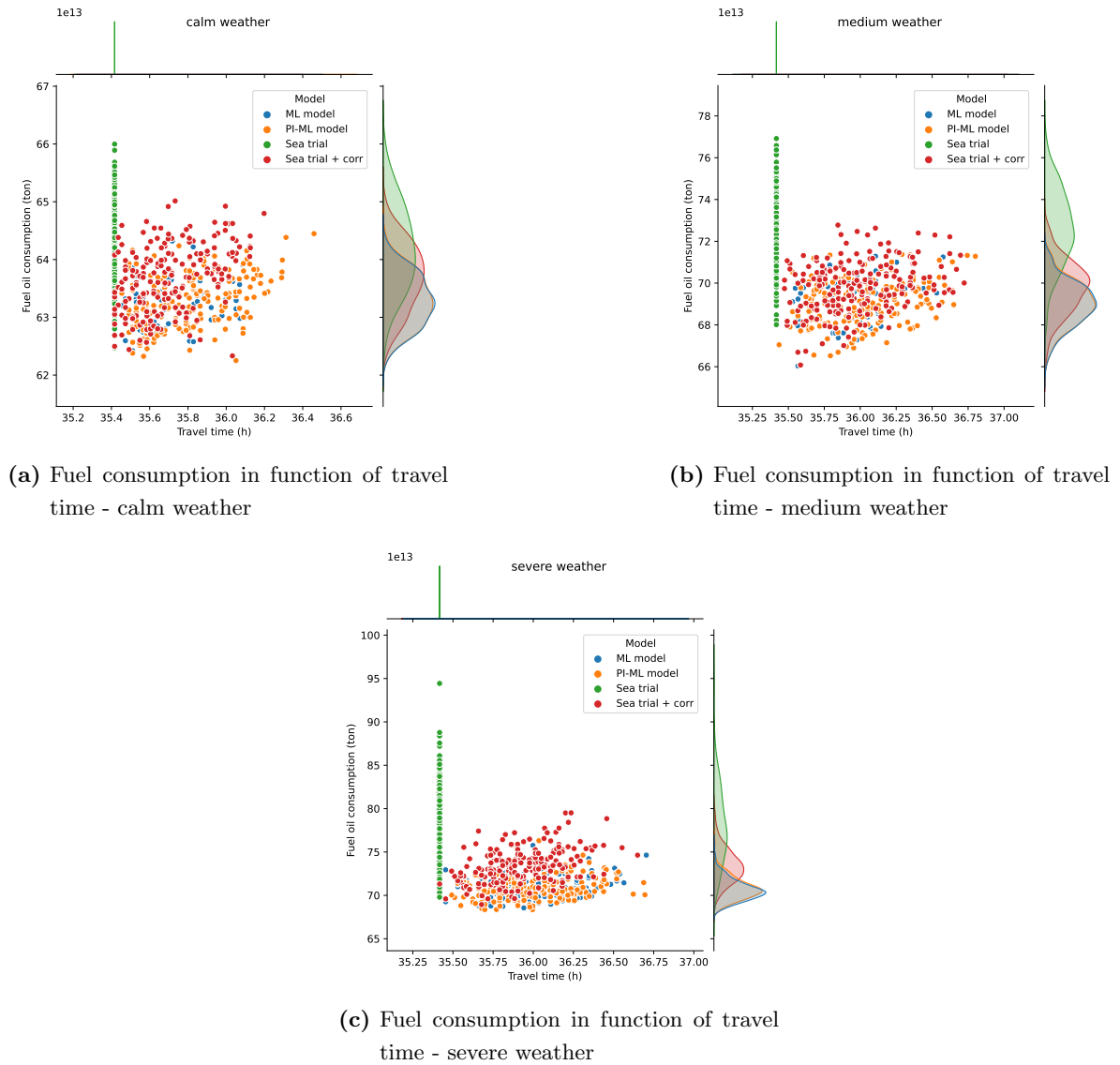


Figure C.2: Fuel consumption calculated by the ML model in function of travel time for different weather categories (200 samples)

Fuel savings (FS) and time extensions (TE) compared to the shortest route (Sea trial)		FOC model							
		Sea trial		Sea trial + corr		ML model		PI-ML model	
		FS	TE	FS	TE	FS	TE	FS	TE
Weather category	Calm	0.00%	0.00%	0.78%	0.21%	1.43%	0.67%	1.41%	0.85%
	Medium	0.00%	0.00%	3.82%	%	5.00%	1.34%	4.94%	1.37%
	Severe	0.00%	0.00%	5.57%	1.54%	9.15%	1.56%	8.84%	1.52%

Table C.1: The average fuel savings (FS) and travel time extensions (TE) of an FOC model's route compared to the shortest route (in %) - FOC recalculated by **ML model** as ground truth

C.2.2 The standard deviations of the time extensions

Travel time extension compared to the shortest route (Sea trial)		FOC model			
		Sea trial	Sea trial + corr	ML model	PI-ML model
Weather category	Calm	0.00%	0.54%	0.58%	0.62%
	Medium	0.82%	0.81%	0.83%	0.73%
	Severe	0.00%	0.64%	0.71%	0.72%

Table C.2: The standard deviation of the travel time extension of an FOC model's route compared to the shortest route (in %)

C.2.3 The standard deviations of the fuel savings

Fuel savings compared to the shortest route (Sea trial)		FOC model			
		Sea trial	Sea trial + corr	ML model	PI-ML model
Weather category	Calm	0.00%	1.24%	1.23%	1.22%
	Medium	0.00%	2.67%	2.40%	2.38%
	Severe	0.00%	4.82%	4.43%	4.43%

Table C.3: The standard deviation of the fuel savings of an FOC model's route compared to the shortest route (in %) - FOC recalculated by **PI-ML model** as ground truth

Fuel savings compared to the shortest route (Sea trial)		FOC model			
		Sea trial	Sea trial + corr	ML model	PI-ML model
Weather category	Calm	0.00%	0.97%	0.92%	0.92%
	Medium	0.00%	2.49%	2.22%	2.24%
	Severe	0.00%	4.93%	4.58%	4.59%

Table C.4: The standard deviation of the fuel savings of an FOC model's route compared to the shortest route (in %) - FOC recalculated by **ML model** as ground truth

Bibliography

- Avgouleas, K. (2008). Optimal ship routing.
- Begovic, E., Bertorello, C., Boccadamo, G., and Rinauro, B. (2018). Application of surf-riding and broaching criteria for the systematic series d models. *Ocean Engineering*, 170:246–265.
- Bellman, R. (1952). On the theory of dynamic programming. *Proceedings of the National Academy of Sciences of the United States of America*, 38(8):716.
- Bentin, M., Zastrau, D., Schlaak, M., Freye, D., Elsner, R., and Kotzur, S. (2016). A new routing optimization tool-influence of wind and waves on fuel consumption of ships with and without wind assisted ship propulsion systems. *Transportation Research Procedia*, 14:153–162.
- Bertsimas, D. and Tsitsiklis, J. (1993). Simulated annealing. *Statistical science*, 8(1):10–15.
- Beşikçi, E. B., Arslan, O., Turan, O., and Ölçer, A. I. (2016). An artificial neural network based decision support system for energy efficient ship operations. *Computers & Operations Research*, 66:393–401.
- Bijlsma, S. J. (1975). On minimal-time ship routing. *Delft University of Technology, Staatsdrukkerij Den Haag, The Netherlands, Doctors Thesis*.
- Calvert, S., Deakins, E., and Motte, R. (1991). A dynamic system for fuel optimization trans-ocean. *The Journal of Navigation*, 44(2):233–265.
- Chen, H. (1978). *A dynamic program for minimum cost ship routing under uncertainty*. PhD thesis, Massachusetts Institute of Technology.
- Colle, C. and Morobé, C. (2022). Saving ai from its own hype: Getting real about the benefits and challenges of machine learning for ship performance modelling aimed at operational optimizations.
- Conference, I. T. T. (2005). Ittc â recommended procedures and guidelines.

- Delitala, A. M. S., Gallino, S., Villa, L. a., Lagouvardos, K., and Drago, A. (2010). Weather routing in long-distance mediterranean routes. *Theoretical and applied climatology*, 102(1):125–137.
- for Standardization, I. O. (2016). Ships and marine technology â measurement of changes in hull and propeller performance â part 2:default method.
- Gkerekos, C. and Lazakis, I. (2020). A novel, data-driven heuristic framework for vessel weather routing. *Ocean Engineering*, 197:106887.
- Gkerekos, C., Lazakis, I., and Theotokatos, G. (2019). Machine learning models for predicting ship main engine fuel oil consumption: A comparative study. *Ocean Engineering*, 188:106282.
- Hagiwara, H. (1989). Weather routing of (sail-assisted) motor vessels. *PhD Thesis, Technical University of Delft*.
- Haltiner, G., Hamilton, H., and 'Arnason, G. (1962). Minimal-time ship routing. *Journal of Applied Meteorology (1962-1982)*, pages 1–7.
- Hinnenthal, J. and Clauss, G. (2010). Robust pareto-optimum routing of ships utilising deterministic and ensemble weather forecasts. *Ships and Offshore Structures*, 5(2):105–114.
- Holtrop, J. and Mennen, G. (1982). An approximate power prediction method. *International Shipbuilding Progress*, 29(335):166–170.
- James, R. W. (1957). *Application of wave forecasts to marine navigation*. New York University.
- Johnson, D. S., Aragon, C. R., McGeoch, L. A., and Schevon, C. (1989). Optimization by simulated annealing: An experimental evaluation; part i, graph partitioning. *Operations research*, 37(6):865–892.
- Kee, K.-K., Simon, B.-Y. L., and Renco, K.-H. Y. (2018). Prediction of ship fuel consumption and speed curve by using statistical method. *J. Comput. Sci. Comput. Math*, 8(2):19–24.
- Kettle, S. (2022). Distance on a sphere: The haversine formula.
- Klompstra, M. B., Olsder, G., and Van Brunschot, P. (1992). The isopone method in optimal control. *Dynamics and Control*, 2(3):281–301.
- Kosmas, O. and Vlachos, D. (2012). Simulated annealing for optimal ship routing. *Computers & Operations Research*, 39(3):576–581.
- Kwon, Y. (2008). Speed loss due to added resistance in wind and waves. *Nav Archit*, 3:14–16.

- Li, Y. and Qiao, C. (2019). A route optimization method based on simulated annealing algorithm for wind-assisted ships. In *IOP Conference Series: Earth and Environmental Science*, volume 295, page 042074. IOP Publishing.
- Lin, Y.-H., Fang, M.-C., and Yeung, R. W. (2013). The optimization of ship weather-routing algorithm based on the composite influence of multi-dynamic elements. *Applied Ocean Research*, 43:184–194.
- Maki, A., Akimoto, Y., Nagata, Y., Kobayashi, S., Kobayashi, E., Shiotani, S., Ohsawa, T., and Umeda, N. (2011). A new weather-routing system that accounts for ship stability based on a real-coded genetic algorithm. *Journal of marine science and technology*, 16(3):311–322.
- Mallawaarachchi, V. (2017). Introduction to genetic algorithms - including example code.
- Mallawaarachchi, V. (2022). Beaufort scale.
- Mao, W., Rychlik, I., Wallin, J., and Storhaug, G. (2016). Statistical models for the speed prediction of a container ship. *Ocean engineering*, 126:152–162.
- Marie, S., Courteille, E., et al. (2009). Multi-objective optimization of motor vessel route. *Marine Navigation and Safety of Sea Transportation*, 9:411–418.
- Mekarapiruk, W. and Luus, R. (2000). Optimal control by iterative dynamic programming with deterministic and random candidates for control. *Industrial & engineering chemistry research*, 39(1):84–91.
- Michalek, D. and Balakrishnan, H. (2009). Identification of robust routes using convective weather forecasts.
- Morobé, C. and Van den Poel, D. (2020). A comparative study of machine learning techniques to predict speed through water and speed loss due to fouling of seagoing vessels.
- national laboratory, P. N. (2022). Physics-informed machine learning.
- Papadakis, N. A. and Perakis, A. N. (1990). Deterministic minimal time vessel routing. *Operations Research*, 38(3):426–438.
- Park, J. and Kim, N. (2015). Two-phase approach to optimal weather routing using geometric programming. *Journal of Marine Science and Technology*, 20(4):679–688.
- Park, M.-W. and Kim, Y.-D. (1998). A systematic procedure for setting parameters in simulated annealing algorithms. *Computers & Operations Research*, 25(3):207–217.
- Pedersen, B. P. (2014). *Data-driven Vessel Performance Monitoring*. DTU Mechanical Engineering.

- Perakis, A. N. and Papadakis, N. A. (1989). Minimal time vessel routing in a time-dependent environment. *Transportation Science*, 23(4):266–276.
- Prpić-Oršić, J., Vettor, R., Faltinsen, O. M., and Guedes Soares, C. (2016). The influence of route choice and operating conditions on fuel consumption and co2 emission of ships. *Journal of Marine Science and Technology*, 21(3):434–457.
- Rere, L. R., Fanany, M. I., and Arymurthy, A. M. (2015). Simulated annealing algorithm for deep learning. *Procedia Computer Science*, 72:137–144.
- Sen, D. and Padhy, C. P. (2015). An approach for development of a ship routing algorithm for application in the north indian ocean region. *Applied Ocean Research*, 50:173–191.
- Shao, W., Zhou, P., and Thong, S. K. (2012). Development of a novel forward dynamic programming method for weather routing. *Journal of marine science and technology*, 17(2):239–251.
- Shin, Y. W., Abebe, M., Noh, Y., Lee, S., Lee, I., Kim, D., Bae, J., and Kim, K. C. (2020). Near-optimal weather routing by using improved a* algorithm. *Applied Sciences*, 10(17):6010.
- Sirimanne, S. N., Hoffman, J., Juan, W., Asariotis, R., Assaf, M., Ayala, G., Benamara, H., Chantrel, D., Hoffmann, J., Premti, A., et al. (2019). Review of maritime transport 2019. In *United Nations conference on trade and development, Geneva, Switzerland*.
- Szlapczynska, J. and Smierzchalski, R. (2007). Adopted isochrone method improving ship safety in weather routing with evolutionary approach. *International Journal of Reliability, Quality and Safety Engineering*, 14(06):635–645.
- Takashima, K., Mezaoui, B., and Shoji, R. (2009). 4 on the fuel saving operation for coastal merchant ships using weather routing. In *Marine Navigation and Safety of Sea Transportation*, pages 457–462. CRC Press.
- Walther, L., Rizvanolli, A., Wendebourg, M., and Jahn, C. (2016). Modeling and optimization algorithms in ship weather routing. *International Journal of e-Navigation and Maritime Economy*, 4:31–45.
- Wang, H., Mao, W., and Eriksson, L. (2020). Efficiency of a voluntary speed reduction algorithm for a ship’s great circle sailing. *TransNav: International Journal on Marine Navigation and Safety of Sea Transportation*, 14(2).
- Wang, H.-B., Li, X.-G., Li, P.-F., Veremey, E. I., and Sotnikova, M. V. (2018). Application of real-coded genetic algorithm in ship weather routing. *The Journal of Navigation*, 71(4):989–1010.

- Wang, K., Yan, X., Yuan, Y., and Li, F. (2016). Real-time optimization of ship energy efficiency based on the prediction technology of working condition. *Transportation Research Part D: Transport and Environment*, 46:81–93.
- Waters, R., Stålberg, M., Danielsson, O., Svensson, O., Gustafsson, S., Strömstedt, E., Eriksson, M., Sundberg, J., and Leijon, M. (2007). Experimental results from sea trials of an offshore wave energy system. *Applied Physics Letters*, 90(3):034105.
- Yang, L., Chen, G., Zhao, J., and Rytter, N. G. M. (2020). Ship speed optimization considering ocean currents to enhance environmental sustainability in maritime shipping. *Sustainability*, 12(9):3649.
- Zhu, X., Wang, H., Shen, Z., and Lv, H. (2016). Ship weather routing based on modified dijkstra algorithm. In *Proc. of 6th International Conference on Machinery, Materials, Environment, Biotechnology, and Computer (MMEBC 2016), China, Tianjin*, pages 696–699.
- Zis, T. P., Psaraftis, H. N., and Ding, L. (2020). Ship weather routing: A taxonomy and survey. *Ocean Engineering*, 213:107697.